

**EXPERIMENTAL STUDY OF DUAL-WAVELENGTH
LASER GENERATION IN YTTERBIUM-DOPED FIBER**

MUHAMMAD AIZI BIN MAT SALIM

**INSTITUTE OF GRADUATE STUDIES
UNIVERSITY OF MALAYA
KUALA LUMPUR**

2018

**EXPERIMENTAL STUDY OF DUAL-WAVELENGTH
LASER GENERATION IN YTTERBIUM-DOPED FIBER**

MUHAMMAD AIZI BIN MAT SALIM

**THESIS SUBMITTED IN FULFILMENT OF THE
REQUIREMENTS FOR THE DEGREE OF
DOCTOR OF PHILOSOPHY**

**INSTITUTE OF GRADUATE STUDIES
UNIVERSITY OF MALAYA
KUALA LUMPUR**

2018

UNIVERSITY OF MALAYA
ORIGINAL LITERARY WORK DECLARATION

Name of Candidate: Muhammad Aizi bin Mat Salim

Matric No: HHE130002

Name of Degree: Doctor of Philosophy

Title of Thesis: Experimental Study of Dual-Wavelength Laser Generation in
Ytterbium -Doped Fiber

Field of Study: Photonics

I do solemnly and sincerely declare that:

- (1) I am the sole author/writer of this Work;
- (2) This Work is original;
- (3) Any use of any work in which copyright exists was done by way of fair dealing and for permitted purposes and any excerpt or extract from, or reference to or reproduction of any copyright work has been disclosed expressly and sufficiently and the title of the Work and its authorship have been acknowledged in this Work;
- (4) I do not have any actual knowledge nor do I ought reasonably to know that the making of this work constitutes an infringement of any copyright work;
- (5) I hereby assign all and every rights in the copyright to this Work to the University of Malaya ("UM"), who henceforth shall be owner of the copyright in this Work and that any reproduction or use in any form or by any means whatsoever is prohibited without the written consent of UM having been first had and obtained;
- (6) I am fully aware that if in the course of making this Work I have infringed any copyright whether intentionally or otherwise, I may be subject to legal action or any other action as may be determined by UM.

Candidate's Signature

Date:

Subscribed and solemnly declared before,

Witness's Signature Date:

Name:

Designation:

UNIVERSITI MALAYA
PERAKUAN KEASLIAN PENULISAN

Nama: Muhammad Aizi bin Mat Salim

No. Matrik: HHE130002

Nama Ijazah: Doktor Falsafah

Tajuk Tesis: Kajian Penjanaan Dwi Panjang Gelombang Laser pada Ytterbium
dopan Gentian

Bidang Penyelidikan: Fotonik

Saya dengan sesungguhnya dan sebenarnya mengaku bahawa:

- (1) Saya adalah satu-satunya pengarang/penulis Hasil Kerja ini;
- (2) Hasil Kerja ini adalah asli;
- (3) Apa-apa penggunaan mana-mana hasil kerja yang mengandungi hakcipta telah dilakukan secara urusan yang wajar dan bagi maksud yang dibenarkan dan apa-apa petikan, ekstrak, rujukan atau pengeluaran semula daripada atau kepada mana-mana hasil kerja yang mengandungi hakcipta telah dinyatakan dengan sejasanya dan secukupnya dan satu pengiktirafan tajuk hasil kerja tersebut dan pengarang/penulisnya telah dilakukan di dalam Hasil Kerja ini;
- (4) Saya tidak mempunyai apa-apa pengetahuan sebenar atau patut semunasabahnya tahu bahawa penghasilan Hasil Kerja ini melanggar suatu hakcipta hasil kerja yang lain;
- (5) Saya dengan ini menyerahkan kesemua dan tiap-tiap hak yang terkandung di dalam hakcipta Hasil Kerja ini kepada Universiti Malaya ("UM") yang seterusnya mula dari sekarang adalah tuan punya kepada hakcipta di dalam Hasil Kerja ini dan apa-apa pengeluaran semula atau penggunaan dalam apa jua bentuk atau dengan apa juga cara sekali pun adalah dilarang tanpa terlebih dahulu mendapat kebenaran bertulis dari UM;
- (6) Saya sedar sepenuhnya sekiranya dalam masa penghasilan Hasil Kerja ini saya telah melanggar suatu hakcipta hasil kerja yang lain sama ada dengan niat atau sebaliknya, saya boleh dikenakan tindakan undang-undang atau apa-apa tindakan lain sebagaimana yang diputuskan oleh UM.

Tandatangan Calon

Tarikh:

Diperbuat dan sesungguhnya diakui di hadapan,

Tandatangan Saksi

Tarikh:

Nama:

Jawatan:

EXPERIMENTAL STUDY OF DUAL-WAVELENGTH LASER GENERATION IN YTTERBIUM-DOPED FIBER

ABSTRACT

This thesis describes the research work that has been carried out on generating dual-wavelength fiber lasers (DWFLs) in the one micron waveband-based ytterbium-doped fiber as an active medium. Various devices were used, including dual-tapered microfiber-based Mach-Zehnder Interferometer (MZI), Side Polished Fiber (SPF), and strain technique was discussed in DWFLs operation with regard to stability, tunability, output power and Side Mode Suppression Ratio (SMSR). A stable Single Longitudinal Mode (SLM) DWFL was successfully demonstrated by employing 2 μm diameter of dual-tapered microfiber MZI with SMSR of 50 dB and wavelength spacing of 0.94 nm. Then, by employing dual-tapered microfiber and tunable band pass filter (TBPF) together, the narrowest wavelength spacing of DWFL was obtained with 0.06 nm and SMSR of 50dB. Another dual-tapered microfiber with diameter of 10 μm was positioned between xyz-translation stages, and then a strain was applied on the microfiber by tuning the micrometer driver. As a result, stable four sets of DWFLs were obtained at displacements from 2 to 190 μm , and these outputs remained consistent after repeated several times. The SPF was also employed into the ring cavity to generate 3 sets of DWFLs with wavelength spacing of 6.89nm, 16.28nm and 22.16nm by adjusting the polarization controller (PC). While in pulse generation of DWFL, both wavelength selective filters and saturable absorbers (SAs) were employed together in the ring cavity to generate dual-wavelength and passively Q-switched operation simultaneously. The wavelength selective filters were dual-tapered microfiber MZI and SPF whereas the saturable absorbers (SAs) used were molybdenum diselenide (MoSe_2), black

phosphorus (BP), titanium dioxide (TiO₂) and zinc oxide (ZnO). The SAs used in our experiments were shown to be new, potentially high quality saturable absorbers. Molybdenum diselenide as SA was used to generate passively Q-switched in DWFL based dual-tapered microfiber MZI. The obtained Q-switched based MoSe₂ had a repetition rate ranging from 15.3 to 35.2 kHz. DWFL based microfiber Q-switched using BP as SAs was successfully demonstrated with tunable repetition rate from 6.5 to 62.5 kHz. Likewise, a passively Q-switched dual-wavelength YDFL using a titanium dioxide as SA and SPF as a wavelength selective filter had a repetition rate from 31.2 to 64.5 kHz. Lastly, zinc oxide together with SPF was proven in generating dual-wavelength passively Q-switched with a repetition rate from 67.6 to 104.2 kHz. The tunable repetition rate, output power, pulse energy and pulse width, and have been discussed in Q-switched operation.

Keywords: Dual-wavelength, microfiber, side polished fiber, saturable absorber, Q-switched

KAJIAN PENJANAAN DWI-PANJANG GELOMBANG LASER PADA YTTERBIUM DOPAN GENTIAN

ABSTRAK

Tesis ini menerangkan kerja-kerja penyelidikan yang telah dijalankan untuk menjana dwi-panjang gelombang laser gentian (DWFLs) dalam rantau 1 mikron berasaskan ytterbium didopan gentian sebagai medium penguatan. Pelbagai peranti telah digunakan seperti dwi tirus gentian mikro berasaskan Mach-Zehnder Interferometer (MZI), gentian sisi digilap (SPF) dan teknik terikan dibincangkan dalam tesis ini dari segi kestabilan, daya talaan, nisbah mod sisi halangan (SMSR) dan kuasa keluaran. DWFL mod tunggal membujur (SLM) yang stabil berjaya dihasilkan dengan menggunakan 2 μ m diameter dwi-tirus microfiber MZI yang mempunyai jarak panjang gelombang 0.94nm dan SMSR sebanyak 50dB. Kemudian dengan menggunakan bersama-sama dwi-tirus gentian mikro dan penapis jalurtalaan (TBPF), jarak gelombang yang paling sempit DWFL diperolehi dengan 0.06 nm dan SMSR 50 dB. Satu lagi dwi-tirus gentian mikro dengan diameter 10 μ m diletakkan di antara pentas xyz dan kemudian terikan dikenakan pada gentian mikro dengan melaraskan pada pemandu mikrometer. Dengan itu menghasilkan empat set DWFLs yang stabil diperolehi pada anjakan dari 2 hingga 190 μ m dan hasilnya tetap konsisten selepas beberapa kali diulang. Gentian sisi yang digilap (SPF) juga digunakan ke dalam rongga cincin untuk menjana 3 set DWFLs dengan jarak panjang gelombang 6.89nm, 16.28nm dan 22.16nm dengan melaraskan pengawal polarisasi (PC). Pada penjanaan denyut DWFL, kedua-dua penapis panjang gelombang terpilih dan penyerap ketepuan (SAs) digunakan bersama-sama dalam rongga cincin untuk menjana dwi-panjang gelombang dan operasi pasif Q-switched serentak. Penapis panjang gelombang terpilih adalah dwi-tirus gentian

mikro MZI dan gentian sisi yang digilap (SPF) manakala penyerap ketepuan (SAs) yang digunakan adalah molibdenum diselenide (MoSe_2), black phosphorus (BP), titanium dioksida (TiO_2) dan zink oksida (ZnO). SAs yang digunakan dalam eksperimen kami telah terbukti berpotensi sebagai penyerap ketepuan baru yang berkualiti. Molybdenum diselenide sebagai SA digunakan untuk menjana pasif Q-switched dalam DWFL berasaskan dwi-tirus microfiber MZI. Q switched berasaskan MoSe_2 yang diperolehi mempunyai frekuensi antara 15.3 - 35.2 kHz. DWFL berasaskan gentian mikro Q-switched menggunakan BP sebagai SAs berjaya dihasilkan dengan kadar frekuensi 6.5 - 62.5 kHz. Begitu juga, pasif Q-switched YDFL dwi-panjang gelombang menggunakan titanium dioksida sebagai SA dan SPF sebagai penapis panjang gelombang terpilih mempunyai frekuensi 31.2 - 64.5 kHz. Akhir sekali, zink oksida bersama-sama dengan SPF terbukti dalam menjana dwi-panjang gelombang pasif Q-switched dengan frekuensi 67.6 - 104.2 kHz. Kadar frekuensi, lebar denyut, kuasa keluaran dan tenaga denyut dibincangkan dalam operasi Q-switched.

Kata kunci: Dwi-panjang gelombang, gentian mikro, gentian sisi yang digilap, penyerap ketepuan, Q-switched

ACKNOWLEDGEMENTS

I wish to convey my sincere appreciation and gratitude to my supervisor, Distinguished Professor Datuk Dr Harith Ahmad and Professor Dr Sulaiman Wadi Harun for the motivation, guidance, knowledge and experience-sharing, criticism, advice and inspiration. Through the journey, I have learned a lot on responsibility, diligence, independence and respect. I am indebted to Dr Saaidal Razalli Azzuhri, Dr Mohd Zulkhikimi Ab Razak, Dr Mohd Afiq Ismail, Mr Mohammad Faizal Ismail and Dr Mohd Zamani Zulkifli for knowledge and experience-sharing, and also providing invaluable assistance throughout the research journey.

I would also like to express my sincerest gratitude to all my friends in the Photonics Research Centre, Farah Diana Muhammad, Mohamad Dernaika, Osayd M Kharraz, Dr Ali Jasim and Dr Zian Cheak Tiu for their kind assistance, opinion and encouragement throughout my study.

My personal full-hearted thank you to my beloved wife, Mdm Raja Nur Azreen binti Raja Abdul Rahman, and my children: Muhammad Irfan, Nur Firzanah and Nur Wafirah for supporting, encouraging and providing motivation in pursuing my degree till the end.

To my beloved parents, Mr Mat Salim bin Hj Yaacob, Mdm Azizah binti Adnan and Mdm Rosiah binti Simat: thank you for your prayers, positive spirit and love for me. I would also like to my siblings for their cooperation, understanding and assistance.

Last but not least, Hj Junus Shukur and to everyone involved in this work both directly and indirectly, my deepest gratitude for your assistance, and may Allah bless your lives.

TABLE OF CONTENTS

Abstract	iii
Abstrak	v
Acknowledgements	vii
Table of Contents	viii
List of Figures	xi
List of Tables.....	xvi
List of Symbols and Abbreviations.....	xvii
List of Appendices	xx
CHAPTER 1: INTRODUCTION.....	1
1.1 Optical Fiber Laser	1
1.2 Dual-Wavelength Fiber Laser.....	1
1.3 Research Methodology	3
1.4 Research Objective	3
1.5 Research Scope.....	4
1.6 Thesis Outline.....	4
CHAPTER 2: THEORETICAL BACKGROUND.....	6
2.1 Ytterbium-Doped Fiber Laser.....	6
2.1.1 Laser Principle.....	6
2.1.2 Ytterbium-Doped Fiber	7
2.2 Dual-Wavelength Fiber Laser.....	11
2.2.1 Mach-Zehnder Interferometer	11
2.2.2 Mechanism of Dual-Tapered Microfiber.....	13
2.2.3 Mechanism of Side Polished Fiber.....	17

2.3	Q-switched Operation	21
2.3.1	Saturable Absorber	25
2.3.2	Mechanism of Saturable Absorber	25
2.3.3	Molybdenum Diselenide (MoSe ₂).....	27
2.3.4	Black Phosphorus (BP)	29
2.3.5	Titanium Dioxide (TiO ₂).....	32
2.3.6	Zinc Oxide (ZnO).....	33

CHAPTER 3: DESIGN, FABRICATION AND CHARACTERIZATION 35

3.1	Introduction.....	35
3.2	Gain Medium	35
3.3	Fiber Laser Design.....	36
3.4	Dual-Tapered Microfiber MZI	39
3.4.1	In House Tapered Machine	39
3.4.2	Commercial Tapered Machine	42
3.5	Side Polished Fiber	43
3.6	Linewidth Characterization	45
3.7	Preparation of Saturable Absorber.....	47
3.7.1	Molybdenum Diselenide	47
3.7.2	Black Phosphorus	50
3.7.3	Titanium Dioxide	52
3.7.4	Zinc Oxide	54
3.8	Modulation Depth Measurement	56

CHAPTER 4: DUAL-WAVELENGTH CONTINUOUS WAVE LASER..... 58

4.1	Introduction.....	58
4.2	Tunable DWFL Based Dual-Tapered Microfiber MZI	59

4.3	Tunable Narrow-Spacing DWFL Using Dual-Tapered Microfiber MZI.....	70
4.4	Tunable DWFL Using A Strain Technique	79
4.5	Tunable DWFL based on Side-Polished Fiber	87
4.6	Summary.....	95
CHAPTER 5: DUAL-WAVELENGTH PULSE LASER		97
5.1	Introduction.....	97
5.2	Q-switched DWFL based microfiber using MoSe ₂ as SA.....	98
5.3	Q-switched DWFL based microfiber using BP as SA.....	105
5.4	Q-switched DWFL based SPF using TiO ₂ as SA.....	112
5.5	Q-switched DWFL based SPF using ZnO as SA	118
5.6	Summary.....	126
CHAPTER 6: CONCLUSION.....		127
6.1	Conclusion	127
	Future Works.....	131
	References	133
	List of Publications and Papers Presented	149
	Appendix A.....	153

LIST OF FIGURES

Figure 2.1: Three processes involved in active gain medium (Durairaj, V. 2013).....	6
Figure 2.2: The electronic structure of Yb ³⁺ ions (Durairaj, V. 2013).....	8
Figure 2.3: The cross-section of absorption and emission of YDF (Rüdiger Paschotta <i>et al.</i> , 1997)	10
Figure 2.4: The Mach-Zehnder Interferometer diagram (Zetie, K., Adams, S., & Tocknell, R. 2000).....	13
Figure 2.5: The cross-section of dual-tapered microfiber (H Ahmad <i>et al.</i> , 2014).....	14
Figure 2.6: Amplification spontaneous emission of dual-tapered microfiber (Ahmad, H., <i>et al.</i> , 2014)	15
Figure 2.7: The cross-section structure of the side polished fiber (S. X. Zhang, Liu, & Ye, 2014).....	17
Figure 2.8: Transmission spectrum of side polished fiber (Ahmad. H., Rashid, F. A. A., <i>et al.</i> , 2016)	19
Figure 2.9: Mechanism of saturable absorber (Kashiwagi & Yamashita, 2010).....	26
Figure 2.10: Suppression of noise in cavity ring via saturable absorber (Kashiwagi, K., & Yamashita, S. 2010).....	27
Figure 2.11: TMD structure with M and X atom (Wilson & Yoffe, 1969)	28
Figure 2.12: Energy structure for TMD (Wilson & Yoffe, 1969)	29
Figure 2.13: Black phosphorus structure with two adjacent puckered sheets linked by phosphorus atom. (F. Xia <i>et al.</i> , 2014).....	30
Figure 2.14: Schematic diagram of saturable absorption of multi-layers BP (Lu, S., <i>et al.</i> , 2015)	31
Figure 2.15: Bulk crystal structure of rutile and anatase with titanium atom in grey and oxygen atom in red (Thompson, T. L., & Yates, J. T. 2006).....	32
Figure 2.16: Wurtzite zinc oxide hexagonal structures. (Wang, Z. L. 2004).....	34
Figure 3.1: Absorption and emission of YDF model DF1100 Fibercore (<i>SM Ytterbium Doped Fiber</i> , 2013).....	36
Figure 3.2: Laser design of a simple ytterbium-doped fiber laser ring cavity.	37

Figure 3.3: Amplified spontaneous emission spectrum of YDF.....	38
Figure 3.4: Lasing spectrum of YDFL.....	38
Figure 3.5: In house tapered machine system	40
Figure 3.6: The cross-section of dual-tapered microfiber	40
Figure 3.7: Amplified spontaneous emission spectrum with microfiber (red) and without microfiber (purple).....	41
Figure 3.8: Packaging microfiber to preserve its properties	41
Figure 3.9: The cross section of microfiber with waist diameter of 10 μm	42
Figure 3.10: The amplified spontaneous emission of YDF with microfiber (blue) and without microfiber (green).....	43
Figure 3.11: The side polished fiber diagram	44
Figure 3.12: The ASE transmission through side polished fiber (blue) and without it (red).....	44
Figure 3.13: Optical heterodyne setup for linewidth measurement (Derickson, 1998)..	46
Figure 3.14: Analysis for (a) XRD, (b) Raman shift, (c) Uv-vis and (d) thin film of MoSe_2	49
Figure 3.15: (a) BP scotch-tape SA, (b) Raman shift analysis, (c) BP tape placed on the surface of fiber ferule and (d) BP tape observed via fiberscope.....	51
Figure 3.16: TiO_2 observed by (a) FEG-SEM, (b) Uv-vis spectroscopy, (c) XRD and (d) image of TiO_2 thin film saturable absorber.....	53
Figure 3.17: (a) FEG-SEM image, (b) XRD pattern, (c) linear absorption and (d) thin film image of ZnO SA.....	55
Figure 3.18: The experimental setup of dual-detector measurement system.....	57
Figure 4.1: Fiber ring laser experimental setup with a dual-tapered MZI microfiber	61
Figure 4.2: Amplified spontaneous emission transmission through microfiber (red) and without it (blue).....	62
Figure 4.3: (a) Dual-wavelength output at 1036.47 nm and 1037.41 nm and (b) dual-wavelength tuning with various wavelength spacing.....	63

Figure 4.4: (a) The dual-wavelength stability scans and (b) power fluctuation for 30 minutes at narrowest wavelength spacing of 0.94 nm	65
Figure 4.5: RF spectrum with (a) microfiber disconnected, and (b) microfiber connected in the ring cavity.....	67
Figure 4.6: FWHM linewidth measurement using a heterodyne linewidth method	68
Figure 4.7: (a) Narrow wavelength spacing of DWFL ring setup, (b) cross section of dual-tapered microfiber MZI (c) amplified spontaneous emission spectrum of microfiber (purple) and excluded microfiber (green)	72
Figure 4.8: (a) The dual-wavelength spectrum with SMSR of 52 dB and (b) Set of dual-wavelengths with tunable spacing from 0.06 nm to 0.22 nm.....	74
Figure 4.9: (a) Wavelength and (b) peak power stability test for wavelength spacing of 0.06 nm at $\lambda_1=1039.42$ nm and $\lambda_2=1039.48$ nm respectively	76
Figure 4.10: (a) Wavelength and (b) peak power stability test for wavelength spacing of 0.09 nm at $\lambda_1=1039.12$ nm and $\lambda_2=1039.21$ nm respectively	77
Figure 4.11 (a) Wavelength and (b) peak power stability test for wavelength spacing of 0.22 nm at $\lambda_1=1039.40$ nm and $\lambda_2=1039.62$ nm respectively	78
Figure 4.12: DWFL based strain technique proposed fiber ring setup	80
Figure 4.13: The cross-section of the microfiber MZI.....	81
Figure 4.14: Amplified spontaneous emission spectrum of microfiber (blue) and excluded microfiber (green) at 175.4 mW. The lasing threshold at 128.8mW (inset) ...	82
Figure 4.15: The dual-wavelength spectrum with SMSR of 48dB	83
Figure 4.16: Set of dual-wavelengths with different wavelength spacing at certain distance from 2 μ m to 190 μ m	84
Figure 4.17: (a) Dual-wavelength (b) peak power and (c) wavelength shift stability test for wavelength spacing of 7.12 nm at $\lambda_1=1034.76$ nm and $\lambda_2=1041.88$ nm respectively	85
Figure 4.18: (a) Dual-wavelength (b) peak power and (c) wavelength shift stability test for wavelength spacing of 11.59 nm at $\lambda_1=1030.18$ nm and $\lambda_2=1041.77$ nm respectively	86
Figure 4.19: YDFL ring cavity experimental setup with a side-polished fiber	88
Figure 4.20: The lasing threshold for the side polished fiber setup in cavity ring.....	89

Figure 4.21: DWFL at 1039.39 nm and 1046.28 nm wavelength.....	90
Figure 4.22: Dual-wavelengths spectrums with different wavelength spacing from 6.89 nm to 22.16 nm	91
Figure 4.23: (a) Wavelength and (b) peak power stability test for wavelength spacing of 6.89 nm at $\lambda_1=1039.39$ nm and $\lambda_2=1046.28$ nm respectively	92
Figure 4.24: (a) Wavelength and (b) peak power stability test for wavelength spacing of 16.28 nm at $\lambda_1=1042.07$ nm and $\lambda_2=1058.35$ nm respectively	93
Figure 4.25: (a) Wavelength and (b) peak power stability test for wavelength spacing of 22.16 nm at $\lambda_1=1043.32$ nm and $\lambda_2=1065.48$ nm respectively	94
Figure 5.1: The characteristic of MoSe ₂ saturable absorber	99
Figure 5.2: Configuration of MoSe ₂ based Q-switched dual-wavelength in YDFL	100
Figure 5.3: Output pulse trains with different frequency and period by increasing pump power at (a) 166.6 mW, (b) 209.7 mW and (c) 261.2 mW.....	102
Figure 5.4: The centered dual-wavelength spectrum at 1035.8 nm and 1040.2 nm, b) Q-switched output pulse train with 34 μ s period, c) 2.2 μ s pulse width and (d) 29.4 kHz fundamental of RF spectra at pump power of 231.6 mW	103
Figure 5.5: (a) The repetition rate and pulse width and (b) the average output power and pulse energy against pump power.....	104
Figure 5.6: The saturable absorption characteristic of the Black Phosphorus SA.....	107
Figure 5.7: Experimental setup of Q-switched DWFLs in YDFL using BP as saturable absorber.....	108
Figure 5.8: The repetition rate and period changes at (a) pump power of 143.9mW, (b) 202.9mW, (c) 239.7mW and (d) 297.1mW.	109
Figure 5.9: Characteristic of Q-switching at repetition rate of 28.1 kHz: (a) dual-wavelength laser, (b) pulse duration, (c) pulse width and (d) frequency domain at pump power of 225.2mW.....	110
Figure 5.10: The repetition rate and pulse width and (b) the average output power and pulse energy in relation to pump power.....	111
Figure 5.11: The saturable absorption distinctive of the TiO ₂ SA.....	113
Figure 5.12: Configuration of titanium dioxide based saturable absorber in one micron region.....	114

Figure 5.13: The pulse train of Q-switched at various pump power at (a) 143.90 mW and frequency of 31.2 kHz, (b) 180.90 mW and frequency of 40.9 kHz and (c) 209.70 mW and frequency of 52.13 kHz, (d) 231.60 mW and frequency of 62.4 kHz.....	115
Figure 5.14: The characteristic of Q-switching at pump power of 188 mW and repetition rate of 43.5 kHz with (a) wavelength spectrum, (b) period, (c) single pulse profile and (d) RF output spectrum	116
Figure 5.15: (a) The repetition rate and pulse width and (b) the pulse energy and average output power corresponding to pump power.	117
Figure 5.16: Saturation absorption characteristic of ZnO	118
Figure 5.17: Configuration of Q-switched dual-wavelength based zinc oxide as saturable absorber in 1 μ m waveband.....	120
Figure 5.18: The pulse traces corresponding to four different stages of input power at (a)188mW, (b) 217.8mW, (c) 246.4mW and (d) 253.4mW	121
Figure 5.19: The dual-wavelength spectrum selected individually at (a) 1038 nm and (b) 1039.2 nm wavelength has same repetition rate of 92.6 kHz at pump power of 253.4 mW. (both insets: Q-switched with repetition rate of 92.6 kHz).....	122
Figure 5.20: The Q-switched dual-wavelength characterization with repetition rate of 104.2 kHz at maximum pump power of 275.3 mW; (a) dual-wavelength spectrum, (b) Q-switched pulse train with period of 9.8 μ s, (c) FWHM of 1.6 μ s and (d) frequency domain spectrum	123
Figure 5.21: (a) The pulse duration and repetition rate, and (b) the pulse energy and average output power corresponding to input pump power.....	125

LIST OF TABLES

Table 3.1: Ytterbium-doped fiber DF1100 Fibercore specification	35
Table 3.2: The Relations of Heterodyne Technique Linewidth (Derickson, 1998).....	46
Table 5.1: Characteristics of Q-switched YDFL by different SAs	126

University of Malaya

LIST OF SYMBOLS AND ABBREVIATIONS

λ	: Wavelength
n	: Refractive index
L_{β}	: Beating length
Δ_{β}	: Propagation constant difference
σ	: Cross-section of laser beam
v	: Volume density
E	: Energy level
l	: Length
h	: Planck constant
t	: time
ν	: Photon frequency
π	: Radians phase shift
α_{linear}	: Non saturable loss
I_{sat}	: Saturable optical intensity
$\Delta\alpha$: Modulation depth
ASE	: Amplification spontaneous emission
BP	: Black Phosphorus
CNT	: Carbon nanotube
CW	: Continuous wave
DWFL	: Dual-wavelength fiber laser
EDF	: Erbium-doped fiber
EDFA	: Erbium-doped fiber amplifier
FEG-SEM	: Field emission gun scanning electron microscope
FWHM	: Full width at half maximum

LD	: Laser diode
LO	: Local Oscillator
LPE	: Liquid phase exfoliation
MMBG	: Multimode fiber Bragg grating
MoSe ₂	: Molybdenum diselenide
MZI	: Mach-Zehnder Interferometer
OC	: Optical coupler
OCT	: Optical coherence tomography
OPM	: Optical power meter
OSA	: Optical Spectrum Analyzer
PC	: Polarization controller
RFSA	: Radio frequency spectrum analyzer
SA	: Saturable absorber
SESAM	: Semiconductor saturable absorber mirror
SLM	: Single longitudinal mode
SMF	: Single mode fiber
SMSR	: Side mode suppression ratio
SPF	: Side polished fiber
TBPF	: Tunable band pass filter
TiO ₂	: Titanium dioxide
TMD	: Transition metal chalcogenides
TMO	: Transition metal oxide
VOA	: Variable optical attenuator
WDM	: Wavelength division multiplexer
XRD	: X-ray diffraction
YDF	: Ytterbium-doped fiber

YDFA : Ytterbium-doped fiber amplifier

YDFL : Ytterbium-doped fiber laser

ZnO : Zinc oxide

University of Malaya

LIST OF APPENDICES

Appendix A: Reprint of selected paper published related to research work	153
--	-----

University of Malaya

CHAPTER 1: INTRODUCTION

1.1 Optical Fiber Laser

Optical fiber laser has been gaining recognition as one of advanced technologies in photonics applications such as telecommunication and computer networking, power transmission where light is converted into electricity, fiber optic sensor, and optical instrument which is used for image enhancement and to analyse properties of photonic component (Chen, L. R., & Gu, X. 2007). Optical fiber laser has several distinct advantages such as longer transmission at higher bandwidth, high stability, low attenuation loss, better beam quality, no effects due to electromagnetic interferences and high thermal resistance.

1.2 Dual-Wavelength Fiber Laser

Dual-wavelength fiber laser (DWFL) research has started to gain attention lately. The attention on enhancing DWFL has been given special consideration especially in 1550nm wavelength range. A variety of techniques have been reported on dual-wavelength laser generation as a result of increasing interest in applications for various fields like high bit rate soliton pulses (Tadakuma, M., Aso, O., & Namiki, S. 2000), radar and photonic beam steering of phased-arrayed antennas in microwave photonic filters (Liu, D., Ngo, N. Q., Ning, G., Shum, P., & Tjin, S. C. 2006) and photonic generation of microwave carrier (Xia, L., Shum, P., & Cheng, T. H. 2007).

Various techniques like inducing polarization hole burning in erbium doped fiber (EDF), increasing the inhomogeneous in gain medium and suppressing wavelength competition effects were demonstrated to generate stable dual-wavelength laser (Qian, J. R., Su, J., & Hong, L., 2008). Feng, X., *et al.*, (2004) employed multimode fiber Bragg gratings (MMBG) for wavelength selection with stronger reflectivity at longer wavelength as compared to a few mode fiber grating (Feng, X., Liu, Y., Yuan, S., *et al.*, 2004), incorporating nonlinear material such as photonic crystal fiber and tapered fiber based on Mach Zehnder Interferometer into ring cavity (Ahmad, H., *et al.*, 2015; Ahmad, H., Salim, M. A. M., Azzuhri, S. R., & Harun, S. W. 2016; Ahmad, H., Soltanian, M. R. K., Pua, C. H., Zulkifli, M. Z., & Harun, S. W. 2013a) work as wavelength selective filters are widely reported in the past few years. There are a few works on wavelength selection filter utilizing single mode fiber Bragg grating for generating a dual-wavelength laser (Li, J. L., Musha, M., Shirakawa, A., Ueda, K. I., & Zhong, L. X. 2006; Wang, H. *et al.*, 2009; Xinhuan, F., Yange, L., Shenggui, F., Shuzhong, Y., & Xiaoyi, D. 2004) incorporating ytterbium-doped fiber (YDF) with spectral range from 970 to 1200 nm (Wright, M. W., & Valley, G. C. 2005). Nevertheless, significant interest has been developed recently in ytterbium-doped fiber lasers (YDFL) that work in the one-micron waveband. Moreover, dual-wavelength laser generation in YDF as active medium (Zhou, P., Wang, X., Xiao, H., Ma, Y., & Chen, J. 2012) is still minimum. It is the aim of this work to explore further on dual-wavelength fiber laser in ytterbium gain medium where applications in optical coherence tomography and free space optical communication are more applicable to the one micron wavelength operation (Yasuno, Y. *et al.*, 2007).

1.3 Research Methodology

The work begins with the study of existing DWFL with various type of wavelength selective filters with different configurations and techniques that are employed in order to achieve stable and tunable wavelength in one micron waveband. DWFL mechanisms can be generated in continuous wave mode and pulse mode operations. In continuous wave mode, the dual-tapered microfiber and side polished fiber are used as wavelength selective filter to generate the DWFL in a ring cavity. Then, the SAs such as molybdenum diselenide, black phosphorus, titanium dioxide or zinc oxide are incorporated in the ring cavity to generate passively Q-switched pulse laser in YDF laser system. The recommendation for future work is concluded to improve the performance of DWFL system.

1.4 Research Objective

The main objectives of this research works are:

- i. To design and characterize a microfiber-based Mach Zehnder Interferometer in generating DWFL
- ii. To design a laser setup in generating narrow spacing DWFL
- iii. To explore the technique applied in generating tunable DWFL
- iv. To employ and characterize a side polished fiber in generating DWFL
- v. To generate Q-switched DWFL-based passive saturable absorber (SA)

1.5 Research Scope

The DWFL operates in one micron region (970 nm to 1200 nm) using YDF laser system in a ring cavity configuration. The wavelength selective filter employed in this work are dual-tapered microfiber and side polished fiber are used to generate DWFL in continuous wave laser mode whereas SAs are used to generate Q-switched pulse laser for passive system.

1.6 Thesis Outline

The purpose of this dissertation is to generate DWFL in the one-micron region using a wavelength selective filter, whereby in our work, dual-tapered microfiber and side-polished fiber are employed in ytterbium-doped fiber ring cavity. Furthermore Q-switched DWFL is also generated using passive saturable absorber.

The thesis comprises of six chapters, lead off by chapter one comprising introduction of the dissertation. In this chapter, the overview of optical fiber laser and DWFL are discussed and a clear objective of the research study is defined.

In chapter 2, the theoretical background of YDF as active medium used in this study is explained to generate YDFL in the one-micron region. The mechanism of dual-wavelength generation in dual-tapered microfiber and side-polished fiber are also explained. Whereas, for pulse mode operation, the mechanism of saturable absorber to generate Q-switched has been delineated in this subdivision.

Chapter 3 accounts for the YDFL experimental setup and its characterization. The fabrication and characterization of wavelength selective filter such as dual-tapered microfiber and side-polished fiber are clarified in terms of method and its specification. Furthermore, the fabrication and analysis of saturable absorber are presented in this section and the modulation depth as well. The saturable absorbers used in this work are molybdenum diselenide (MoSe_2), black phosphorus (BP), titanium dioxide (TiO_2) and zinc oxide (ZnO).

The results and discussion of successful DWFL in continuous wave are presented in Chapter 4. In this section, DWFLs generated using dual-tapered microfiber MZI and side-polished fibers are studied in terms of output power, tunability, SMSR and stability. The study begins with the generation of DWFLs, and is continued with researches on narrow wavelength spacing of DWFLs and the strain technique is applied to tune the DWFLs system.

In chapter 5, the results for Q-switched DWFLs are presented here. In this work, the successful Q-switched DWFL is demonstrated by incorporating both wavelength selective filters and passive saturable absorber in the YDFL ring cavity. Molybdenum diselenide (MoSe_2), black phosphorus (BP), titanium dioxide (TiO_2) and zinc oxide (ZnO) are used as SAs to generate Q-switched pulse YDFL and the characteristics in terms of repetition rate, output power, pulse energy and pulse width are studied in this section.

Ultimately the closing section is chapter 6, which concludes the dissertation. Each chapter in the dissertation and recommendation of future work are summarized and suggested in this section.

CHAPTER 2: THEORETICAL BACKGROUND

2.1 Ytterbium-Doped Fiber Laser

An ytterbium-doped fiber laser is a type of laser whereby the active gain medium is an optical fiber doped with ytterbium rare-earth element. A Ytterbium-doped fiber is discussed in this chapter, starting with laser principle, rare-earth element, the particular properties and its characteristics that offer wide range of applications in the one-micron region.

2.1.1 Laser Principle

The absorption, spontaneous emission and stimulated emission are three main processes happening due to interaction of light and an optically active gain medium.

Figure 2.1 shows the processes involved in two energy levels, E_1 and E_2 , respectively.

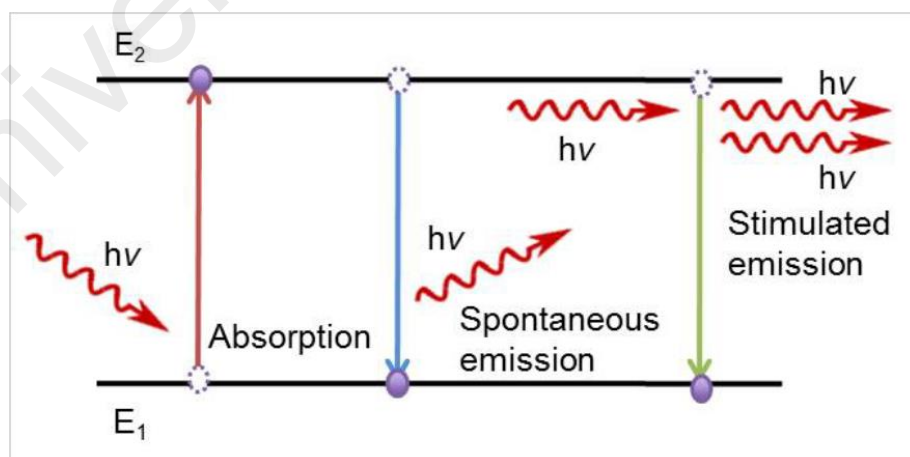


Figure 2.1: Three processes involved in active gain medium (Durairaj, V. 2013)

Electrons of an atomic or molecular medium reside in the ground-state energy level, E_1 . Then a photon with frequency, ν and energy, E is incident on medium and is given by the equation as follows:

$$E = h\nu = E_2 - E_1 \quad (2.1)$$

The photon energy is transferred to electrons in ground-state, E_1 resulting the electrons to be excited to a higher energy level, E_2 , whereby this process is also known as absorption and can result in more electrons being present in the excited state energy level, E_2 in contrast to ground-state, E_1 or also known as population inversion.

Spontaneous emission is a process where the excited electron moving down to the ground-state by photon emission without the effect of external electromagnetic field. Usually, spontaneous emission happens in every pathway and causes spatially incoherent radiation. However, once a photon with energy, E interact with an excited electron, it results in a new emission of photon with same frequency, polarization, phase and pathway as the incident photon known as stimulated emission. A highly coherent beam can be achieved by intensifying the stimulation of emission process.

2.1.2 Ytterbium-Doped Fiber

In 1988, ytterbium-doped fiber (YDF) was first demonstrated, operating at wavelength ranging from 1035 to 1078nm (Hanna, D. *et al.*, 1988). Initially, ytterbium-doped fiber was not popular due to the existence of erbium- and neodymium-doped fiber that were commonly used due to their advantages. For example EDF has operating wavelength from 1520 nm to 1600 nm which lies in telecommunication region and has broad pumping wavelength ranging from 510 to 1480nm. While neodymium-doped

fiber has shown a four level energy system and is highly efficient at the lasing wavelength of 1060 nm by pumping at 800nm. On the other hand, their disadvantages such as excited-state absorption in EDF and limited emission bandwidth in neodymium-doped fiber limit their applications in fiber laser. Thus, the new interest in YDF surfaced. Paschotta, R., *et al.*, (1997) studied various advantages in ytterbium -doped fiber (Paschotta, R., Nilsson, J., Tropper, A. C., & Hanna, D. C. 1997) and this brought about great attention to further explore the characteristics of this rare-earth fiber.

Figure 2.2 shows the electronic structure of Yb^{3+} ions (Pask et al., 1995) in light amplification which involves two main energy levels. There are the ground level ($^2F_{7/2}$) and a higher excited level ($^2F_{5/2}$). Due to Stark effect, pump and laser transitions take place between various sub-energy levels, which split these main energy levels through red and green arrows respectively.

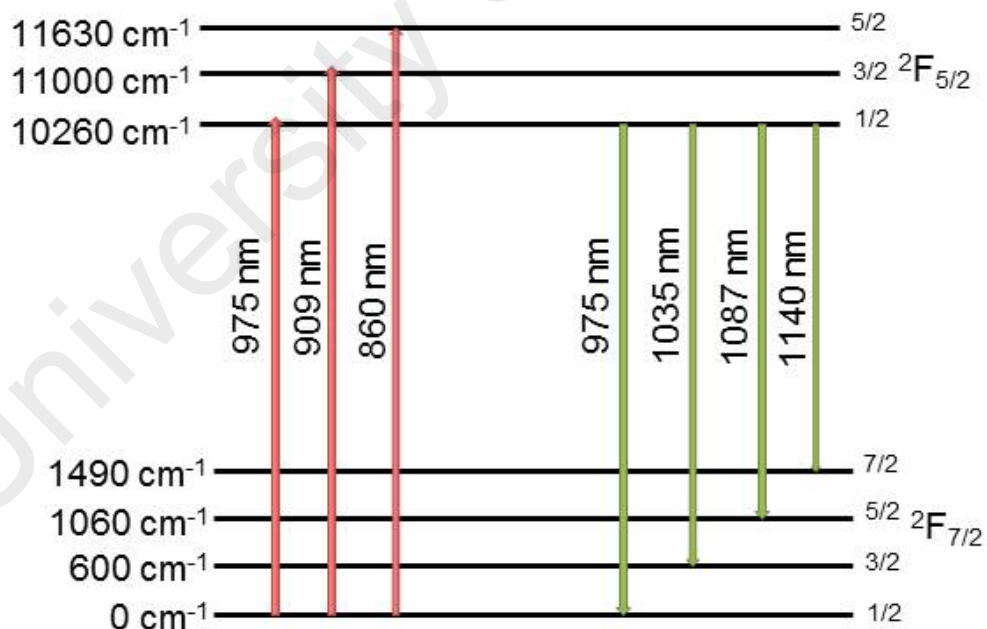


Figure 2.2: The electronic structure of Yb^{3+} ions (Durairaj, V. 2013)

The main advantage of YDF is that it has only one excited-state manifold associated in laser transition. The extremely low quantum defect is due to small energy gap between the ground and the excited state. Therefore, high power efficiency is achievable; reducing thermal effects, quenching and excited-state absorption (Paschotta, R., *et al.*, 1997). However, a pronounced quasi-3-level behavior is disadvantageous due to low quantum defect.

The pump and seed wavelengths influence the quasi-3-level or 4-level behavior of YDF. The lower laser transition state is close to the ground level for emitting wavelength less than 1080 nm, similar to a quasi-3-level system. Significant population in this level causes re-absorption losses (Paschotta, R., *et al.*, 1997) in un-pumped gain medium thus requires higher laser threshold as compared to neodymium-doped fiber (Nilsson, J. *et al.*, 2004). The laser transition is higher than ground level for emitting wavelength further than 1080nm, which shows a 4-level behavior. Population inversion is achieved easily as a result of large energy gap between the ground level and lower laser level thus reducing laser threshold in the system.

Figure 2.3 shows the emission and absorption cross section of ytterbium in germanosilicate glass (Paschotta, R., *et al.*, 1997) as a common host medium based on simple electronic structure of ytterbium ions. There are two peaks of absorption cross-sections that offer great selection for pump wavelengths. The broad absorption cross-section at 910 nm is relatively low and requires strong pumping to obtain high gain. Strong pumping can be applied to obtain almost 97% upper state populations (Paschotta, R., *et al.*, 1997). Amplified spontaneous emission (ASE) can occur with strong pumping at 975nm, thus limiting the maximum gain amplification at longer wavelengths. Nevertheless, at 975nm, the absorption and emission cross-section have

nearly the same magnitude, only 50% of the upper-state populations is achieved and the narrow absorption peak shows great sensitivity at this pump wavelength.

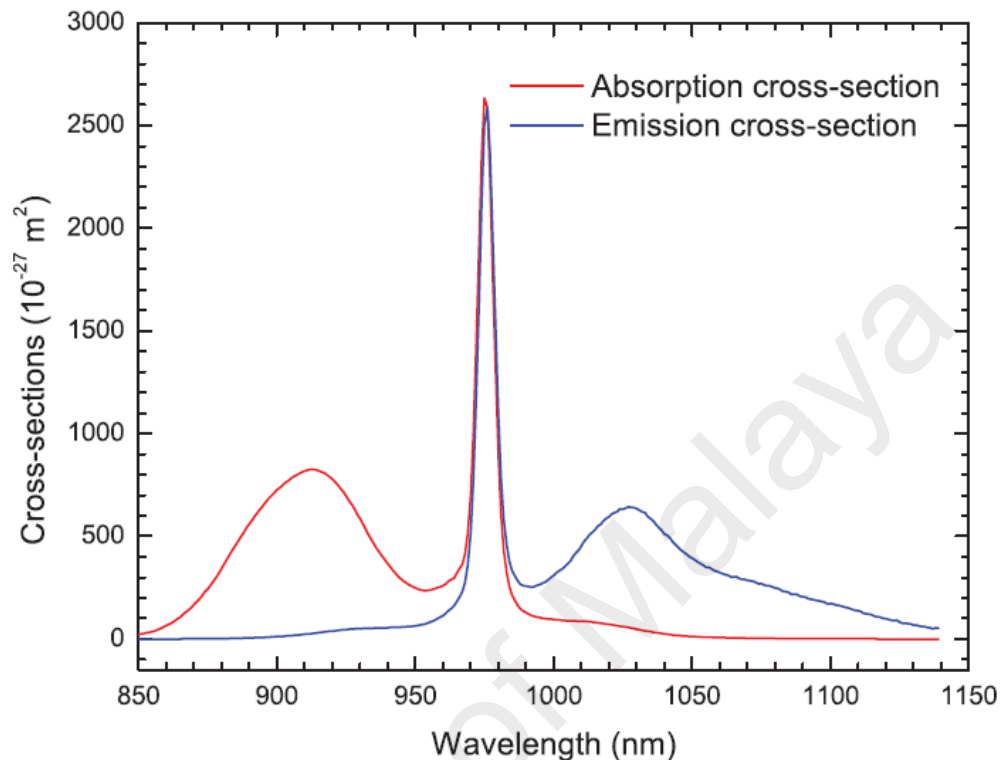


Figure 2.3: The cross-section of absorption and emission of YDF (Rüdiger Paschotta *et al.*, 1997)

Gain can be accomplished at 975nm narrow emission peak or broader wavelength ranging from 1000 nm to 1100nm where the broad amplification is appropriate for ultra-short pulse amplification. At 975nm amplification wavelength, the re-absorption loss in an unpumped fiber is very high because of strong 3-level behavior and the fiber length has to be carefully optimized. Strong lifetime quenching was observed in Yb-doped fibers although it was initially believed that quenching effects should be prevented by low quantum defect (Paschotta, R., *et. al.*, 1997). Although re-absorption loss and ASE are disadvantages of YDF, many other advantages like high power efficiency, low thermal effect and large gain bandwidth made it an attractive choice in ultra-short pulse propagation and high-power application.

2.2 Dual-Wavelength Fiber Laser

Dual-wavelength fiber lasers have gained significant attention in the photonics field because of its potential in generating microwave and terahertz (THz) radiation, topography, optical communication, laser processing, precision spectral analysis, range finding and optical remote sensing, medical instrumentation, and optical clock synchronization. The tapered fiber based Mach-Zehnder Interferometer (MZI) was employed as comb filter in generating DWFL (Harun, S. W., Lim, K. S., Jasim, A. A., & Ahmad, H. 2010), to generate tunable multi-wavelength up to 17 wavelengths (Peng, W., Yan, F., Li, Q., Tan, S., *et al.*, 2013), to record a highly stable DWFL (Ahmad, H., *et al.*, 2016) and was also used as narrow single longitudinal mode fiber using an inline MZI (Ahmad, H., *et al.*, 2014). In this work, we design a dual-tapered Mach-Zehnder Interferometer based on microfiber and side-polished fiber that acts as a wavelength-selective filter to generate dual-wavelength laser.

2.2.1 Mach-Zehnder Interferometer

The Mach-Zehnder interferometer is a particularly simple instrument to exhibit interference by division of amplitude. Firstly, light beam is separated into two sections using a beam splitter and later combined again using a second beam splitter. Based on the relative phase needed by the beam through out both ways, the beam will be reflected by the second beam splitter with an efficiency between 0 and 100%.

The schematic diagram of Mach-Zehnder Interferometer is shown in Figure 2.4. On the upper path from source to detector A, as light goes through the beam splitter's glass, it has π phase shift at first reflection (50%), another π phase shift at second reflection

(100%) and no phase shift at transmission. The phase shift for distance travelled is $2\pi l_1/\lambda$ and the phase shift for traversing the glass substrates is $2\pi t/\lambda$. Therefore, the total phase shift for upper path is:

$$2\pi + 2\pi \left(\frac{l_1+t}{\lambda} \right) \quad (2.2)$$

where l_1 is the total length of light travelling at upper path from source to detector and t is path length of light through the beamsplitter which consider the refractive index of the glass and coating, and actual distance of travelled light passes through at an angle. On the lower path, same on its path to detector A, π phase shift at 100% reflector, and second beamsplitter (50%). A phase shift for distance travelled is $2\pi l_2/\lambda$ and phase shift for passing through the glass is $2\pi t/\lambda$. Therefore, the difference in phase shift between two paths is denoted by the equation below:

$$\delta = 2\pi \left(\frac{l_1-l_2}{\lambda} \right) \quad (2.3)$$

where l_2 is total length of light travelling at lower path from source to detector. Comparing to phase shift difference between two paths from source to detector B, the following equation is derived:

$$\pi + \delta = \pi + 2\pi \left(\frac{l_1-l_2}{\lambda} \right) \quad (2.4)$$

Thus, when $\delta = 0$, constructive and destructive interferences are achieved on the way to detector A and detector B, respectively.

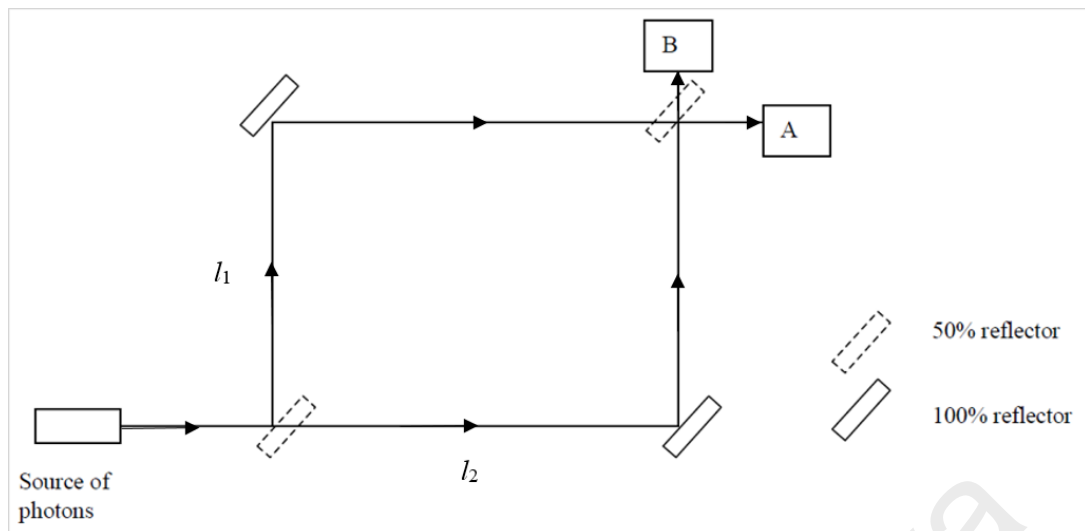


Figure 2.4: The Mach-Zehnder Interferometer diagram (Zetie, K., Adams, S., & Tocknell, R. 2000)

2.2.2 Mechanism of Dual-Tapered Microfiber

Figure 2.5 illustrates the dual-taper fiber MZI, where the propagation of light is deemed to be from left to right. This MZI taper's fabrication uses the heat-and-pull method. This method exploits mass conservation principle by pulling a fiber that had been heated to soften the glass. There are four variations of this techniques, which are flame brushing, micro-heater brushing, drawing tower, and self-modulated taper-drawing. In this work, the flame brushing technique was proposed to fabricate the tapered fiber due to its low development cost. This method uses very small and highly hot flame repeatedly travelling under a portion of optical fiber. This soften-glass optical fiber is then stretched through a permanent strain under applied stress. The flame torch and the optical fiber are attached onto translation stages, which are connected to a computerized system in order to control the taper dimensions and shape, thus ensuring lowest optical transmission loss of the microfiber (Ismaeel, R., Lee, T., Ding, M., Belal, M., & Brambilla, G. 2013).

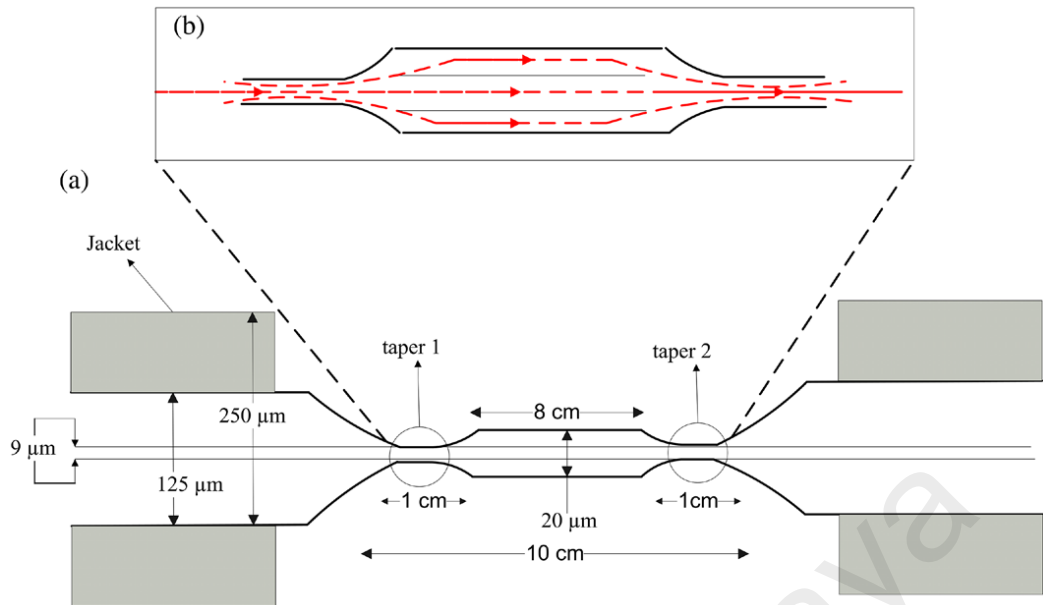


Figure 2.5: The cross-section of dual-tapered microfiber (H Ahmad *et al.*, 2014)

The jacket in the entire tapered region of the fiber has been detached. Two sections, each 1 cm in length, are narrowed down to the taper 1 and taper 2 (core level), where because of huge differences between the air refractive indices and the core, these parts serve as multimode optical fibers. Most of the modes in core–air areas are cladding modes. Single to multimode transitions occur in taper 1 region, where excitation of the cladding modes occurs due to partially coupled core mode in the tapered area . As shown in Figure 2.5 (b), the mid section coming after taper 1 serves as the MZI arms, where the light generates an accumulation of phase shift after propagating into the arms without coupling. The shift φ is derived as (Zhang, Q., Zeng, X., Pang, F., Wang, M., & Wang, T. 2012):

$$\varphi = \frac{2\pi}{\lambda} (n_{eff\ core} - n_{eff\ cladd})L \quad (2.5)$$

where $n_{eff\ core}$ is the effective index of the core and $n_{eff\ cladd}$ is the effective index of the cladding. L is the length of interferometer. Before coupling into the single mode fiber, the arms combine together at taper 2. The differences in the propagation constants lead

to spatial mode beating as a result of the interference between the cladding and the core modes. The strong beating lead to ripple effect on the spectrum as seen in Figure 2.6.

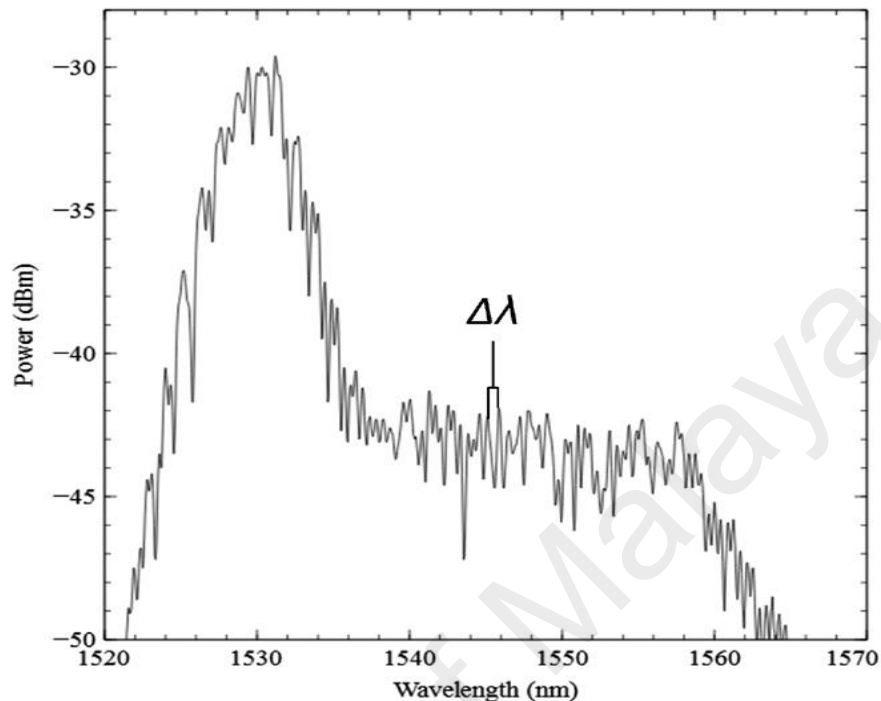


Figure 2.6: Amplification spontaneous emission of dual-tapered microfiber
(Ahmad, H., *et al.*, 2014)

To monitor the effects of spatial mode beating on the spectrum and aid optimization of the MZI during fabrication, a broadband light source is injected into the fiber. An OSA (Anritsu MS9780A) is used to monitor these effects, with Figure 2.6 illustrating the spectrum from MZI taper fiber. The broadband spectrum at the MZI taper fiber output, as illustrated in Figure 2.6, which has an average peak-to-peak beating distance is labelled as ' $\Delta\lambda$ ' for future reference purpose. The beating and coupling of the core and cladding modes in MZI tapered fiber yielded the frequency comb structure. Different length and diameter of tapering fiber will further prompt different beating effects. Wavelength difference, $\Delta\lambda$, is obtained through the following equation (Peng, W., *et al.*, 2013):

$$\Delta\lambda = \frac{\lambda^2}{\Delta n_{eff}L} \quad (2.6)$$

where Δn_{eff} is the effective index difference of the core and cladding modes, and L is the length of interferometer.

Beating length can be derived as a function of propagation constant (Poustie, A. J., Harper, P., & Finlayson, N. 1994):

$$L_{\beta} = \frac{2\pi}{\Delta\beta} \quad (2.7)$$

where $\Delta\beta$ is the propagation constant difference between core and cladding modes and L_{β} is the beating length. If the diameter or length of the core-tapered regions decreases, there will be an increase in the propagation constant of the beating modes. The beating length becomes smaller. In conclusion, narrower and sharper peaks will be obtained when a longer tapered area or smaller diameter is used (Villatoro, J., Minkovich, V. P., & Monzón-Hernández, D. 2006). If a MZI fiber taper is built based on the specifications above, a very narrow linewidth can be obtained, which restricts noise and retains stability with minimum power loss.

2.2.3 Mechanism of Side Polished Fiber

A rough explanation on the operation of the device is made based on the weak coupling approach whereby the evanescent coupling of power from the fiber mode to the highest-order mode of the overlay waveguide occurs. The principle of optical fiber filters can be explained using Fresnel's law too. The structure of the filter is as seen in Figure 2.7.

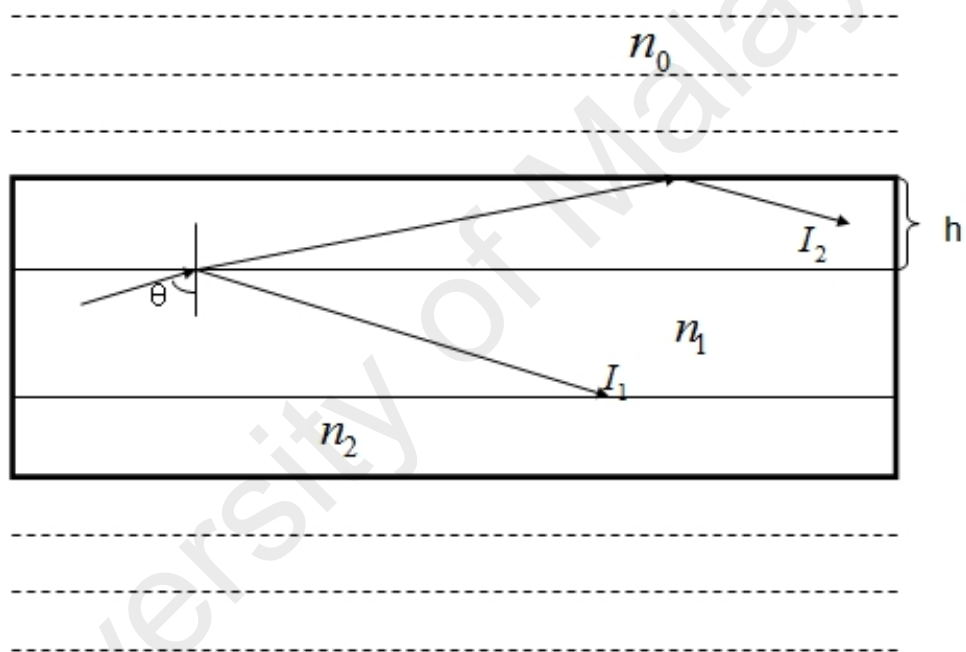


Figure 2.7: The cross-section structure of the side polished fiber (S. X. Zhang, Liu, & Ye, 2014)

With white light as the source of light, the incident light was projected through the fiber end. Incident light dropping below the critical angle of total reflection incident on the interface between the core and the cladding will lead to refraction occurring at both parts, and reflection being produced at the top and bottom of cladding layer. The wavelength, λ , of the incident light to the fiber core and cladding interface is at θ angle,

as depicted in Figure 2.7. Whereas, n_o , is the refractive index of the outside (n_o is less than that of the cladding), h is the thickness of the cladding layer, n_1 is the refractive index of the fiber core, and n_2 is the cladding refractive index.

Cladding layer is where the incident light is directed to through the core. A part of the incident light is reflected at the core-cladding interface in order to generate the first batch of reflected light, I_1 . Second reflected light beam, I_2 , is formed when the other part of the incident light is moving in the cladding reflected at cladding-external medium interface. Interference happens between two beams of reflected light, which is considered as parallel-plate interference light.

Hence, the interference is caused by two modes, which are core and cladding mode (Jiang, L., Yang, J., Wang, S., Li, B., & Wang, M. 2011). The side polished fiber structure can be considered as a Mach-Zehnder Interferometer. The transmission of MZI when the SPF is in the air is shown in Figure 2.8 and can be derived as (Li, L., Xia, L., Xie, Z., & Liu, D. 2012):

$$I(\lambda) = I_{core} + I_{cladd} + 2\sqrt{I_{core} I_{cladd}} \cos \varphi \quad (2.8)$$

Where I_{core} and I_{cladd} are the intensity of light in the core and the cladding mode of the SPF, respectively. The phase shift, φ between core and cladding modes after transmission along the polished area can be represented as:

$$\varphi = 2\pi\Delta n_{eff}L / \lambda \quad (2.9)$$

Where Δn_{eff} is the effective refractive index difference between the core and cladding modes, L is a length of MZI side polished fiber and λ is a propagation light wavelength.

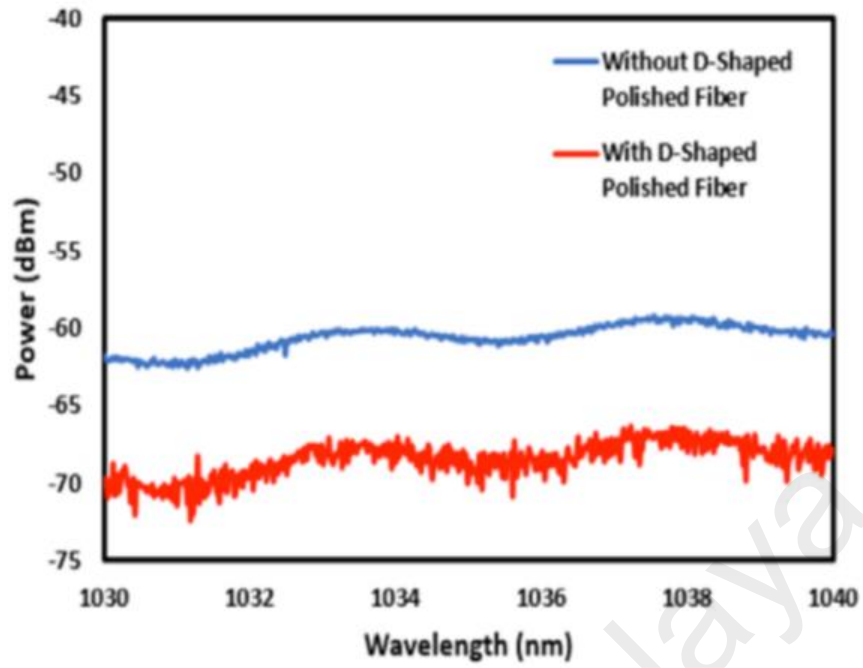


Figure 2.8: Transmission spectrum of side polished fiber (Ahmad. H., Rashid, F. A. A., *et al.*, 2016)

For minimum interference signal, $\varphi = (2m + 1)\pi$, the m^{th} order of wavelength peak attenuation can be derived as:

$$\lambda_m = \frac{2\Delta n_{eff}L}{2m+1} \quad (2.10)$$

The changing of Δn_{eff} or L will shift the attenuation of peak wavelength. Therefore, the free spectral range (FSR) or wavelength spacing between two minima interference can be derived as:

$$\Delta\lambda_m = \frac{4n_{eff}L}{(2m+1)(2m-1)} \approx \frac{\lambda_m^2}{\Delta n_{eff}L} \quad (2.11)$$

From Equation 2.11, the narrower MZI side polished fiber FSR can be obtained by increasing the length of polished area. This parameter give SPF a potential device for a specific application such as polarization-maintaining fiber (Zamarreño, C. R., Zubiate, P., Sagües, M., Matias, I., & Arregui, F. 2013) and intermodal interferometer (Gao, L., Zhu, T., Zeng, J., & Chiang, K. S. 2013).

University of Malaya

2.3 Q-switched Operation

Q-switching can be defined as a simple technique that modulates the intra cavity losses or the quality factor, Q of a laser cavity that is defined as a ratio between the energy stored in the system, W to the energy losses per oscillation cycle, ΔW as follows (Avadhanulu, M. 2001) :

$$Q = 2\pi \frac{\text{Energy stored in the resonator}}{\text{Energy lost in a cycle}} = \frac{W}{\Delta W} \quad (2.12)$$

For a laser, Q is very high due to the gain medium supplying energy to the oscillating modes. There are losses which limit Q to a high value. If L is the length of the cavity, σ is the cross-sectional area of laser beam and v is the volume density of energy, then the energy store in the resonator is as follow:

$$W = \sigma Lv \quad (2.13)$$

There are two equal volume densities of energy fluxes moving in opposite direction and therefore the energy lost during one cycle is given by the following equation:

$$\Delta W = \left(\frac{v}{2}\right) \sigma L (1 - e^{-2f}) \quad (2.14)$$

when $f \ll 1$, we can approximate $e^{-2f} \sim 1 - 2f$, then,

$$\Delta W = v\sigma Lf \quad (2.15)$$

If T is the period of laser radiation and $2L/v$ is the duration of one cycle, then

$$\Delta W = \frac{\sigma Lv}{\left(\frac{1}{2}\right)v\sigma fT} = \frac{2L}{f\lambda} \quad (2.16)$$

But
$$\frac{2L}{\lambda} = m \quad (2.17)$$

Therefore
$$Q = \frac{m}{f} \quad (2.18)$$

We can express the condition necessary for lasing, using $\alpha_o L = f$ and substituting lasing threshold condition into equation 2.18, we obtain $Q = \frac{m}{\alpha_o L}$. Using equation 2.17, we get

$$Q = \frac{2}{\alpha_o \lambda} \quad (2.19)$$

Therefore, the laser threshold is dependant on the reciprocal of the quality factor. The higher the Q-factor, the lower the lasing threshold.

Q-switched pulsed operation can be achieved by eliminating cavity feedback or in other words by keeping the laser within the cavity and oscillating in such a way that the cavity loss can be significantly increased. The active medium is largely built up by pumping process and lasing in the beginning can be hindered by a low Q factor due to the loss per oscillations which brings no positive feedback from the cavity. The lower Q factor leads to higher loss per roundtrip in the resonator and vice versa. This situation provides the build-up process of elevated population inversion and as laser operation cannot occur at such a time, only can be occurred by stimulated emission when the stored energy of the photons in the active medium increases by pumping process. The gain medium must have a long upper-state lifetime to reach a stored energy that is high enough for continuous pumping so that energy is not lost. Ultimately, the saturation energy must not be too low, so that the gain is not excessive, in order to ensure that the premature onset of lasing can be suppress. The loss from initial spontaneous emission or noise level in the laser cavity affects the stored energy in photons that reached some maximum level and this is why the gain is getting saturated. At this point, the cavity loss is abruptly reduced or switched from high Q-factor to low Q-factor, consequently allowing the feedback in the cavity and the process of optical amplification by stimulated emission to begin. Intensity of the laser in the cavity is greatly increased and the rapid oscillation becomes sufficiently powerful that it begins

to saturate or deplete within a very short time. The short pulse laser is known as giant pulse. The peak power in the giant pulse can be three or four orders magnitude more intense than the continuous wave (CW) oscillation level created in the same laser using the same laser pumping rate (Mahad, F. D., Supa'at, M., & Sahmah, A. 2009; Siegman, A. E. 1986).

The Q-switched pulsed performances can be characterized based on repetition rate, average output power, pulse width, and pulse energy. The repetition rate that is measured is in the kHz range and pulse width lie in the μs range. When compared to mode locked pulse operation, the tendency of Q-switched operation to achieve higher pulse energies can be observed and the pulse width are also larger (Popa *et al.*, 2011) as the time taken to restore the extracted energy between two successive pulses is dependent on the lifetime of absorbed photons in the active medium. In mode-locking approach, the single pulse will be generated in time period ranging from picoseconds to femtoseconds by fixing the random phase among longitudinal modes of the laser cavity originating from the interference of cavity modes (Popa *et al.*, 2011). However, mode locking pulse have drawbacks in terms of requiring an appropriate laser cavity configuration and is more complicated in order to achieve a stable operation compared than Q-switching technique due to several factors. For example, the intra cavity components' nonlinear properties and dispersion influence the stability of mode locked operation whereby it has to be well-balanced. Since these parameters affect the laser cavity, the experimental set up needs to be carefully designed. The repetition rate is dependent to the inverse of cavity round-trip time based on the equation below (Xinju, 2010):

$$\Delta f = \frac{c}{nL} \quad (2.20)$$

Where Δf is the repetition rate (Hz), c is the velocity of light in the vacuum (ms^{-1}), L is the length of laser cavity (m), and n is the refractive index.

Q-switching pulse laser operation gained significant interest in industrial applications, especially in long pulse, like instance material processing, medicine (Skorczakowski *et al.*, 2010), long-pulse nonlinear experiments (Laroche, M., *et al.*, 2002), range finding and environmental sensing since it has advantages with regard to cost, easy integration into the laser cavity and efficient operation rate of output pulse energy to input power as compared to mode-locked pulse, that relate to nonlinearity parameters and the dispersion in the cavity in order to achieve a stable operation.

In general, Q-switched pulse lasing can be obtained through an active or a passive manner. The usage of active system normally needs an electro-optic or acousto-optic modulator (Kivisto, S., *et al.*, 2009; Williams, R. J., Jovanovic, N., Marshall, G. D., & Withford, M. J. 2010; Zhao, H. M., *et al.*, 2007) which could turn out to be complex. This disadvantage could be eliminated through the use of a passive modulator that is also known as saturable absorber (SA). Therefore, in this study, SA is employed to generate passively Q-switched in ring cavity set up.

2.3.1 Saturable Absorber

Saturable absorber is defined as a device or an optical instrument with optical losses which declines at high optical intensities. Therefore, it permits the generation of passively Q-switched pulses. This situation can occur in different mediums such as dyes, glasses, crystals doped with ions, semiconductors, carbon nanotubes and graphene (Siegman, A. E. 1986; Sun, Z., Hasan, T., & Ferrari, A. C. 2012).

2.3.2 Mechanism of Saturable Absorber

In this section, the propagation of light through the saturable absorber is discussed. The mechanism of saturable absorber in a laser cavity is shown in Figure 2.9. Electron carriers are excited to the conduction band from the valence band whenever it is excited by photon with sufficient energy and at this point, the saturable absorber absorbs the light. When there is strong excitation, the absorption becomes saturated due to the depletion of possible final states of the pump transition. In general, pulse formation is favored as an intensity increase passes through the absorber. Incident light at low intensities is absorbed and excites carrier to the conduction band. When the incident light intensity increases, the conduction band becomes saturated and no more vacant states are available for carriers in the valence band to excite, consequently making the absorption lower.

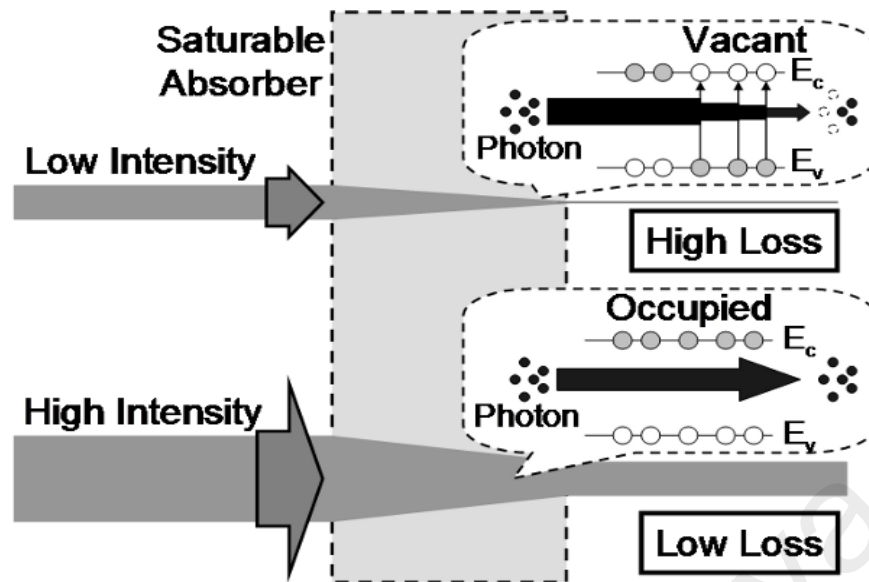


Figure 2.9: Mechanism of saturable absorber (Kashiwagi & Yamashita, 2010)

In order to investigate the proper saturable absorber in generating Q-switched pulse operations, several factors to attain good performance of output pulse laser were highlighted. ((Ando, Y., Zhao, X., Shimoyama, H., Sakai, G., & Kaneto, K. 1999) and (Popa *et al.*, 2010)) proposed that there are parameters for saturable absorber that should be highlighted, like linear absorption, total non-saturated absorption of the saturable absorber must be relatively high to achieve a high pulse energy and short pulse duration. Besides that, the saturation fluence and non-saturable losses should be low to minimize power losses. Meanwhile, the recovery time should be ultrafast, in picoseconds, and the damage threshold value should be high so that the saturable absorber is compatible within the compact fiber laser system(Cho, W. B., *et al.*, 2011; Xing, G. H., Guo, H. C., Zhang, X. H., Sum, T. C., & Huan, C. H. A. 2010). Basically, the saturable absorber reflection or transmission depends on the intensity of light where the light with low intensity will be absorbed by the material and the light with high intensity will be released depending on the material recovery time.

As a SA is placed in a laser cavity as shown in Figure 2.10, the profile of gain medium's amplified spontaneous emission (ASE) noise is formed to be a pulse train. In each round trip, light passes through the SA as high intensity noise with low loss, and low intensity noise with high loss, resulting in high intensity difference. Eventually, laser begins to oscillate in pulsed state.

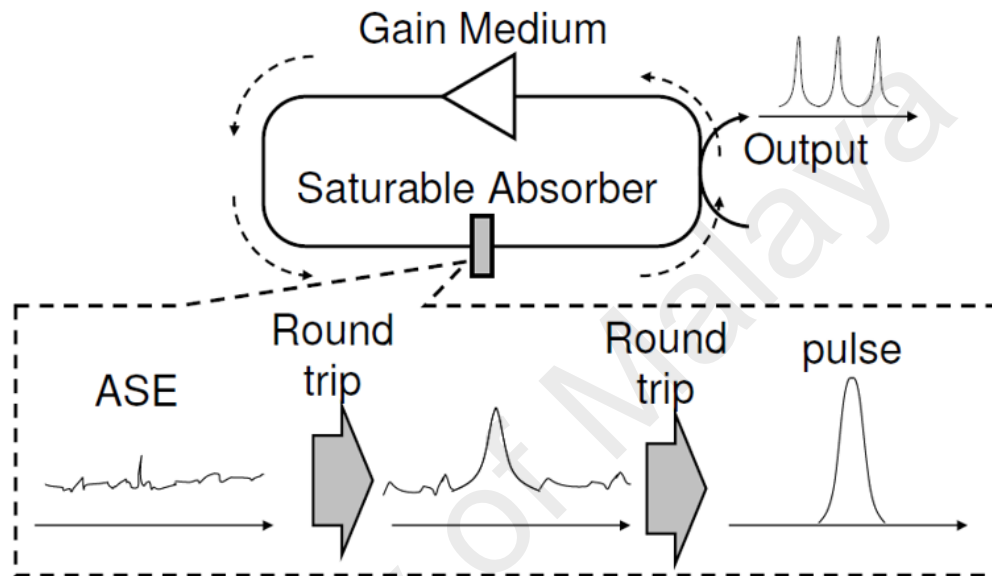


Figure 2.10: Suppression of noise in cavity ring via saturable absorber

(Kashiwagi, K., & Yamashita, S. 2010)

2.3.3 Molybdenum Diselenide (MoSe₂)

Recently, transition metal dichalcogenides (TMD) based optical materials such as molybdenum diselenide (MoSe₂) has been gaining interest among researchers. A chalcogenide is a chemical mixture of one chalcogen ion and electropositive element. In this case, a layer consists of single hexagonal plane transition metal (M), which is molybdenum (Mo) atoms, covalently bonded between two hexagonal planes of

chalcogen (X) atom, which is selenium (Se) as shown in Figure 2.11. The layers are in turn bounded by van der Waals forces (Wilson & Yoffe, 1969). MoSe₂ from semiconducting TMDs has great potentials in photonic and optoelectronic application due to its characteristics on few layers properties which are dependant on the layer quantities in material. The behavior of MoSe₂ is observed and found to display a crossover from an indirect 1.1 eV (1128 nm) bandgap to a direct 1.55 eV (800 nm) bandgap (Tongay *et al.*, 2012), whereby dimensionality reduces due to the emergence of strong excitonic effects (Woodward, R. I., & Kelleher, E. J. 2015).

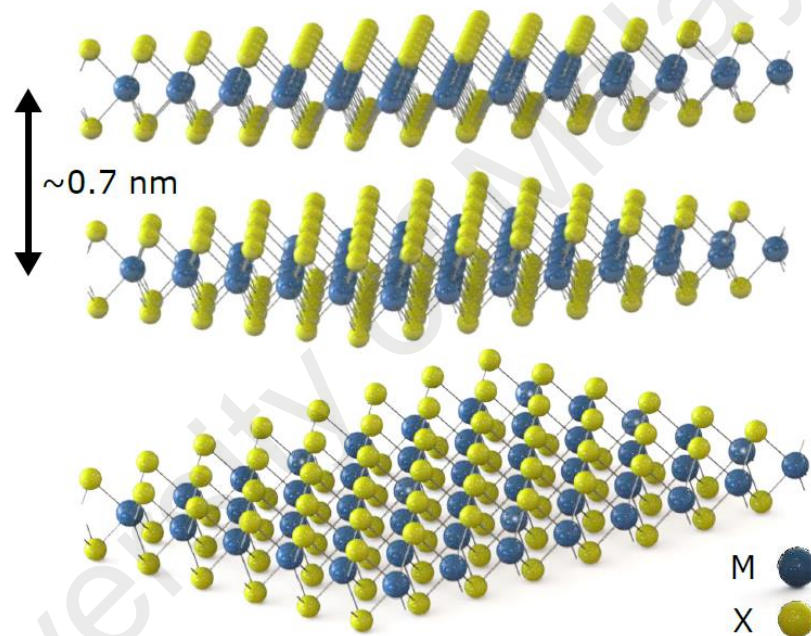


Figure 2.11: TMD structure with M and X atom (Wilson & Yoffe, 1969)

An electron leaving a hole in the valence band into conduction band is called photo-excitation. The weak interaction of electron-hole due to separation renders it as a free carrier. Nevertheless, the electrons' proximity can lead to the creation of attractive Coulombic interaction thus resulting in a bound-state quasi particle that is referred as an exciton (Peter & Cardona, 2010). As a result, exciton occupies an energy level that lies under the conduction band as shown in Figure 2.12.

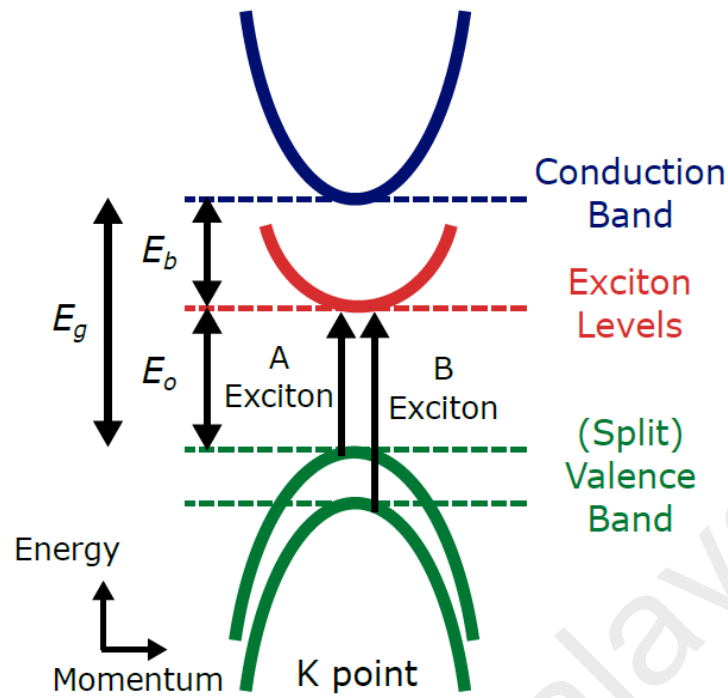


Figure 2.12: Energy structure for TMD (Wilson & Yoffe, 1969)

Several reports identified MoSe_2 as a promising material for thermoelectric, photodetector and pulse-laser applications (Kumar, S., & Schwingenschlogl, U., 2015; Lu, X., *et al.*, 2014; Xia, J. *et al.*, 2014) because of its amazing optoelectronic properties like high optical nonlinearity, strong photoluminescence and ultrafast dynamic carriers for mono and few-layers form (Woodward, R. I., *et al.*, 2015).

2.3.4 Black Phosphorus (BP)

Black Phosphorus (BP) is another 2D material with most stable allotrope of phosphorus due to its orthorhombic crystal structure as shown in Figure 2.13 with its unique properties like highly anisotropic electric conductance and strain-controlled anisotropic electric mobility (Churchill, H. O., & Jarillo-Herrero, P. 2014; Koenig, S. P., Doganov, R. A., Schmidt, H., Neto, A. C., & Oezylmaz, B. 2014; Xia, F., Wang, H.,

& Jia, Y. 2014). A stable and linked ring structure of BP is formed by a phosphorus atom which is linked to three adjacent phosphorus atoms where each ring has six phosphorus atoms.

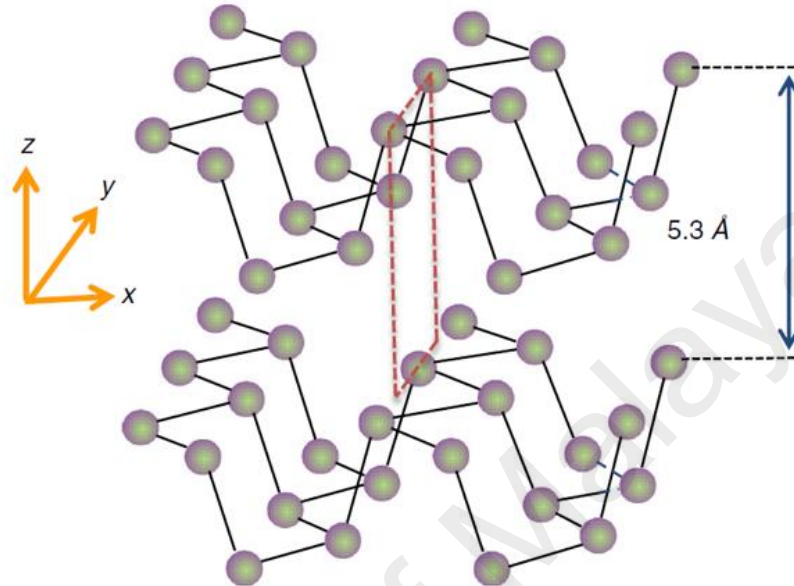


Figure 2.13: Black phosphorus structure with two adjacent puckered sheets linked by phosphorus atom. (F. Xia *et al.*, 2014)

The schematic diagram of excitation process on BP for linear and non linear light absorption is shown in Figure 2.14. An incident light with photon energy, $E = h\nu$ is absorbed and electrons from valence band (red) are excited to conduction band (yellow) as depicted in Figure 2.14(a). Hot electrons rapidly thermalize to create hot Fermi-Direct distribution after the photo-excitation. At the same time, electron-hole pairs block inter-band transition partially at the valence band. Thus, optical absorbance decreases. Subsequently, intra-band scattering cools down the thermalized carrier and resulting in electron-hole recombination domination as shown in Figure 2.14(b) until the relaxation of the equilibrium electron and hole distribution. These processes are referred to as linear transition with weak excitation. On the other hand, Figure 2.14(c) shows the population of photo-generated carriers that rises notably by strong excitation, causing

half of the photon energy is filled thus hindering further absorption as a result of Pauli blocking process which is impossible for two electrons filling at the same state.

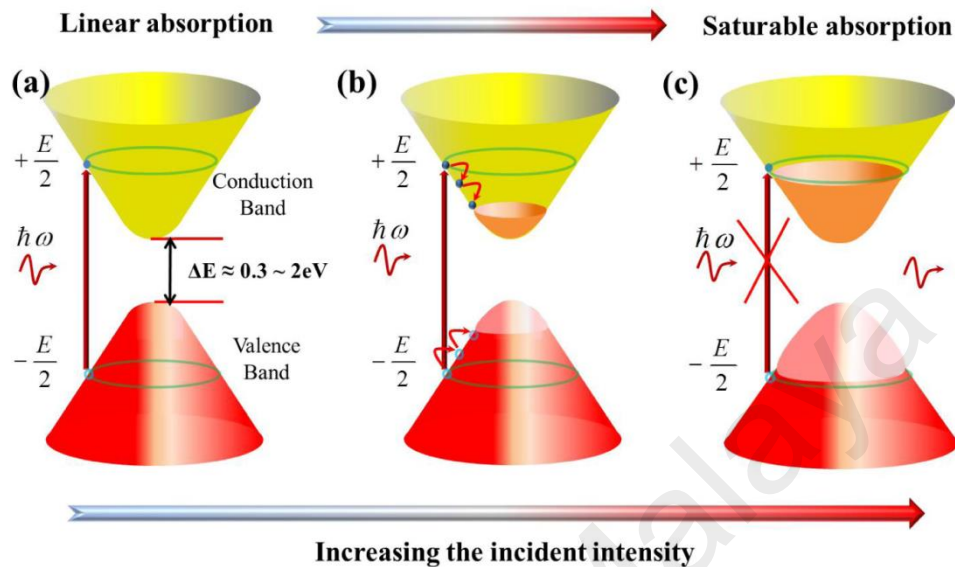


Figure 2.14: Schematic diagram of saturable absorption of multi-layers BP (Lu, S., *et al.*, 2015)

BP has a layer-dependent direct band-gap which increases as layers decreases from 0.3 eV in bulk state to 2 eV in monolayer BP (Churchill, H. O., & Jarillo-Herrero, P. 2014; Xia, F., *et al.*, 2014). BP can retain the direction of electron transition at different thickness which can absorb more photons and allow large modulation depth in SA. The narrow gap of multilayer BP renders it a suitable saturable absorber as compared to graphene with zero band-gap and TMD materials with large band-gap (Koenig, S. P., *et al.*, 2014). The BP saturable absorber was first identified at the wavelength of 1.5 micron and 2 micron region by BP particles deposited on side-polished fiber optic while sticking onto the scotch tape (Jiang, T., Yin, K., Zheng, X., Yu, H., & Cheng, X. A. 2015). Besides that, there are various techniques using BP as saturable absorber such as deposited around the microfiber (Luo, Z. C., *et al.*, 2015), mechanical exfoliation technique (Chen, Y., *et al.*, 2015) and BP gold-film mirror (Kong, L., *et al.*, 2015) which is the only available Q-switched reported in the one micron region.

2.3.5 Titanium Dioxide (TiO₂)

TiO₂ is a semiconductor which is normally utilized as a pigment in paints, ointments and even toothpastes (Braun, J. H., Baidins, A., & Marganski, R. E. 1992). Moreover, TiO₂ is also used as photocatalysis (titanium dioxide photocatalysis); aiding in breaking down organic compounds when illuminated by sunlight, killing bacteria and cancer cells. There are four major crystal structures for TiO₂ which are stable rutile, metastable anatase, brookite and TiO₂ (B) (Yin, Z. F., Wu, L., Yang, H. G., & Su, Y. H. 2013). The rutile and anatase structures are studied extensively and made of titanium atom with six oxygen atoms surrounding it in a somewhat distorted octahedral configuration as shown in Figure 2.15. Rutile structure is orthorhombic structure with slight distortion where the cell is stretched beyond a cubic shape. However, the distortion of cubic lattice is more notable in the anatase structure, leading to its symmetry being lower than that of the orthorhombic.

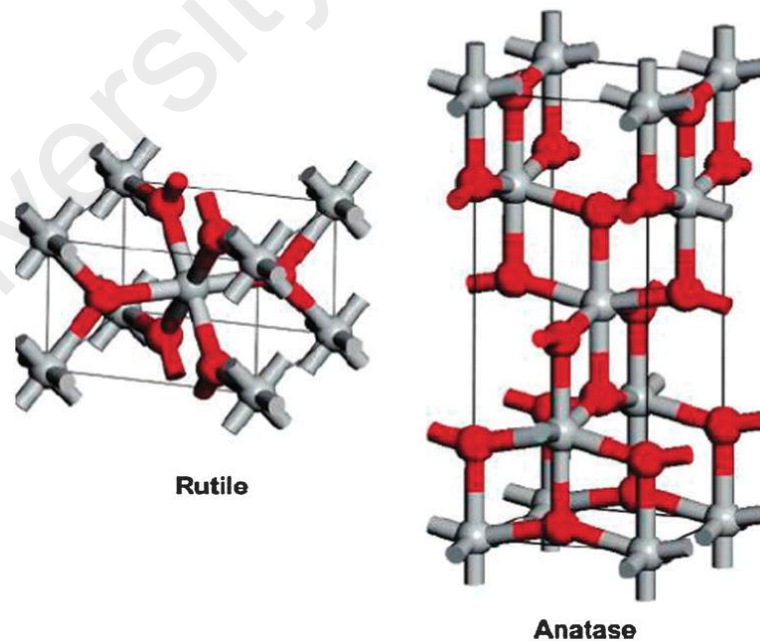


Figure 2.15: Bulk crystal structure of rutile and anatase with titanium atom in grey and oxygen atom in red (Thompson, T. L., & Yates, J. T. 2006).

When selecting materials for saturable absorber, the material needs to have several requirements. The material must be able to absorb at the intended operating wavelength, has nonlinear optical absorption and ultrafast recovery time. After an open-aperture Z-scan was performed on anatase and rutile TiO₂, it was concluded that an anatase TiO₂ exhibits significant nonlinear optical response and possess saturable absorption characteristic (Iliopoulos et al., 2009). When being tested using femtosecond time-resolved pump-probe technique, the recovery time is found to be 1.5 ps at room temperature, suggesting a strong potential of this material in optical switching devices (Elim, H., Ji, W., Yuwono, A., Xue, J., & Wang, J. 2003). Despite having a bandgap of ~3.2 eV (~387 nm), TiO₂ SA is found to be able to absorb at visible (Kuznetsov, V. N., & Serpone, N. 2006) and infrared spectra (Luxon & Summitt, 1969), thus exhibiting the potentials of TiO₂-based saturable absorber for generating pulse output.

2.3.6 Zinc Oxide (ZnO)

Zinc oxide (ZnO) is a metal oxide semiconductor from the II-VI group and is being researched based on their optical and electrical properties. There are two main crystal structure of ZnO which are wurtzite and zincblende. The most common and stable structure at ambient conditions is the wurtzite crystal structure. Figure 2.16 shows the wurtzite crystal structure of ZnO which has a hexagonal structure with lattice parameters of $a = 0.3296$ and $c = 0.52065$ nm. Furthermore, the structure consists of a number of alternating planes made of tetrahedrally coordinated O²⁻ and Zn²⁺ ions, stacked alternately through out the c -axis, resulting in non-central symmetric structure.

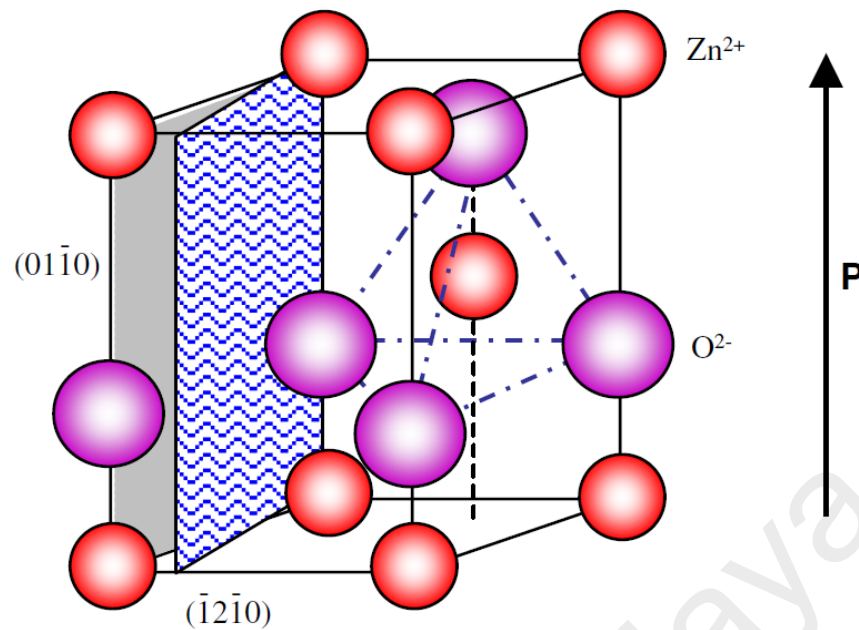


Figure 2.16: Wurtzite zinc oxide hexagonal structures. (Wang, Z. L. 2004)

The main interest on this SA was due to its 3.4 eV direct band gap (Jagadish, C., & Pearton, S. J. 2011; Mang, A., & Reimann, K., 1995), and a huge energy of 60 meV (Bagnall, D., *et al.*, 1997; Jagadish, C., & Pearton, S. J. 2011; Reynolds, D. C., Look, D. C., & Jogai, B. 1996) at room temperature for its electrical properties. Their optical properties are useful for non-linear optical devices (Larciprete, M., *et al.*, 2006) where ZnO thin films show second and third order nonlinear optical properties. This semiconductor has several remarkable properties which lead to broad application such as amenability to wet chemical etching adds flexibility in designing, processing and integrating optoelectronics devices, radiation hardness for applications in space or at high altitude and low power threshold for optical pumping (Janotti, A., & Van de Walle, C. G. 2009). These characteristics are suitable for emerging applications in electronics like light-emitting diodes and thin-film transistors, energy-saving or heat-protecting windows, gas sensor, ultra violet laser diode, nanotechnology-based devices and transparent electrodes in liquid crystal displays (Janotti, A., & Van de Walle, C. G. 2009). Therefore, we employed ZnO as a SA in this experiment.

CHAPTER 3: DESIGN, FABRICATION AND CHARACTERIZATION

3.1 Introduction

A simple fiber laser cavity is first designed in order to generate laser which operates in continuous wave. The single wavelength laser generated from a simple fiber laser design will be employed to generate dual-wavelength laser by incorporating wavelength selective filter in the cavity. The fiber laser design and measurements, fabrication and characterization of wavelength selective filter, and saturable absorber are presented in this section.

3.2 Gain Medium

A ytterbium-doped fiber (YDF) model DF100 Fibercore was used in this work with the specifications of fibers as summarized in Table 3.1. The absorption and emission cross-sections are plotted in Figure 3.1

Table 3.1: Ytterbium-doped fiber DF1100 Fibercore specification

Parameter	DF1100 Fibercore
Absorption at 977nm	1300 dB/m
Attenuation at 1200nm	5.7dB/km
Core concentricity	0.19 microns
Cut-off wavelength	810nm
Fiber diameter	124.8 microns
Mode field diameter	5.1 microns
Numerical aperture	0.17
Operating wavelength	1085 nm

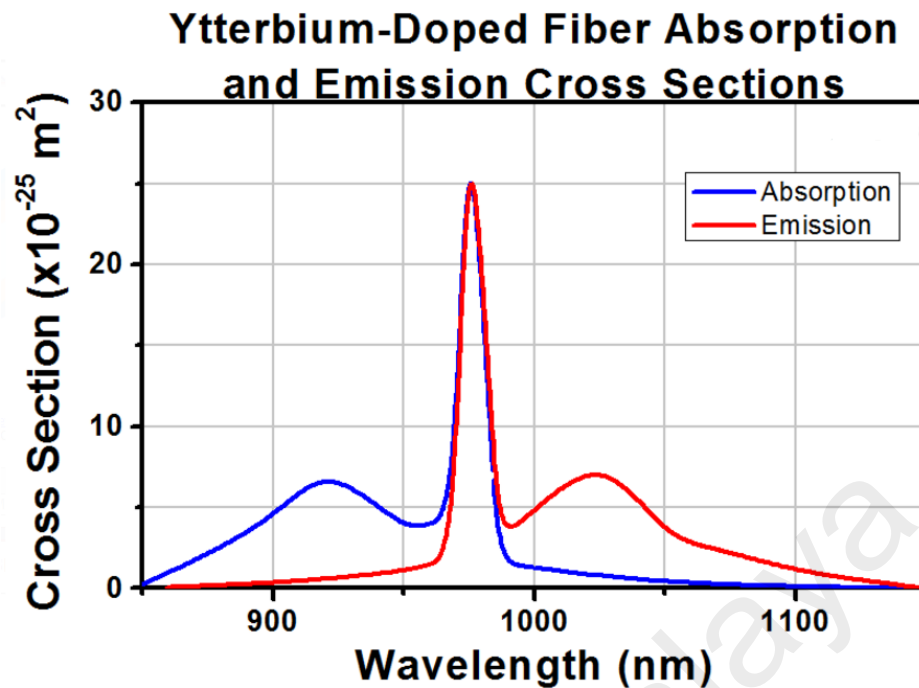


Figure 3.1: Absorption and emission of YDF model DF1100 Fibercore (*SM Ytterbium Doped Fiber, 2013*)

3.3 Fiber Laser Design

A ytterbium-doped fiber laser (YDFL) is produced based on the design of ring cavity setup. A simple ring cavity fiber laser consists of pumping source, wavelength division multiplexer (WDM), active gain medium, isolator and optical coupler (OC), and are typically formed as a loop with unidirectional propagation of light. A ring cavity of YDFL is shown in Figure 3.2.

In this work, we used fiber laser ring cavity design as it has several advantages such as minimum power fluctuation, minimal amplified spontaneous emission (ASE) background and higher side mode suppression ratio (SMSR) which makes it an applicable design for dual-wavelength fiber laser (Ahmad, H., Latif, A. A., Zulkifli, M. Z., Awang, N. A., & Harun, S. W. 2012).

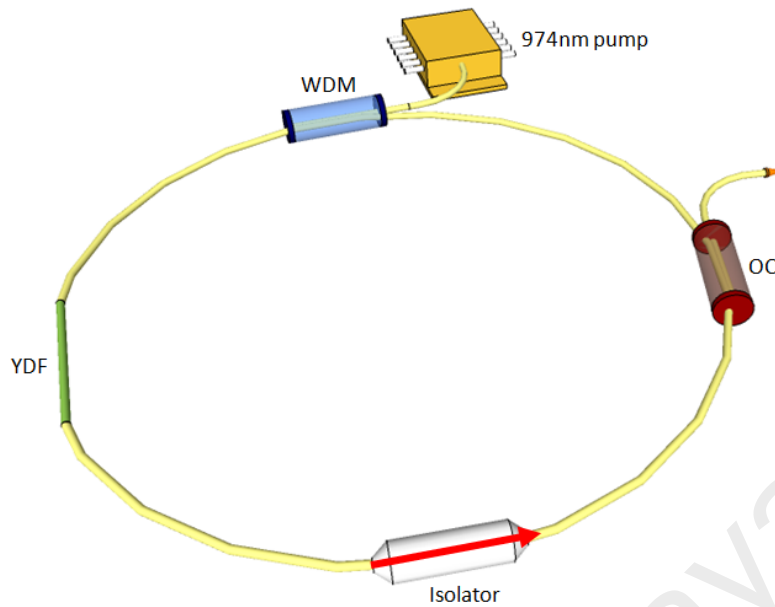


Figure 3.2: Laser design of a simple ytterbium-doped fiber laser ring cavity.

A laser diode (LD) model Oclaro is employed as a pumping source. The laser diode can supply continuous wave laser output at maximum output power of 600mW at room temperature by varying the driving current. However, for this work, the output power is pumped up to 300mW due to limitation on fiber optic component used in ring cavity. The laser diode has a central wavelength of 974nm and spectral width of 0.2 nm. The LD is pumped to 70 cm long YDF model DF1100 Fibercore through wavelength division multiplexing (WDM) as LD is connected to 980 port of WDM while YDF is spliced to common port of WDM. Then, the ytterbium active fiber output is attached to an isolator to prevent back reflection of light and then is channeled to input port of 90:10 optical coupler. The 90% port of OC is looped back to 1060 port of WDM to form a ring cavity design whereas the 10% port is used to characterize the laser output generated using optical spectrum analyzer (OSA) model AQ6373 Yokogawa.

The ASE spectrum of the cavity is illustrated in Figure 3.3 before it reaches the lasing threshold of 42 mW. Figure 3.4 shows the single lasing spectrum of YDFL in a ring cavity has a center wavelength of 1064 nm. The fiber laser's lasing wavelength can be shifted within gain spectrum depending on the length of YDF, pump power and

optical coupler as a feedback employed in the configuration. In order to generate dual-wavelength fiber laser, the wavelength selective filter must be employed in the ring cavity. In this work, we use dual-tapered microfiber and side polished fiber as wavelength selective filter. The fabrication and characterization of these wavelength selective filters are discussed in this section.

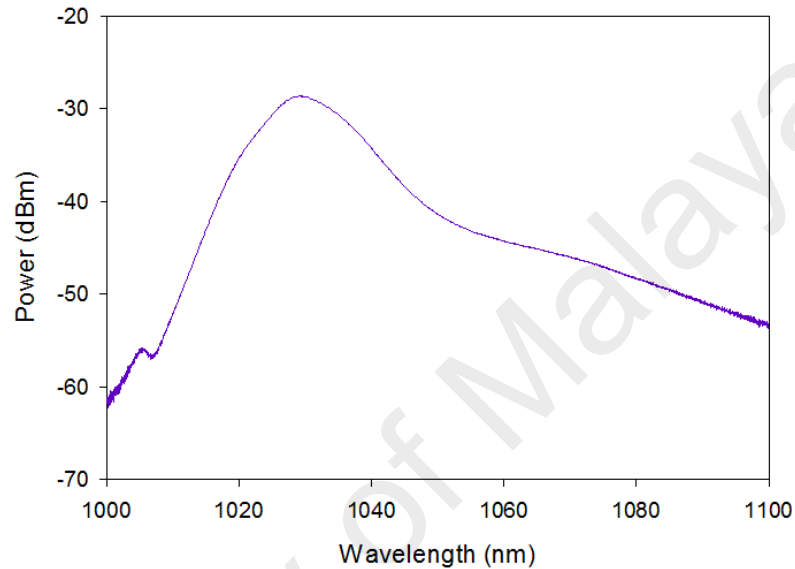


Figure 3.3: Amplified spontaneous emission spectrum of YDF.

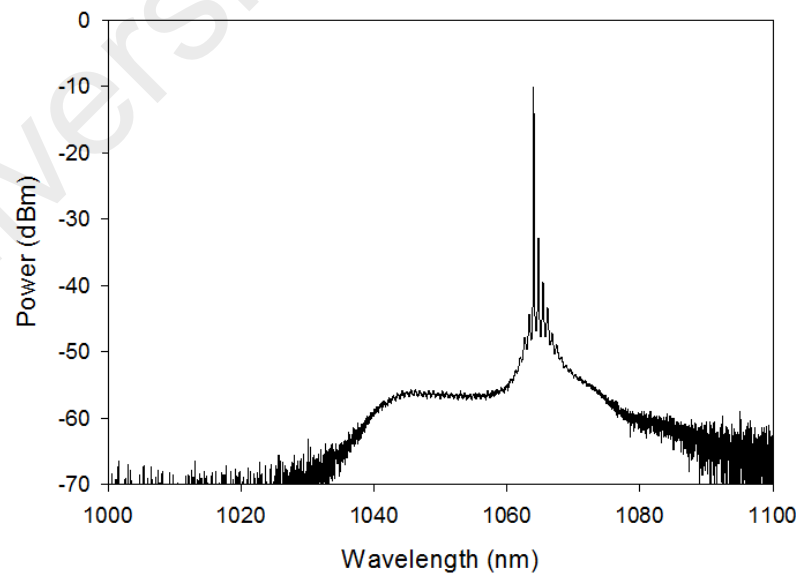


Figure 3.4: Lasing spectrum of YDFL

3.4 Dual-Tapered Microfiber MZI

In this section, the fabrication of wavelength selective filter that is dual-tapered microfiber is discussed with two waist diameter of 2 μm and 10 μm . These microfibers are used in this work to generate DWFL. The dual-tapered microfiber with 2 μm waist diameter is fabricated by using in-house tapered machine whereas 10 μm waist diameter is fabricated by using commercial tapered machine.

3.4.1 In House Tapered Machine

Initially, single mode fiber is tapered in the desired region by using in-house tapered machine as shown in Figure 3.5. A 70 mm in-house fabricated microfiber has a waist diameter of 2 μm as illustrated in Figure 3.6. This microfiber is used as a multimodal interference medium in order to form a narrowband filter. The fabrication of microfiber employs a single mode fiber with a standard size of 9/125 μm core/cladding diameter operating through the flame brushing technique (Brambilla, G., Jung, Y., & Renna, F. 2010), where heating and stretching were applied onto the optical fiber. The structure of the microfiber enables it to support higher order modes.

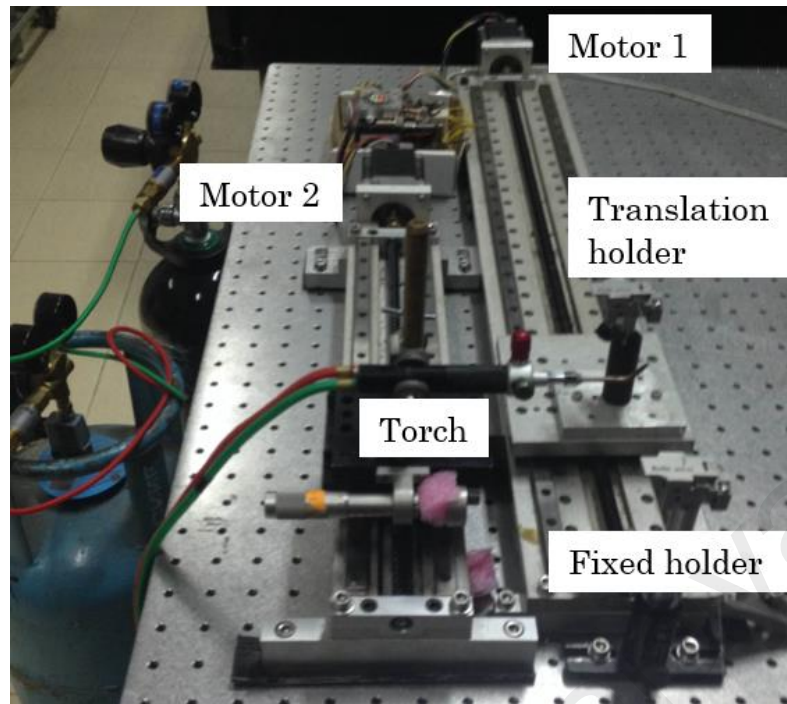


Figure 3.5: In house tapered machine system

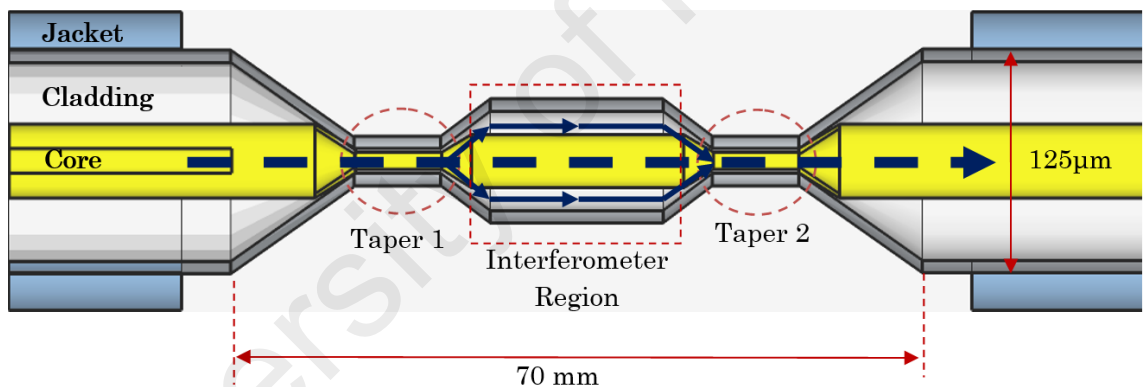


Figure 3.6: The cross-section of dual-tapered microfiber

These microfiber parameters contribute to stability, generate narrow linewidth and suppress mode competition due to wavelength-dependent loss. The interference spectrum is shown in Figure 3.7, where the ASE depicted in purple represents the spectrum of ASE directly from the YDFA output, while the red line depicts the spectrum of ASE following the microfiber. The interference peak is observed and depicted by the red line in Figure 3.7 (from the inset), which implies narrow linewidth upon closure of the cavity ring.

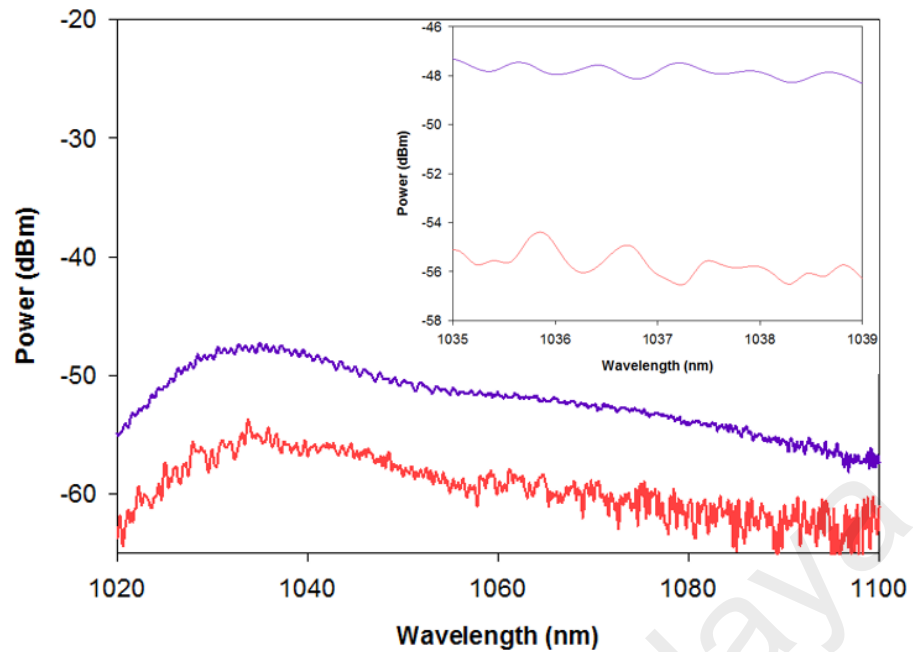


Figure 3.7: Amplified spontaneous emission spectrum with microfiber (red) and without microfiber (purple).

The microfiber has a diameter of 2 μm , rendering it very fragile and sensitive to external environment and foreign matter, like dust, which can induce mode hopping, instability and loss of power. Consequently, the microfiber was wrapped up similar to Jasim, A. A., *et al.*, (2012)'s study, to isolate it from the external environment while preserving its properties as shown in Figure 3.8.



Figure 3.8: Packaging microfiber to preserve its properties

3.4.2 Commercial Tapered Machine

The commercial machine named Vytran GPX-3000 series is used to fabricate dual-tapered microfiber. This machine has a graphite filament that is able to produce controllable heat, tuned from room temperature up to maximum temperature of 3000 °C. The desired specification of taper profile can be set by using this machine and in this case, the taper waist diameter is set at 10 μ m, the taper transition length is set to 2 mm and the taper waist length is 10 mm as shown in Figure 3.9.

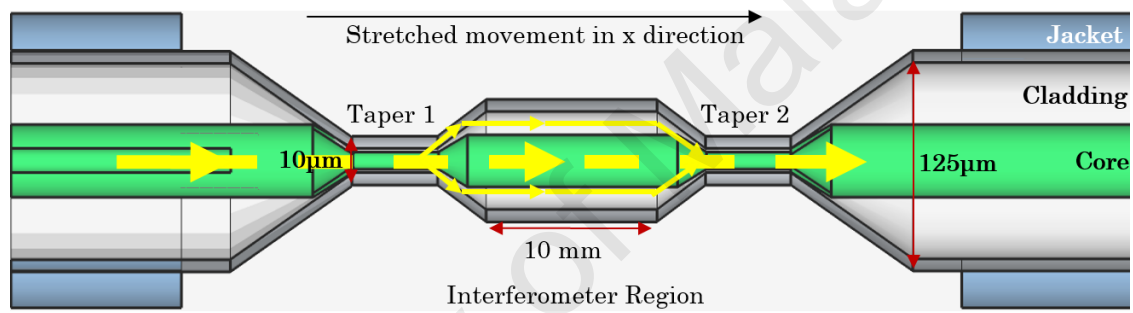


Figure 3.9: The cross section of microfiber with waist diameter of 10 μ m

The heat-and-pull technique was used during the fabrication process of tapered fiber. Initially, the jacket was first detached at the desired tapered area. Two areas were tapered to the core level and denoted as taper 1 and taper 2 with each length being 10 mm. Both tapered region have the function of multimode fiber due to huge difference in refractive index between core fiber and air (Ahmad, H., *et al.*, 2014).

The transmission spectrum of dual-tapered microfiber with an unpolarized ASE source pumped at 175.4 mW is shown in Figure 3.10 which clearly observe the interference spectrum and results in the narrow lasing when the ring cavity is formed.

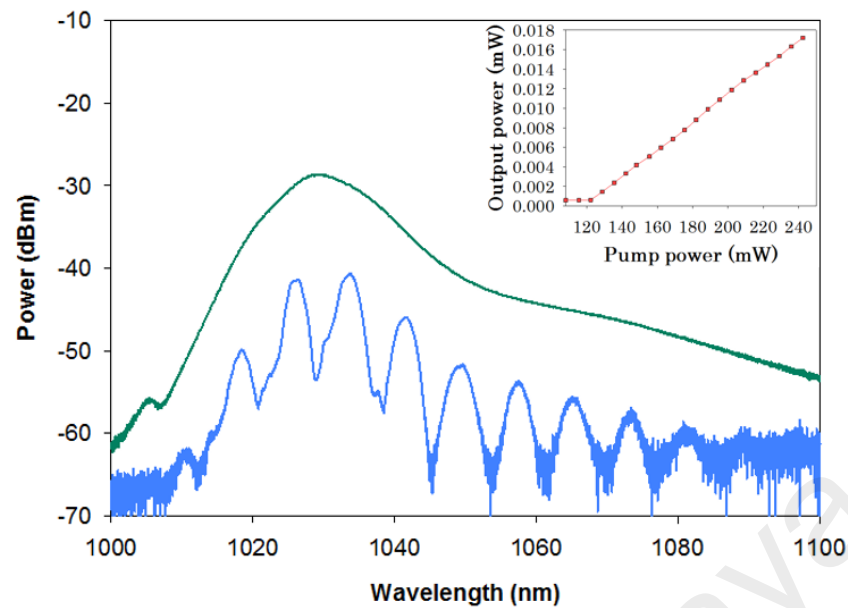


Figure 3.10: The amplified spontaneous emission of YDF with microfiber (blue) and without microfiber (green).

3.5 Side Polished Fiber

Another wavelength selective filter used in the experiment is side polished fiber (SPF). The SPF or also known as D-shaped fiber (Phoenix Photonics Side Polished Optical Fiber: Model Number SPF-S-SM) was acquired from Phoenix Photonics Ltd. The SPF was fabricated from a standard SMF (SMF-28) with a core/cladding diameter of 8.2/125 μm . Figure 3.11 illustrates the sideview of our SPF. It has a polished area with a length of 17 mm and an insertion loss of ~ 3 dB. By removing a section of the cladding, the side polishing fiber enables access to the evanescent field of the wave propagating in the standard single mode optical fiber. The ASE transmission through side polished fiber is shown in Figure 3.12

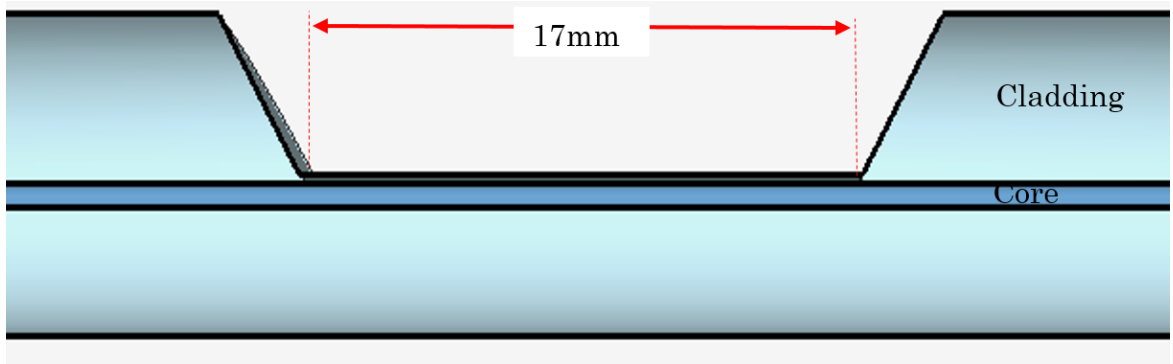


Figure 3.11: The side polished fiber diagram

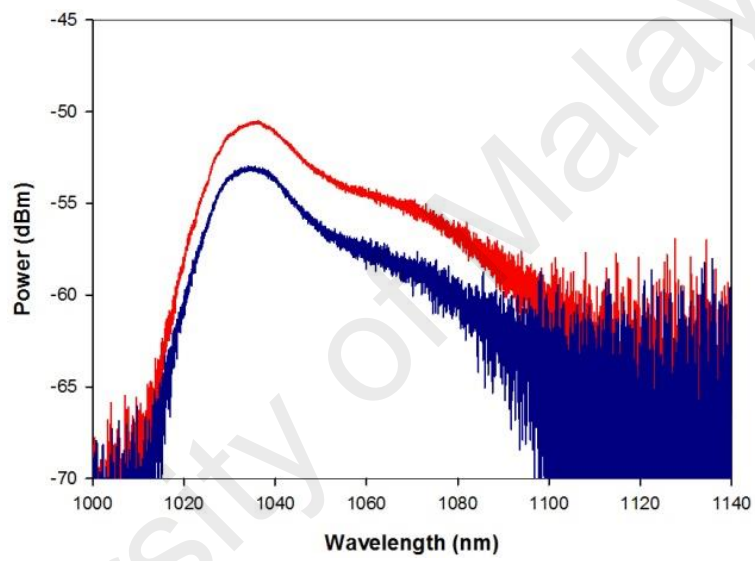


Figure 3.12: The ASE transmission through side polished fiber (blue) and without it (red)

3.6 Linewidth Characterization

Linewidth is commonly defined in terms of full width at half maximum (FWHM) of the optical power spectrum. In this section, heterodyne measurement technique using a local oscillator method had been used to characterize linewidth of single longitudinal mode laser. The main component required for this operation is a stable and narrow linewidth reference laser.

The experimental setup of optical heterodyne using a local oscillator method is shown in Figure 3.13. Local oscillator (LO) or reference laser is tuned appropriately and is fixed during the experiment process. Light source from LO is attached to polarization controller (PC) to align the polarization state of LO. Both the laser signal and LO are combined by 50:50 optical coupler and then divided into two portions. One portion is channeled into photodetector which then converts the optical interference to electrical signal and which will then be analyzed using Radio Frequency Spectrum Analyzer (RFSA). Another portion is channeled into Optical Spectrum Analyzer (OSA). The LO frequency is tuned just lower than the average frequency of signal laser that will create a heterodyne beat tone between LO and each frequency in signal spectrum.

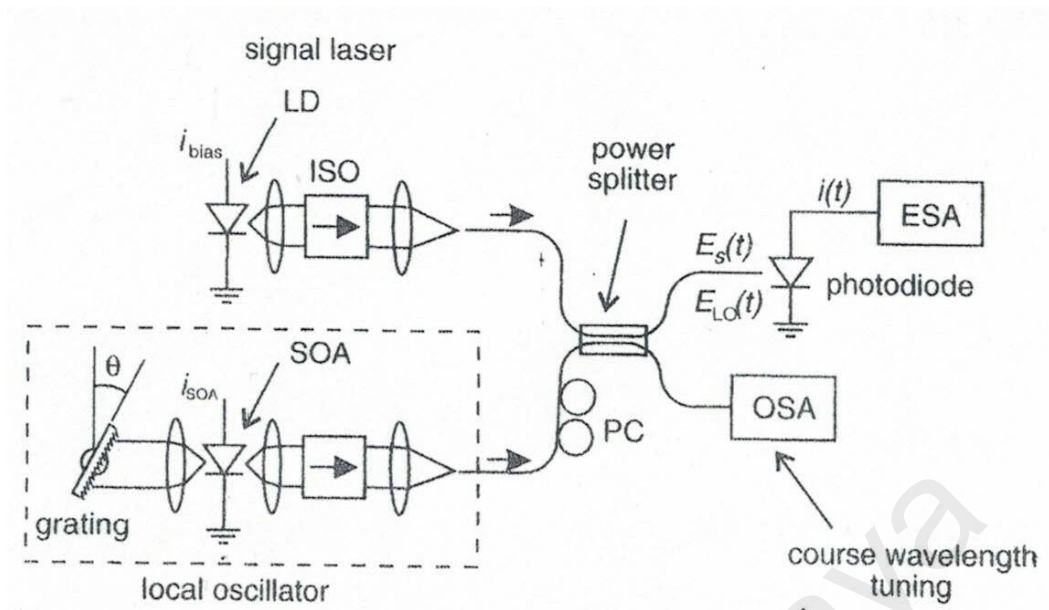


Figure 3.13: Optical heterodyne setup for linewidth measurement (Derickson, 1998)

As a common case of Lorentzian shaped spectrum, the relation between the measured full width at specific power and the FWHM linewidth is shown in Table 3.2.

Table 3.2: The Relations of Heterodyne Technique Linewidth (Derickson, 1998)

Measured Full-Width Point	Corresponding Width
- 3dB	$\Delta\nu$
- 10dB	$\sqrt{9} \Delta\nu$
- 20dB	$\sqrt{99} \Delta\nu$
- 30dB	$\sqrt{999} \Delta\nu$

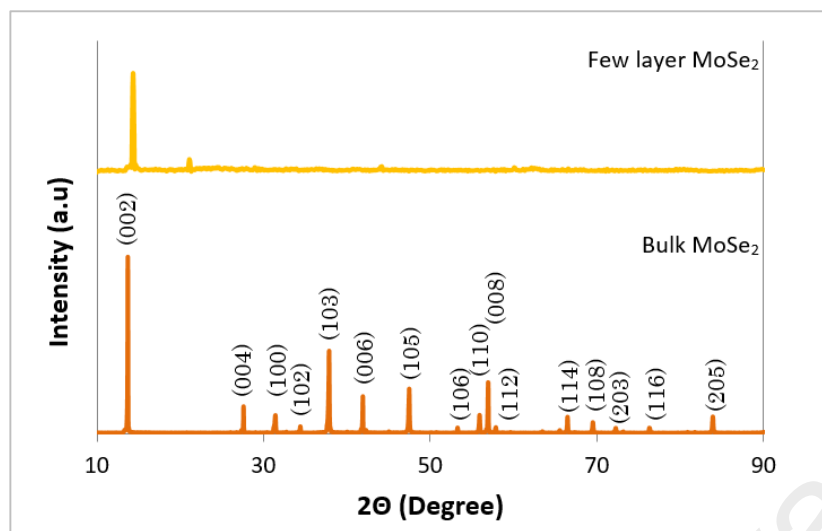
3.7 Preparation of Saturable Absorber

Saturable absorber is used in this work to generate Q-switched pulse. There are four type of saturable absorber employed in ring cavity, which are Molybdenum diselenide (MoSe_2), black phosphorus (BP), Titanium dioxide (TiO_2) and Zinc oxide (ZnO). In this section, the fabrication of saturable absorber and its characterization are also presented.

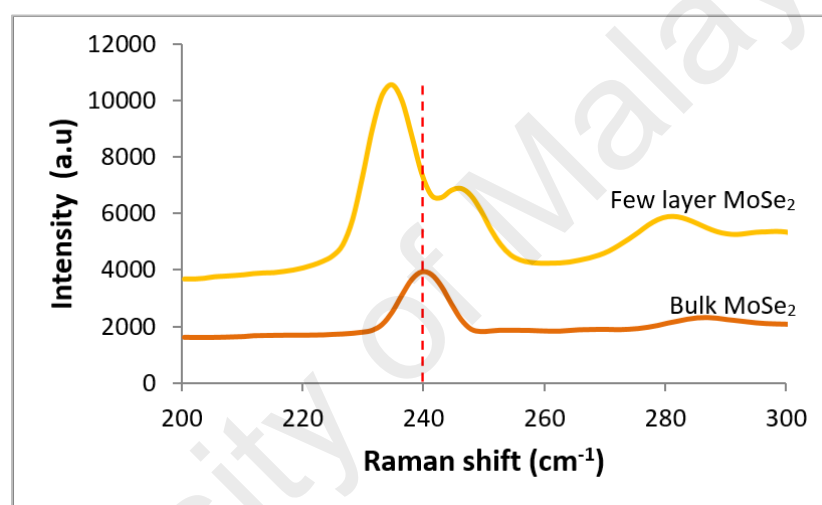
3.7.1 Molybdenum Diselenide

In this experiment, the preparation and fabrication of a few layers MoSe_2 was made through liquid phase exfoliation (LPE) and it begins with making a few layers MoSe_2 as described in our previous work (Ahmad, H., Suthaskumar, M., Tiu, Z., Zarei, A., & Harun, S. W. 2016). In the exfoliation process, N-methyl-2-Pyrrolidine (NMP) solvent was added to bulk powder with 5 mg/ml concentration. The solution was treated for ultrasonication for about 8 hours. By centrifuging the exfoliated MoSe_2 suspension for approximately 30 minutes, the bulk MoSe_2 is removed. The top two third supernatant solution was pipetted out for analysis. The purchased bulk MoSe_2 and exfoliated MoSe_2 were first characterized using a Bruker D8 Advanced at 1.5406 \AA excitation wavelength for X-ray diffraction (XRD) as shown in Figure 3.14 (a). Then, both bulk and few layers were analyzed using Renishaw inVia confocal Raman Microscope at 488nm of excitation wavelength and a power of 3.5mW for Raman Spectra measurement as depicted in Figure 3.14 (b). The out-of-plane vibration (A_g^1) for bulk MoSe_2 is centered at 240 cm^{-1} , while the few layer MoSe_2 was centered around 235 cm^{-1} . This peak shift verifies the exfoliation of the few MoSe_2 layers. Furthermore, the SPECORD 210-Plus

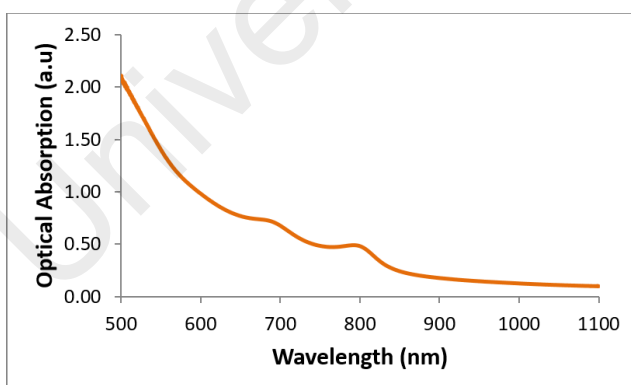
UV-Vis Spectrometer was used to characterize linear absorption of MoSe₂ as provided in Figure 3.14 (c) with two peaks trace observed at ~697 nm and ~800 nm respectively. Then, the few layers of MoSe₂ solution were developed to produce a thin film as shown in Figure 3.14 (d). Ultrasonic bath was used to agitate particles in the solution for about 10 minutes. Eventually, 200 mg of polyvinyl alcohols were dissolved in 15 ml deionized water with the concentration of 10 mg/ml and were mixed with 15 ml of the few layers MoSe₂ solution. The solution mixture (30 ml) was stirred and heated constantly at a temperature of 80 °C using magnetic stirrer for around 6 hours to reduce the solution to approximately 10 ml. A glass substrate is used to evaporate the remaining solution in an oven for approximately 4 hours at 80 °C to obtain the MoSe₂ thin film.



(a)



(b)



(c)

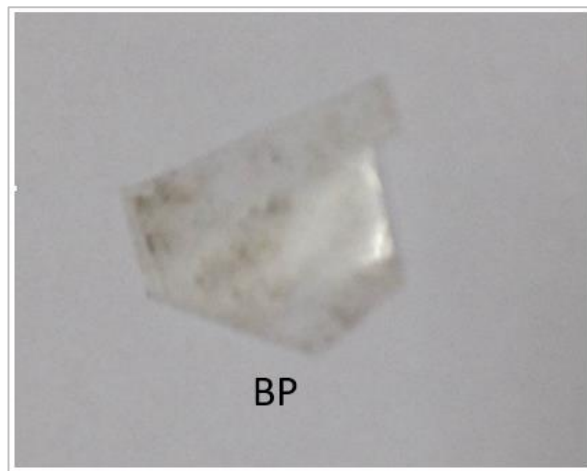


(d)

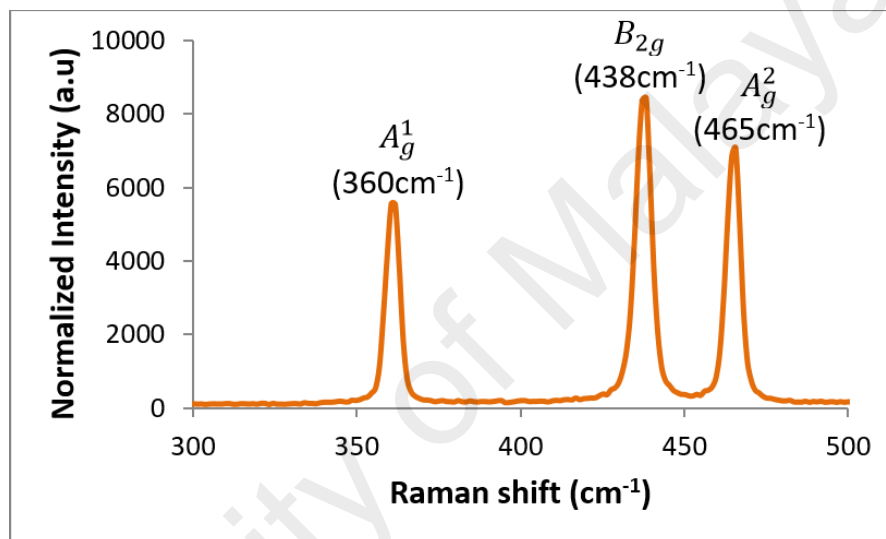
Figure 3.14: Analysis for (a) XRD, (b) Raman shift, (c) Uv-vis and (d) thin film of MoSe₂

3.7.2 Black Phosphorus

Mechanical exfoliation method was used to fabricate BP-based SA (also known as ‘scotch-tape method’) (Chang, Y. M., Kim, H., Lee, J. H., & Song, Y. W. 2010) in this study. Through this method, BP with high purity was separated using scotch-tape into a very thin layer. A BP scotch-tape SA is shown in Figure 3.15(a). Relatively thin flakes were removed from a retail BP crystal (hq graphene) of 99.995% purity using a clear scotch tape. The BP tape was studied with Raman spectroscopy as shown in Figure 3.15(b). Raman spectrum was traced via a spectrometer where a 514 nm beam of a He-Ne laser was emitted on the tape for 10 ms with an exposure power of 10 mW. The result showed three distinct Raman peaks at 360 cm^{-1} , 438 cm^{-1} and 465 cm^{-1} , related to the A_g^1 , B_{2g} and A_g^2 vibration modes of layered BP. Whereas, the B_{2g} and A_g^2 modes coincide with the in-plane oscillation of phosphorus atoms in BP layer and the A_g^1 modes corresponds to the out-of-plane vibration. The BP layers were then transferred onto a fiber pigtail as illustrated in Figure 3.15(c) and the image of BP was observed using fiberscope EXPO Model FIP-400as depicted in Figure 3.15(d). Subsequently, the BP tape was placed between the fiber optic ferrules and later incorporated into fiber laser ring cavity. Mechanical exfoliation has its advantages with its simplicity, where the entire fabrication process has not involved any complicated chemical procedures and costly instruments.



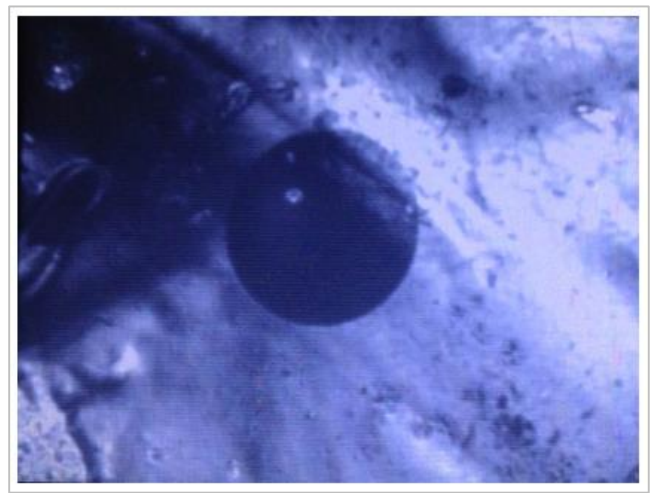
(a)



(b)



(c)

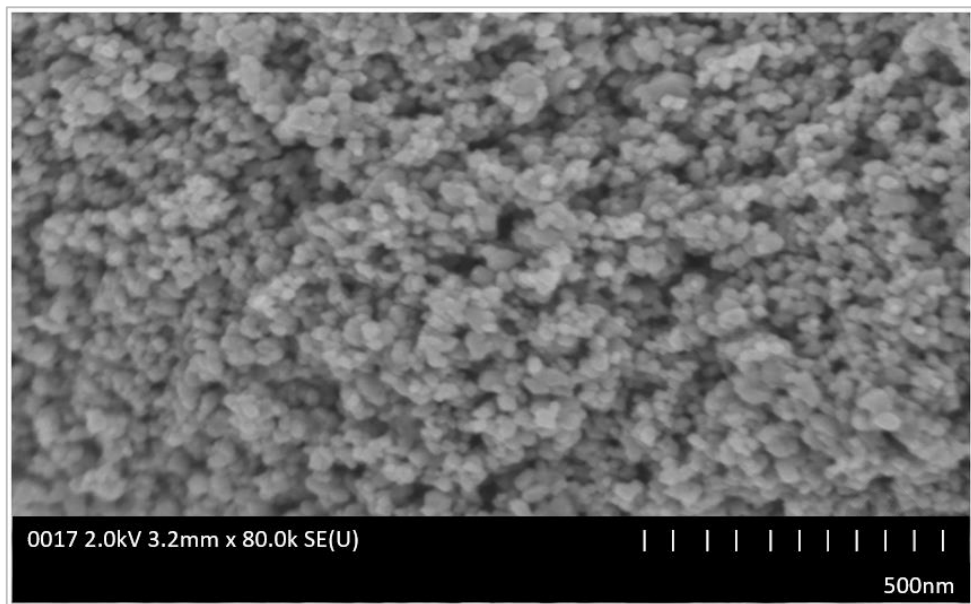


(d)

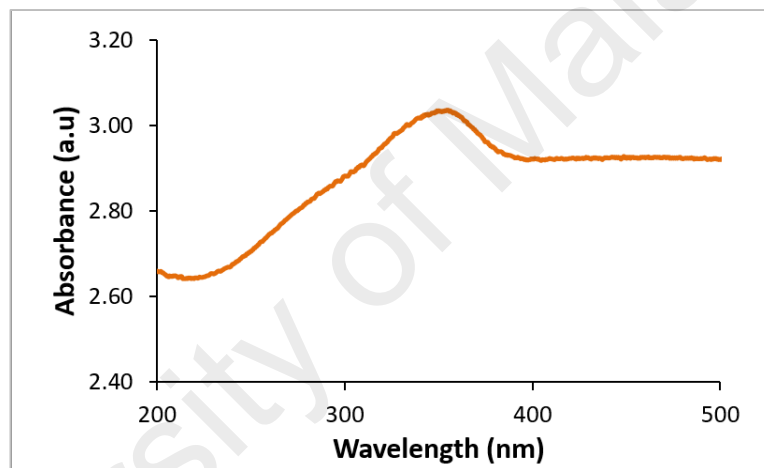
Figure 3.15: (a) BP scotch-tape SA, (b) Raman shift analysis, (c) BP tape placed on the surface of fiber ferule and (d) BP tape observed via fiberscope.

3.7.3 Titanium Dioxide

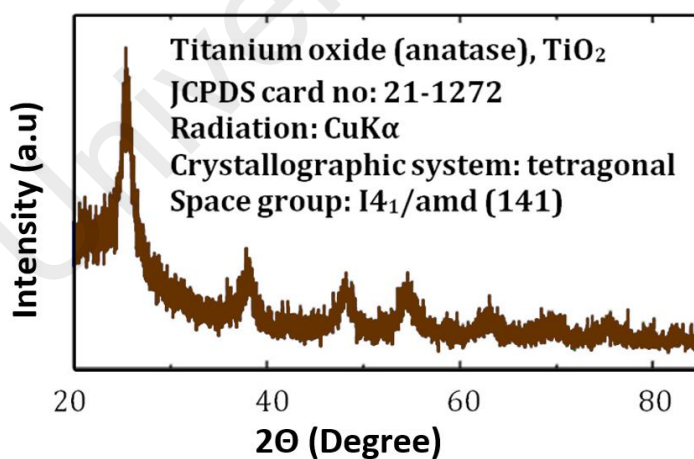
The TiO₂ nanostructures were procured from Sigma Aldrich (Malaysia) Sdn. Bhd. and used without further purification. The TiO₂ provided was of the anatase group. Polymer thin film based on agar and TiO₂ was developed to assess the performance of TiO₂ saturable absorber. The thin film was produced by ultrasonically stirring a mixture of 0.05 g of TiO₂ and 50 ml of deionized water for 30 minutes. Then, 1 g of agar was added to the mixture and heated at 300 °C for 15 minutes. The mixture was continuously stirred before being poured onto a 4-ml mold. The mixture was left to dry in a 27 °C environment for 5 days. Thickness of the thin film was 0.10 ± 0.01 mm when measured. Figures 3.16 (a), (b) and (c) display the field emission gun scanning electron microscopy (FEG-SEM) image, Uv-Vis spectrum image of thin film, the X-ray diffractions (XRD) pattern of the TiO₂ respectively. The nanostructure sizes were about 20-50 nm. The TiO₂ exhibits a strong absorption band at around 354 nm. The TiO₂ provided was of the anatase group and the performance of TiO₂ as a saturable absorber was tested by embedding it into a polymer based thin film (or Polymer thin film based on agar and TiO₂ has been used as a layer to carry out the test.) The thin film as shown in Figure 3.16 (d) was developed by heating 1g of agar in a 50 ml of deionized water for 15 minutes at 300 °C before 0.05 g of TiO₂ was added. The mixture was continuously stirred before being poured into a 25 ml mold. The mixture was left to dry in 27 °C for 3 days.



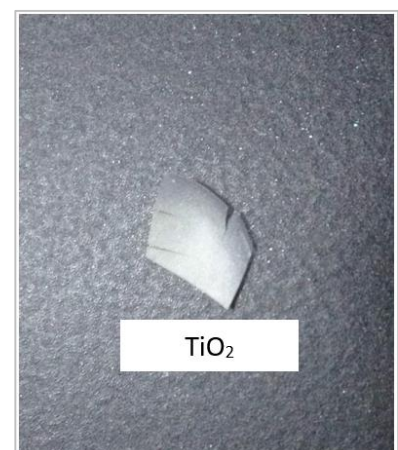
(a)



(b)



(c)

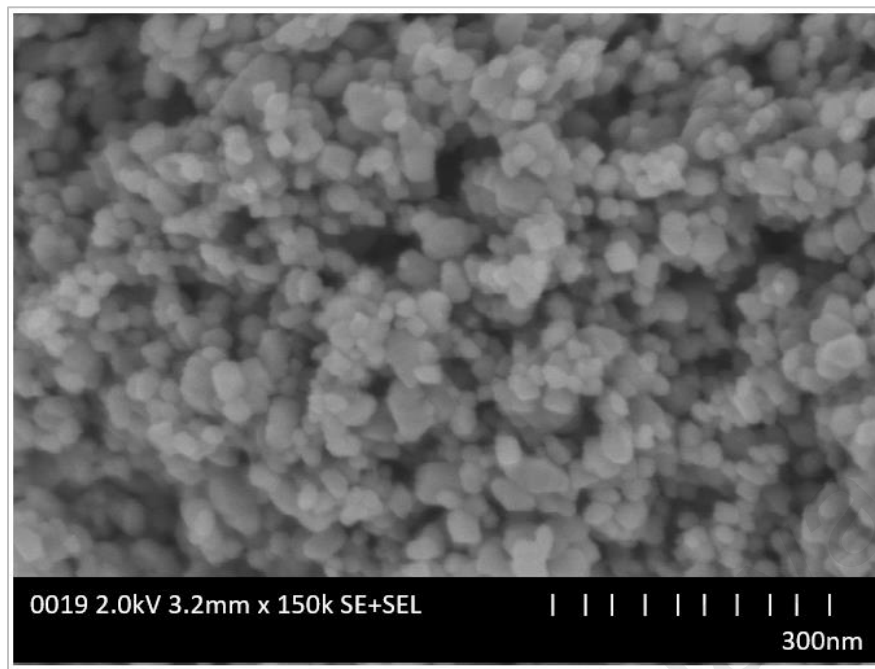


(d)

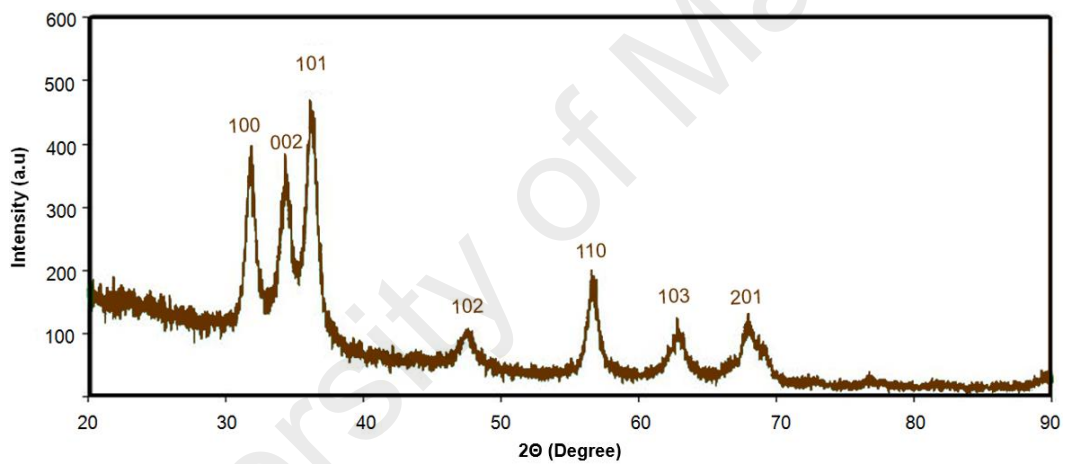
Figure 3.16: TiO₂ observed by (a) FEG-SEM, (b) Uv-vis spectroscopy, (c) XRD and (d) image of TiO₂ thin film saturable absorber

3.7.4 Zinc Oxide

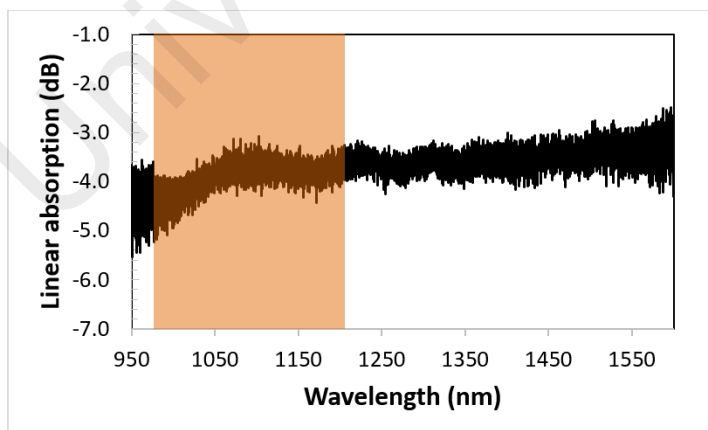
In this experiment, ZnO nanostructures was acquired from Sigma Aldrich (Malaysia) Sdn. Bhd. and used without further purification. A thin film polymer based on agar and TiO₂ was fabricated to assess the potential of the ZnO as a saturable absorber. The thin film was prepared by ultrasonically stirring a mixture of 5% wt of ZnO powder that was added into a mixture of silane and ethanol with a weight ratio of 1:1 for 30 minutes. Then, 10% sulfuric acid was added and the mixture was continuously stirred for 5 more minutes. The mixture was left to dry in an environment at 27°C for 3 days. Figure 3.17 (a), (b), (c) and (d) show the field emission gun scanning electron microscopy (FEG-SEM) image, X-ray diffractions (XRD) pattern, linear absorption and thin film image of the ZnO SA. The thin film thickness was measured to be 0.15 ± 0.01 mm and the sizes of nanostructures were in the range of 20-50 nm.



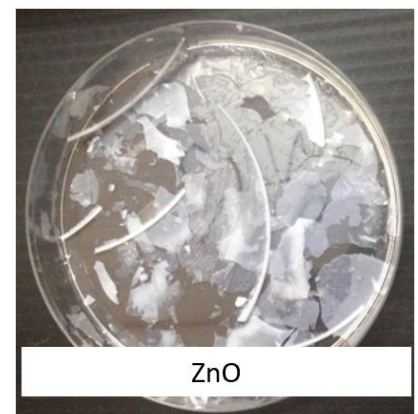
(a)



(b)



(c)



(d)

Figure 3.17: (a) FEG-SEM image, (b) XRD pattern, (c) linear absorption and (d) thin film image of ZnO SA

3.8 Modulation Depth Measurement

The characterization of saturable absorber can be measured by its modulation depth. In this section, the measurement of modulation depth is discussed and the modulation depth and saturation intensity results of each type of SA used in this work is presented in chapter 5.

The experimental setup to measure the properties of nonlinear saturable absorption for SA is represented in Figure 3.18. The dual-detector measurement system was used to measure the modulation depth of SA (Ahmad, H., Soltanian, M. R. K., *et al.*, 2015). These measurement systems consist of mode-locked erbium-doped fiber laser (EDFL), incorporating CNT based SA as pulse seed, an amplifier, a variable optical attenuator (VOA) (Anritsu MN9610B), a 50:50 optical coupler and two optical power meter (OPM) model Thorlabs PM100USB. The pulse generated has a frequency of 27.6 MHz and 0.51 ps pulse width and was amplified using a commercial low-dispersion Keopsys EDFA to sufficiently saturate the SA sample. Then, the mode locked pulse signal broke after going through the amplifier, therefore by correctly tuning the LD current, the pulse shape from the pulse seed can be preserved. A VOA was utilized to control the pump power launched through the SA. The amplified mode-locked pulse is divided into two parts by a 50:50 optical output coupler. One part hits the ZnO thin film before going into an OPM while the other part acts as a reference (travels directly into another OPM). The saturable absorption graph was fitted using the following formula (Luo, Z., *et al.*, 2015):

$$\alpha = \frac{\Delta\alpha}{(1 + \frac{I}{I_{sat}})} + \alpha_{linear} \quad (3.1)$$

where α_{linear} , I_{sat} , $\Delta\alpha$, correspond to the non-saturable loss, saturable optical intensity and modulation depth, respectively. The modulation depth and saturable intensity of the saturable absorber employed in this work can be measured as explained in chapter 5.

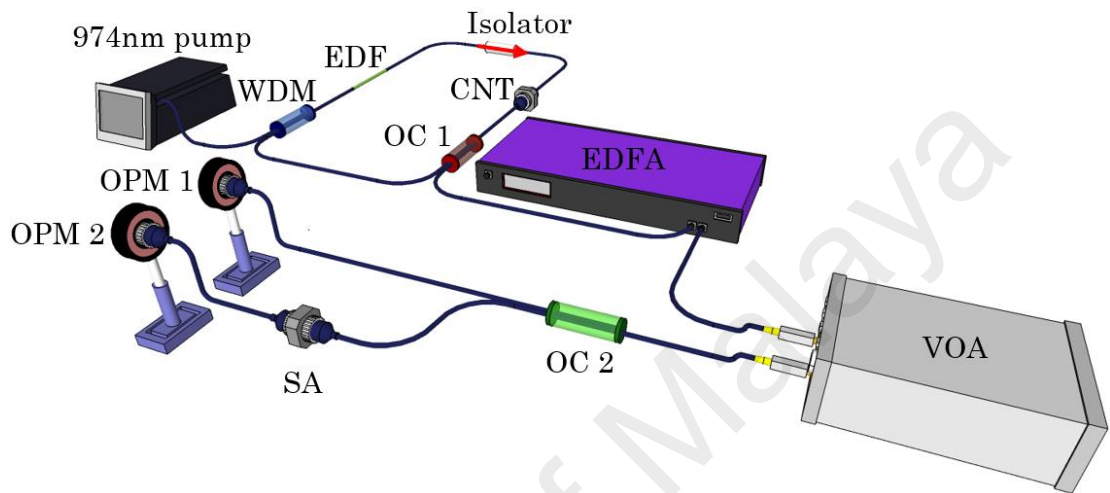


Figure 3.18: The experimental setup of dual-detector measurement system

CHAPTER 4: DUAL-WAVELENGTH CONTINUOUS WAVE LASER

4.1 Introduction

Multi-wavelength lasers have gained popularity as they can be employed in various applications like remote sensing, industrial devices and optical communications as wavelength division multiplexing (WDM) sources. Majority of current researches on such lasers focus extensively on C-band erbium-doped fiber (EDF) lasers because of its applicability in optical communications. Nevertheless, ytterbium-doped fiber lasers (YDFL) working in the one-micron region gained the interest of researchers lately. YDFL is widely known in applications such as optical coherence tomography (OCT) and biomedical devices for its use in laser cutting, welding, marking and drilling.

Various setups for YDF lasers have been proposed. These include applying the use of a Lyot filter and an unpumped YDF in two Sagnac loop configurations in a ring cavity setup to generate multi-wavelengths (Yue, Z., Chui, P. C., & Wong, K. K. Y. 2013). Another setup uses 15 m of YDF along with a single mode fiber Bragg grating (FBG) in a linear cavity (Xinhuan, F., *et al.*, 2004). A setup employing multiple ring cavities with a tunable band pass filter has also been reported (Feifei, Y., Sigang, Y., Hongwei, C., Minghua, C., & Shizhong, X. 2011). These arrangements achieve a single longitudinal mode in the 1 μm region at the expense of long cavity length, bulky cavities, requiring complicated designs and expensive filtering elements.

In the recent years, DWFL has gain significant attention due to its specific features such as high bit rate soliton pulses (Tadakuma, M., *et al.*, 2000) for radar and photonic beam steering of phased-arrayed antennas in microwave photonic filters (Liu, D., *et al.*,

2006) and photonic generation of microwave carrier (Xia, L., *et al.*, 2007). Moreover, most of the researches on DWFL using EDF as active medium for 1550nm region have been demonstrated. For example, by using FBG (Zhang, F., Chu, P. L., Lai, R., & Chen, G. R. 2005), polarization hold-burning method (Qian, J. R., *et al.*, 2008), introducing a filter (Ahmad, H., Soltanian, M. R. K., Pua, C. H., Zulkifli, M. Z., & Harun, S. W. 2013b) and many more designs were suggested to generate dual-wavelength spectrum.

On the other hand, very few researches were made on the generation of dual - wavelength in the one micron area, particularly using YDF. This prompted further interest in this research. Furthermore, the desirable applications for DWFL in the one micron region in space optical communication (Wright, M. W., & Valley, G. C. 2005) and optical coherence tomography (Yasuno, Y., *et al.*, 2007) have driven and motivated for further studies using YDF as gain medium in DWFL generation.

4.2 Tunable DWFL Based Dual-Tapered Microfiber MZI

Recently, researches has explored the significant optical properties of microfiber or tapered fiber by heating and stretching single mode fibers (SMF) using flame-brushing technique. Using this method, a narrow waist region of microfiber that exhibits complicated structures (Brambilla, G. 2010), for example Mach-Zehnder interferometer (Lu, P., Men, L., Sooley, K., & Chen, Q., 2009) and nonlinear fiber (Agrawal, G. 2001) can be fabricated. A tapered fiber will stimulate higher order modes, resulting in a spatial mode beating (Jian, F., Ying-Ying, X., Shao-Fang, T., Yang, L., & Shuo, S. 2010) that implies a interference comb spectrum which corresponds to wavelength-dependent loss (Li, Y., & Bao, X. 2008). Therefore, by exploiting optical properties of tapered fiber, such as its waist diameter, refractive index contrast and length of tapered

region, the interference characteristics of the tapered fiber can be manipulated and controlled.

This work proposes, and experimentally demonstrates a novel dual-wavelength ytterbium fiber ring laser that is very simple and compact by incorporating dual-tapered microfiber based Mach Zehnder Interferometer (MZI). The incident beams propagate into tapered region that consists of 70 mm length of tapered fiber with 2 μm in taper waist diameter. This interaction generates a higher order mode and spatial mode beating resulting in interference comb spectrum. The laser emission will occur when completing optical component connection in a ring cavity. The lasing occurs in single longitudinal mode with side mode suppression ratio (SMSR) in excess of 50 dB. The interference response of the microfiber is responsive to polarization state. Therefore, by adjusting the laser cavity state of polarization through a polarization controller (PC), the dual-wavelength lasing generation with different wavelength spacing were successfully demonstrated and reported here.

The laser setup of 1 μm laser system is shown in Figure 4.1. Ytterbium-doped fiber amplifier (YDFA) is formed together with a wavelength division multiplexer (WDM) coupler, with one input connected to a 974 nm pump and the output linked to a 70 cm YDF. The other port of the WDM is connected to a 10/90 fused biconical coupler. The absorption rate of the YDF (DF1100 Fibercore) at 977 nm is 1300 dB/m, with 5.7 dB/km of attenuation at 1200 nm. The cladding diameter is 124.8 μm , with a mode field diameter of 5.1 μm and a numerical aperture of 0.17. The output of YDFA is fusion-spliced to an polarization insensitive isolator so that ring laser operates unidirectionally. The output of isolator is then linked to the polarization controller (PC) to manage the state of polarization in the setup by adjusting three adjustable waveplate from the PC. The PC output is linked to a 70 mm in-house fabricated microfiber. The

waist diameter of the microfiber is 2 μm . This microfiber is used as a multimodal interference medium in order to form a narrowband filter. Furthermore, to form a ring cavity, the input port of 90/10 optical coupler is connected to the microfiber, the 10% output port is attached to the optical spectrum analyzer model AQ 6373 Yokogawa, with 0.02 nm resolution and the 90 % output port is coupled back into the YDFA input. The fabrication of microfiber employed a single mode fiber with standard size of 9/125 μm core/cladding diameter operating on a flame brushing technique (Brambilla, G., *et al.*, 2010) as discussed in chapter 3, where heating and stretching was applied onto the optical fiber. The dual-tapered MZI structure of the fiber enables it to support higher order modes.

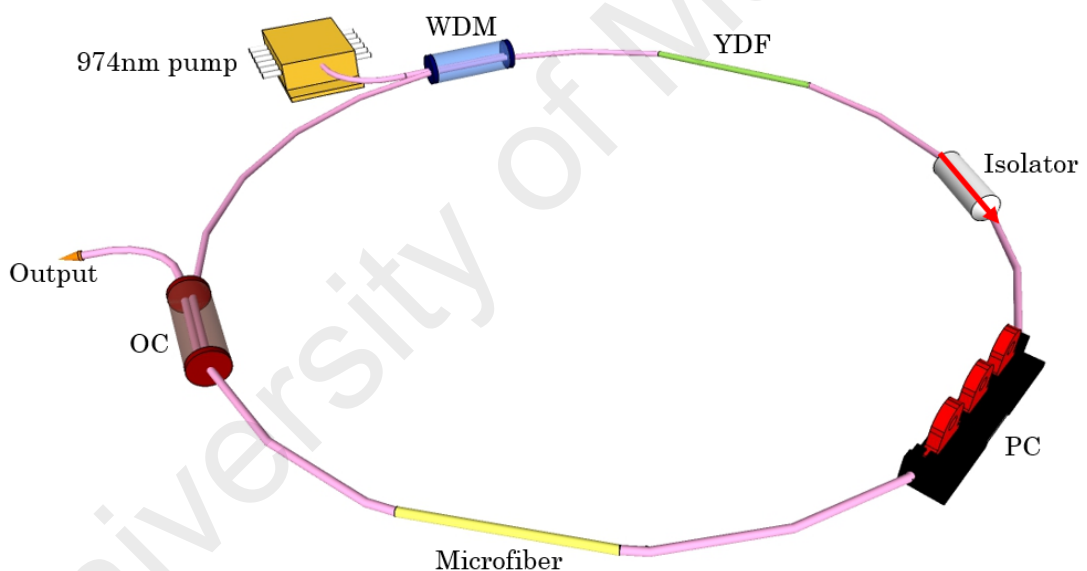


Figure 4.1: Fiber ring laser experimental setup with a dual-tapered MZI microfiber

The interference spectrum is shown in Figure 4.2, where the amplified spontaneous emission (ASE) depicted in blue, represents the spectrum of the ASE directly from the YDFA output, while the red arrow depicts the spectrum of amplified spontaneous emission following the dual-tapered MZI microfiber. The interference spectrum is observed and illustrated in red in Figure 4.2, implying narrow linewidth upon closure of

the cavity ring. The lasing normally occurs at the interference peaks, and by simply adjusting the polarization using PC, the peak switches to another peak. Both peaks are supported by the cavity.

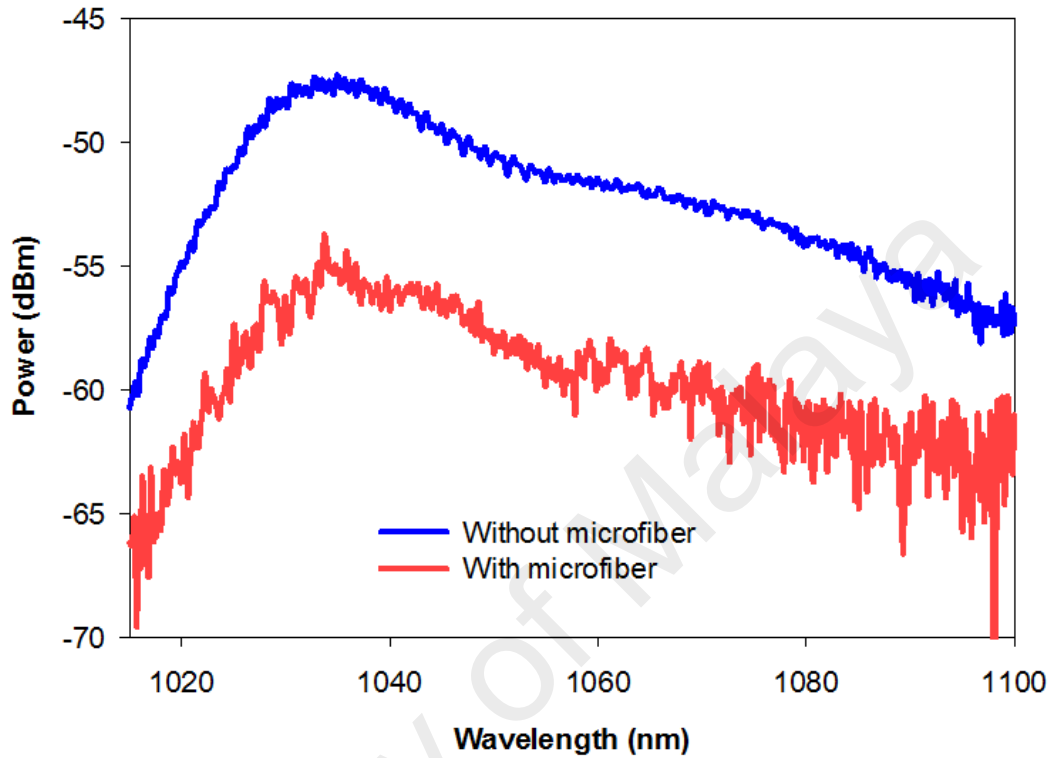
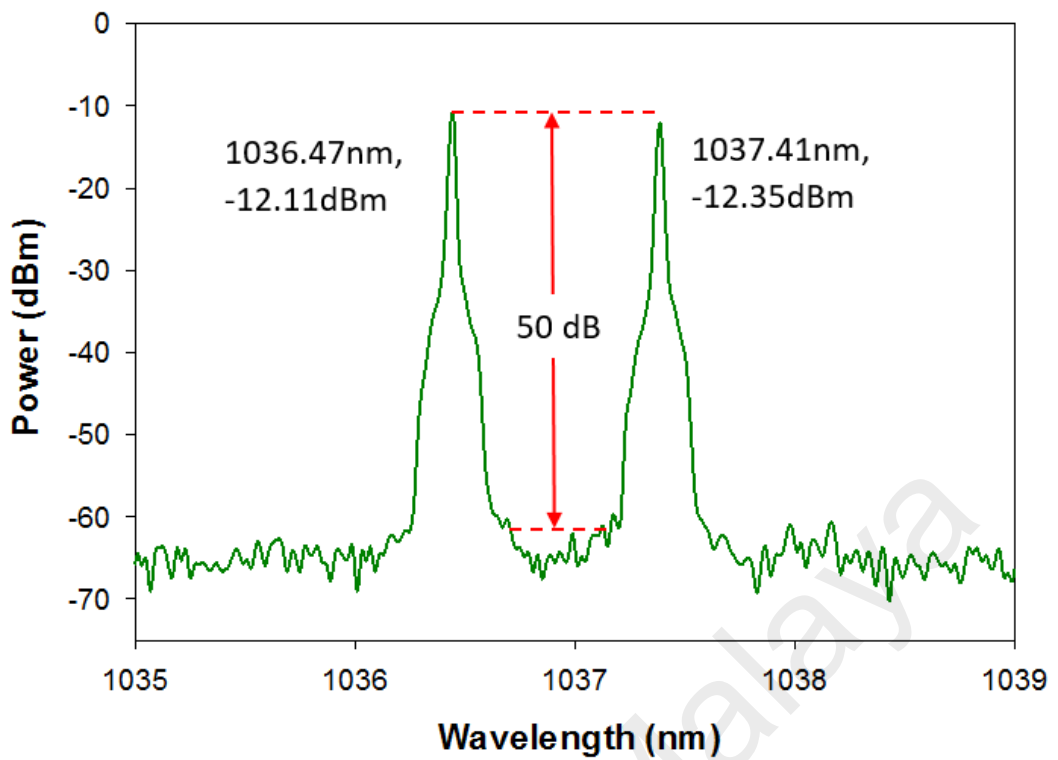
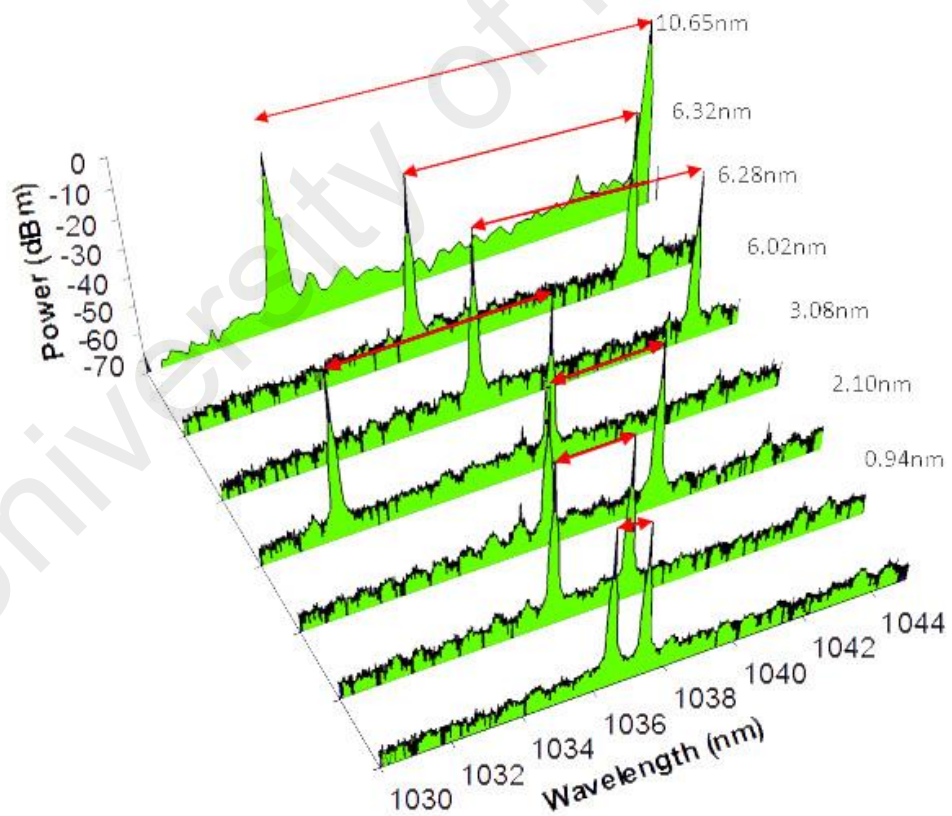


Figure 4.2: Amplified spontaneous emission transmission through microfiber (red) and without it (blue)

The microfiber introduces a high suppression ratio to the other cavity modes and the ASE, leading to a relatively high power lasing output operating at one longitudinal mode. Figure 4.3 (a) shows a dual-wavelength spectrum obtained after the adjustment of the PC. The dual-wavelength has 0.94 nm wavelength spacing and central wavelength at 1036.47 nm and 1037.41 nm respectively. A slight adjustment to the PC caused the wavelength of lasing to switch over another wavelength as illustrated in Figure 4.3 (b) with various wavelength spacing.



(a)

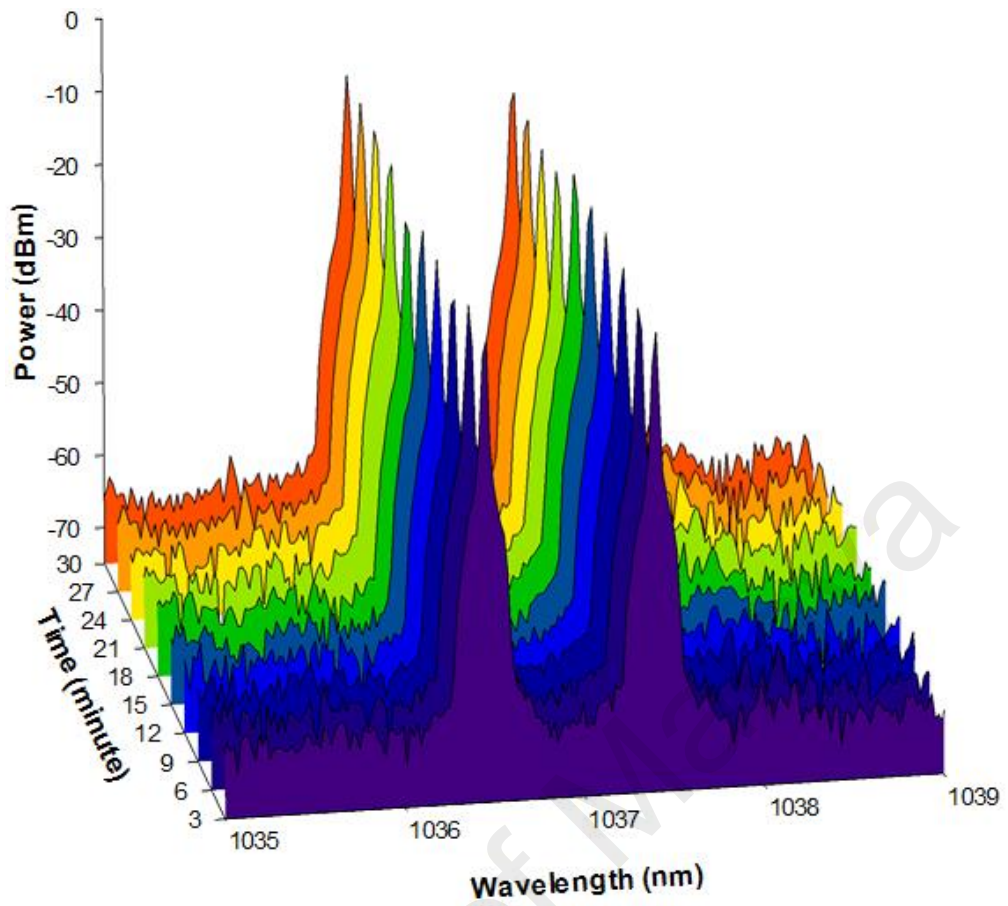


(b)

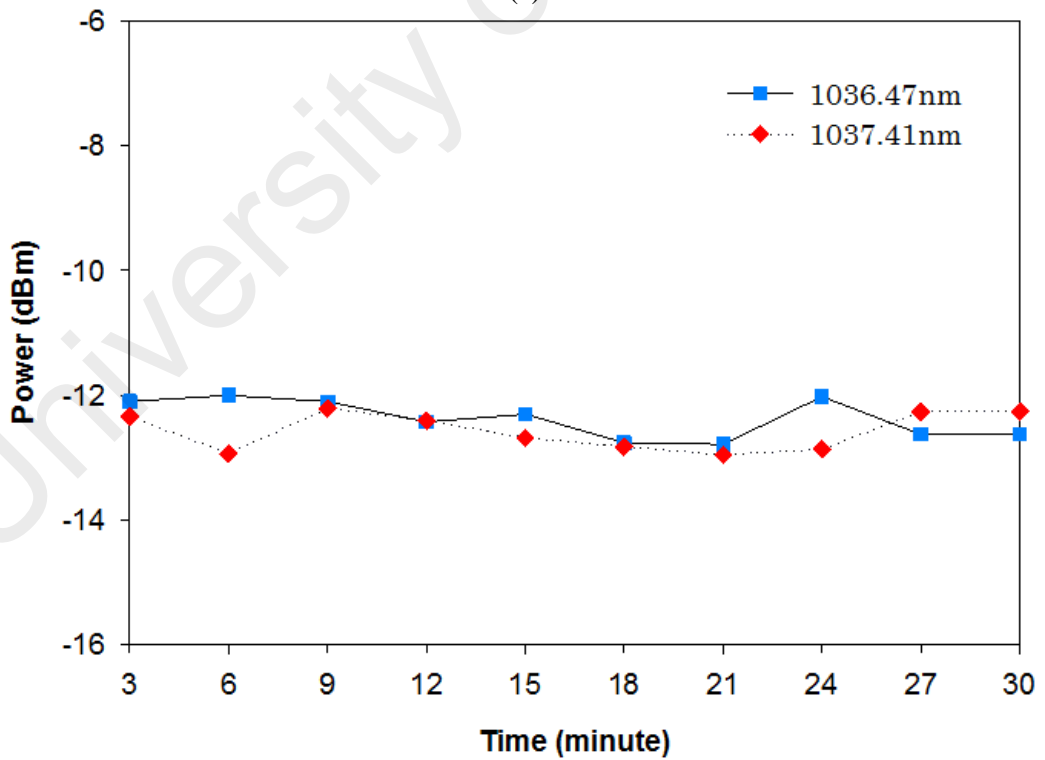
Figure 4.3: (a) Dual-wavelength output at 1036.47 nm and 1037.41 nm and (b) dual-wavelength tuning with various wavelength spacing.

The spectrum of the dual-wavelength's temporal test for 30 minutes at 1036.47 nm and 1037.41 nm is shown in Figure 4.4. During the 30-minute scan, the maximum measured power fluctuation was 0.8 dBm. The dual lasing is stable and fixed, taking into account the fact that the experiment was run at room temperature. This proved that the dual -wavelengths are sustainable over time and has low power fluctuations of around 0.8 dBm. It was possible to generate seven different tuning configurations by controlling the polarization state by tuning the polarization controller, in which dual-wavelengths with different wavelength spacing were obtained.

University of Malaya



(a)

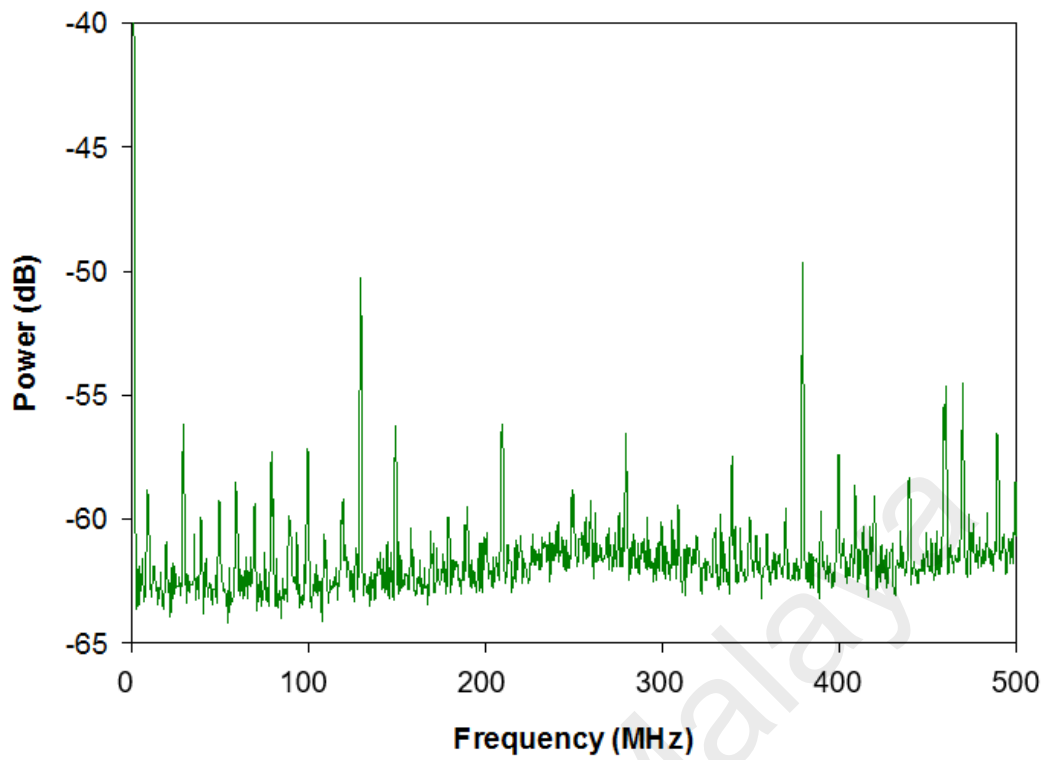


(b)

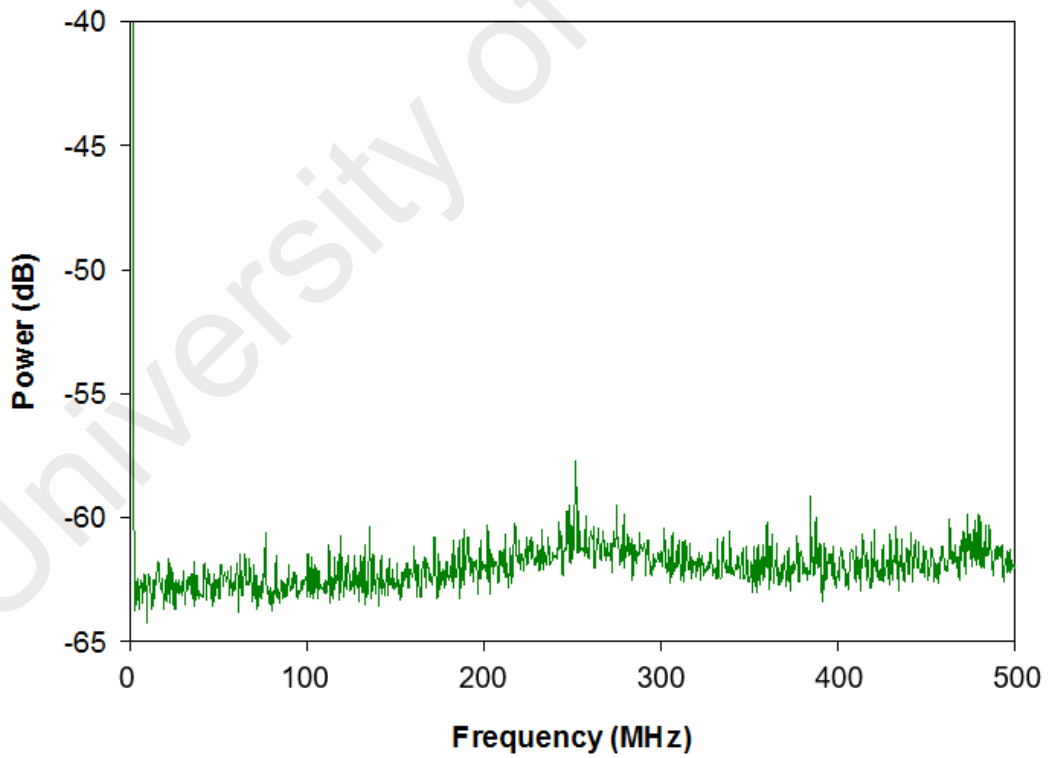
Figure 4.4: (a) The dual-wavelength stability scans and (b) power fluctuation for 30 minutes at narrowest wavelength spacing of 0.94 nm

Verification of the SLM operation in the proposed setup was undertaken by connecting the 10% output from the coupler to a RF analyzer (Anritsu MS2683A with a detection range from 9 KHz to 7.8 GHz) via a Thorlabs D400FC fiber optic photo detector in order to analyse the spectrum's beating signal. An initial observation of the beating mode, wherein the dual-tapered fiber was disconnected from the cavity setup, across a scan range from 0 to 500 MHz is illustrated in Figure 4.5 (a). It is evident that the spectrum is quite noisy and unstable due to mode-hopping within the cavity. Connecting the dual-tapered fiber to the cavity setup caused the beating noise to disappear, with no mode-hopping observed in the resulting spectrum as illustrated in Figure 4.5 (b).

University of Malaya



(a)



(b)

Figure 4.5: RF spectrum with (a) microfiber disconnected, and (b) microfiber connected in the ring cavity.

Measurement of the SLM full width at half maximum (FWHM) linewidth involves the application of heterodyne technique linewidth relations method as described by (Derickson, 1998) in Chapter 3 and is denoted by the following equation:

$$\sqrt{99}\Delta\nu = \Delta f_{20\text{dB}} \quad (1)$$

where $\Delta\nu$ is the FWHM linewidth and $\Delta f_{20\text{dB}}$ is the frequency difference for a measured full width point at 20 dB. The measured FWHM linewidth resulting from the heterodyne method is illustrated in Figure 4.6. Applying the equation in 1 $f_2 = 3.63 \times 10^8$ Hz and $f_1 = 3.59 \times 10^8$ Hz, resulting in a $\Delta\nu$ linewidth value of 294.15 kHz, thus providing a verification of SLM operation in the experiment.

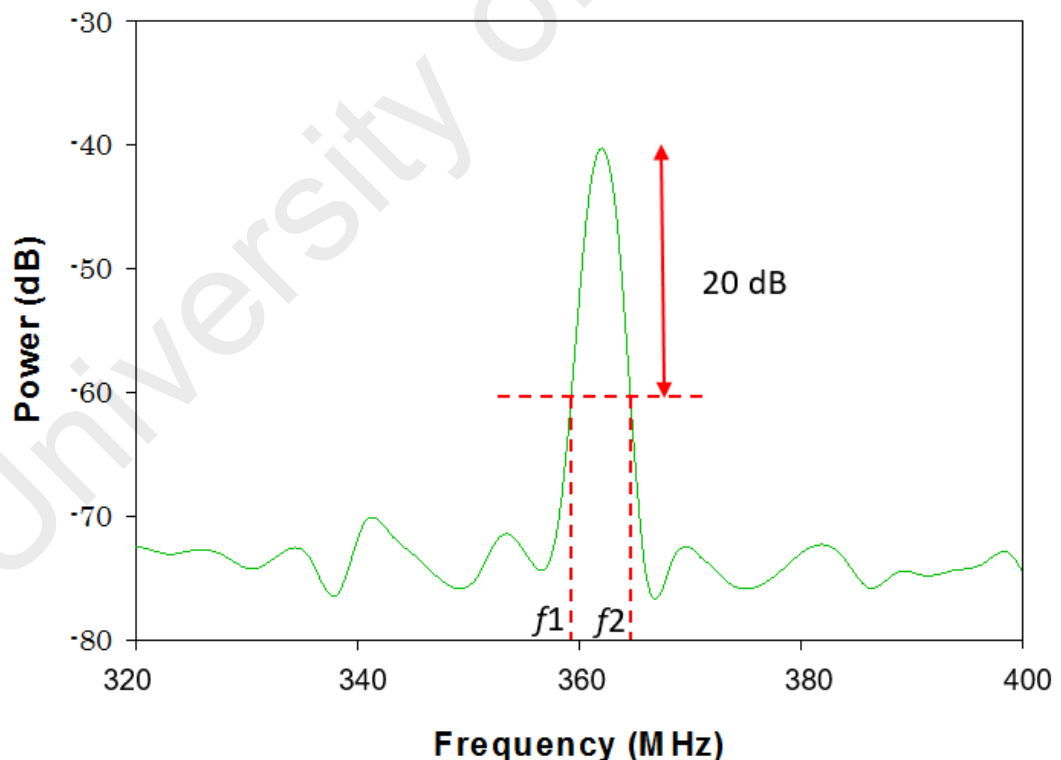


Figure 4.6: FWHM linewidth measurement using a heterodyne linewidth method

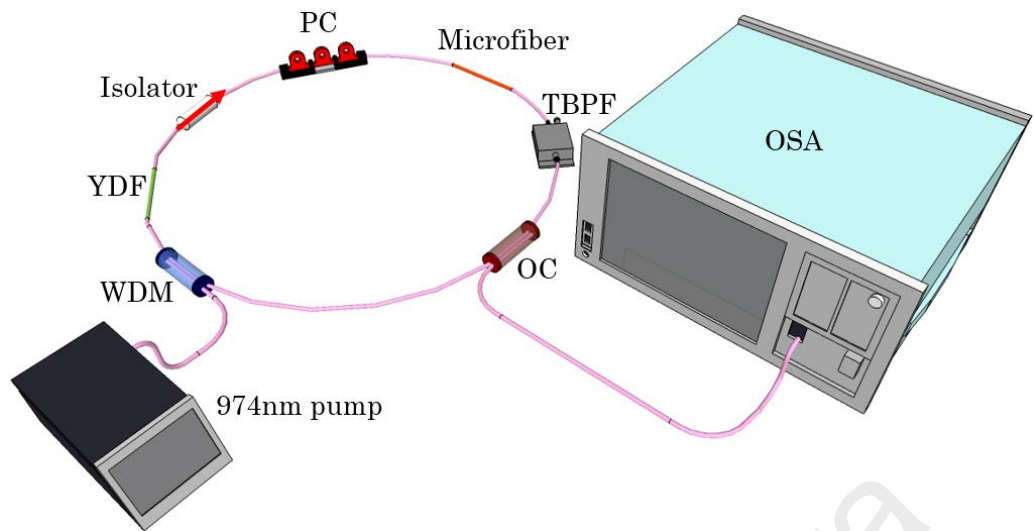
The generation of DWFL by employing dual-tapered microfiber MZI has similar results in terms of SMSR and power stability when compared to researches using FBG (Feng, X., Liu, Y., Fu, S., Yuan, S., & Dong, X. 2004; Wang, H., *et al.*, 2009). However, the fabrication of FBG is costly as it requires equipments such as phase mask and UV laser (Song, Y., Zhan, L., Hu, S., Ye, Q., & Xia, Y. 2004) as opposed to in-house fabrication of microfiber which is cheaper and uses reliable components. In comparison to the similar approach used for SLM operation with YDF (Zhou, Y., Chui, P. C., & Wong, K. K. Y. 2013), the proposal demonstrated in this paper achieved a comparable SMSR and a higher linewidth in the kHz range when utilizing a simpler setup and lesser equipments for SLM output. With regards to the proposed dual-tapered microfiber MZI, the generation of dual-wavelength using a less complex setup, lower cost of installation, and highly stable operation in room temperature are the key advantages in the 1 μm wavelength region. Consequently, the proposed dual-tapered MZI fiber is proven to be an excellent choice as a wavelength filter, and fits applications such as micromachining, OCT and optical wireless (Yu, Y., Liaw, S., Hsu, W., Shih, M., & Chen, N. 2015).

4.3 Tunable Narrow-Spacing DWFL Using Dual-Tapered Microfiber MZI

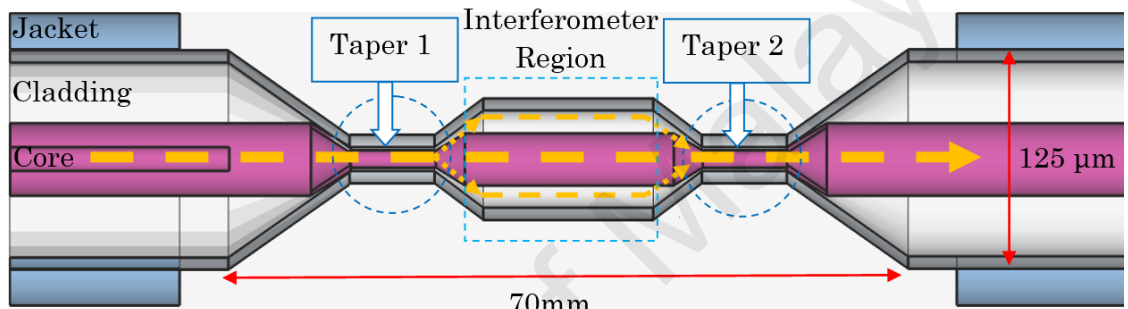
In this work, both dual-tapered microfiber MZI and tunable band pass filter (TBPF) are successfully employed in a simple YDF laser ring cavity for narrow spacing of dual-wavelength operation. The TBPF is incorporated into the cavity setup to confine DWFL oscillation in narrow wavelength spacing. The proposed setup exhibits 3 sets of DWFL with narrow wavelength spacing of 0.06, 0.09 and 0.22 nm and has high SMSR of ~50 dB, wavelength shift less than 0.01 nm and low power fluctuation less than 0.8 dBm resulting in stable operating condition in a simple setup.

The laser setup of narrow spacing DWFL in 1 μm laser system is shown in Figure 4.7 (a). Ytterbium-doped fiber amplifier (YDFA) is formed together with a wavelength division multiplexer (WDM) coupler, with one input attached to a 974 nm pump and the output linked to a 70 cm YDF as gain medium. The other port of the WDM is connected to a 90:10 fused biconical coupler. The absorption rate of the YDF (DF1100 Fibercore) at 977 nm is 1300 dB/m, with 5.7 dB/km of attenuation at 1200 nm. The cladding diameter is 124.8 μm , with a mode field diameter of 5.1 μm and a numerical aperture of 0.17. To ensure the ring laser operates unidirectionally, the output of the YDFA is fusion-spliced to an optical insensitive isolator. The output of isolator is then linked to the polarization controller (PC) to manage the polarization state in the setup by adjusting three adjustable waveplate from the PC. The PC output is linked to a dual-tapered in-house fabricated microfiber. The waist diameter of the microfiber is 2 μm . This microfiber is used as a multimodal interference medium in order to form a narrowband filter. Then, the microfiber output is attached to TBPF (Agiltron Inc.) to achieve narrow wavelength spacing by confining the DWFL oscillation. Furthermore, to form a ring cavity, the input port of 90:10 optical coupler is connected to the TBPF. The 10% output port is used to analyze the generated signal by directly attaching it to the

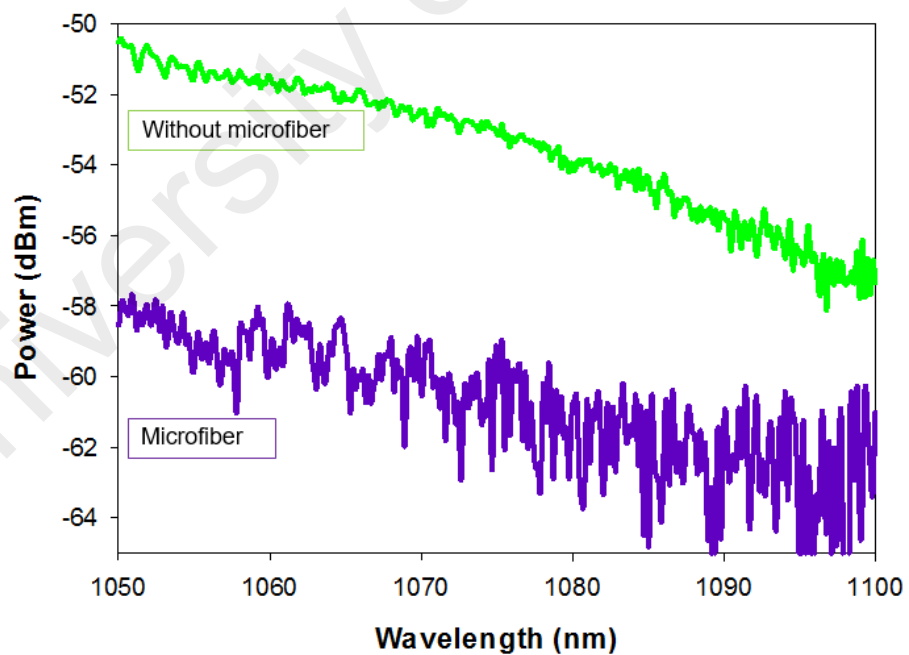
optical spectrum analyzer model AQ 6373 Yokogawa, with 0.02 nm resolution and then the 90 % output port is coupled back into the YDFA input. The schematic diagram of dual-tapered microfiber is shown in Figure 4.7 (b) with taper waist diameter of 2 μm . Figure 4.7 (c) illustrated the amplified spontaneous emission (ASE) directly from the YDFA output (green), while the purple color represents the spectrum of amplified spontaneous emission following the dual-tapered microfiber. The interference spectrum is observed and represented by purple line, which implies narrow linewidth upon closure of the cavity ring. The lasing normally occurs at the interference peaks, and by simply adjusting the polarization using the PC, the peak switches to another peak. Both peaks are supported by the cavity.



(a)



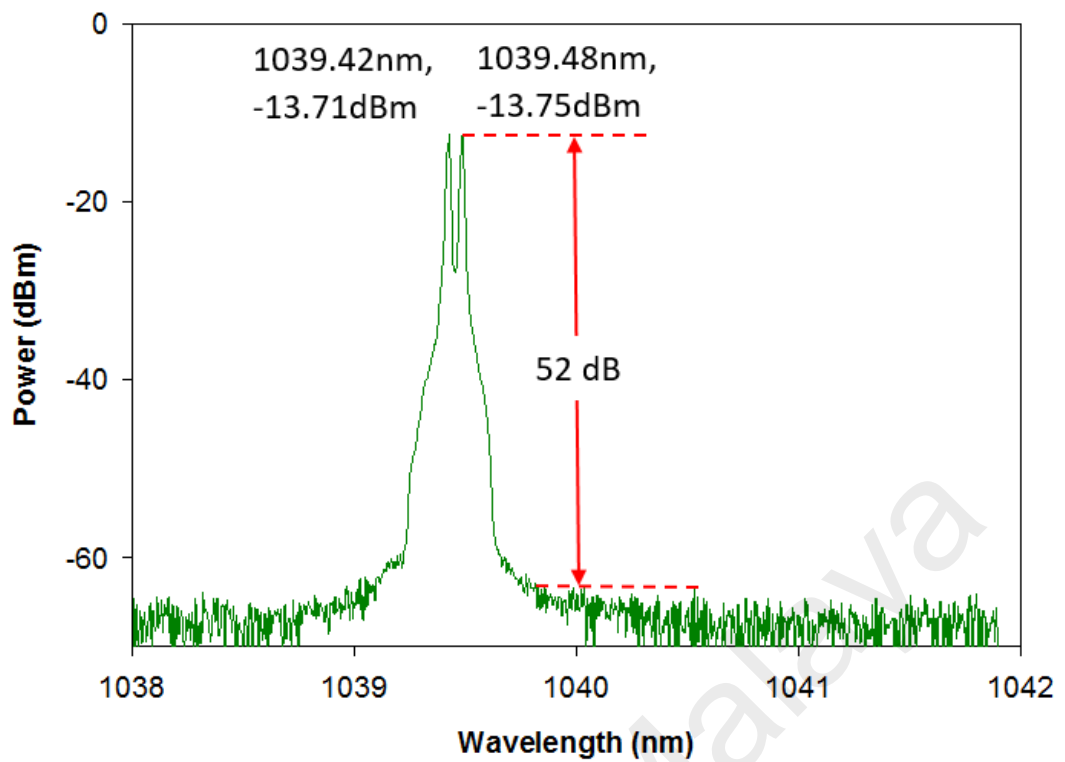
(b)



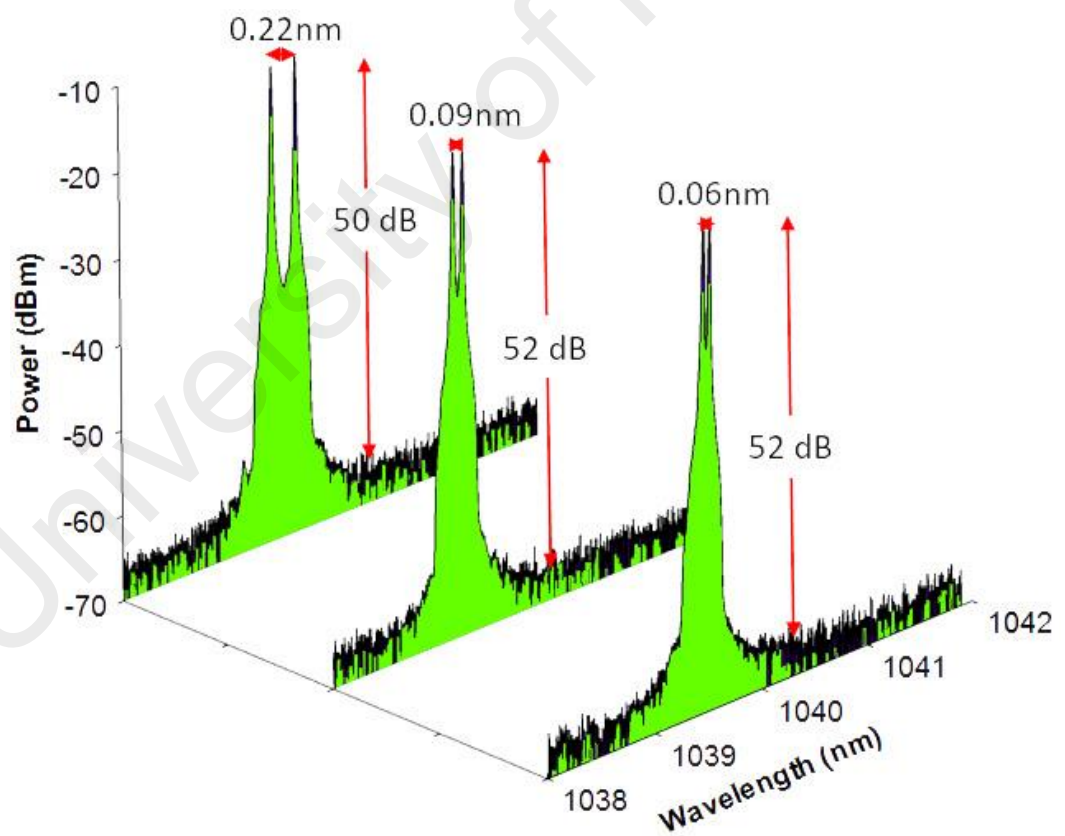
(c)

Figure 4.7: (a) Narrow wavelength spacing of DWFL ring setup, (b) cross section of dual-tapered microfiber MZI (c) amplified spontaneous emission spectrum of microfiber (purple) and excluded microfiber (green)

In this experiment, the LD pump power is increased to 275 mW in order to obtain a highly stable laser performance. The dual-tapered microfiber based MZI produces a spectral filtering effect in laser cavity. This spectral filtering effect influences the emission of laser in generating dual-wavelength laser. Therefore, the PC and TBPF, when adjusted appropriately, results in the spectral shifting which instantaneously changes the laser characteristics. Adjusting the PC allows rotation of polarization state and adjustment of birefringence in order to balance the loss and gain in the cavity. Proper tuning of the TBPF and then adjusting the PC enables the generation of dual-wavelength in narrow wavelength spacing. Initially, the TBPF with tuning range from 1015 nm to 1079 nm is tuned at single wavelength lasing centered at 1039 nm, and the PC is fine-tuned to obtain DWFL. The spectrum output of DWFL obtained is depicted in Figure 4.8 (a), with wavelength and power at 1039.42 nm and -13.71 dBm, and 1039.48 nm and -13.75 dBm, respectively. The dual-wavelength's wavelength spacing is about 0.06 nm, which is due to the intra cavity birefringence. The side mode suppression ratio (SMSR) is about 52 dB. Furthermore, the variation of wavelength spacing can be obtained by re-adjust the PC and in this manner, three set of dual-wavelength are achieved with cavity length of 6 m in simple DWFL setup. Figure 4.8 (b) shows all sets of dual-wavelength with different wavelength separation with (SMSR) observed to exceed 50 dB. Higher SMSR indicates higher stability of dual-wavelength laser that was achieved in this set up. Referring to Figure 4.8 (b), the 3 sets are 0.06 nm from central wavelength of 1039.42 nm to 1039.48 nm, 0.09 nm at central wavelength from 1039.12 nm to 1039.21 nm and 0.22 nm from central wavelength of 1039.40 nm to 1039.62 nm.



(a)

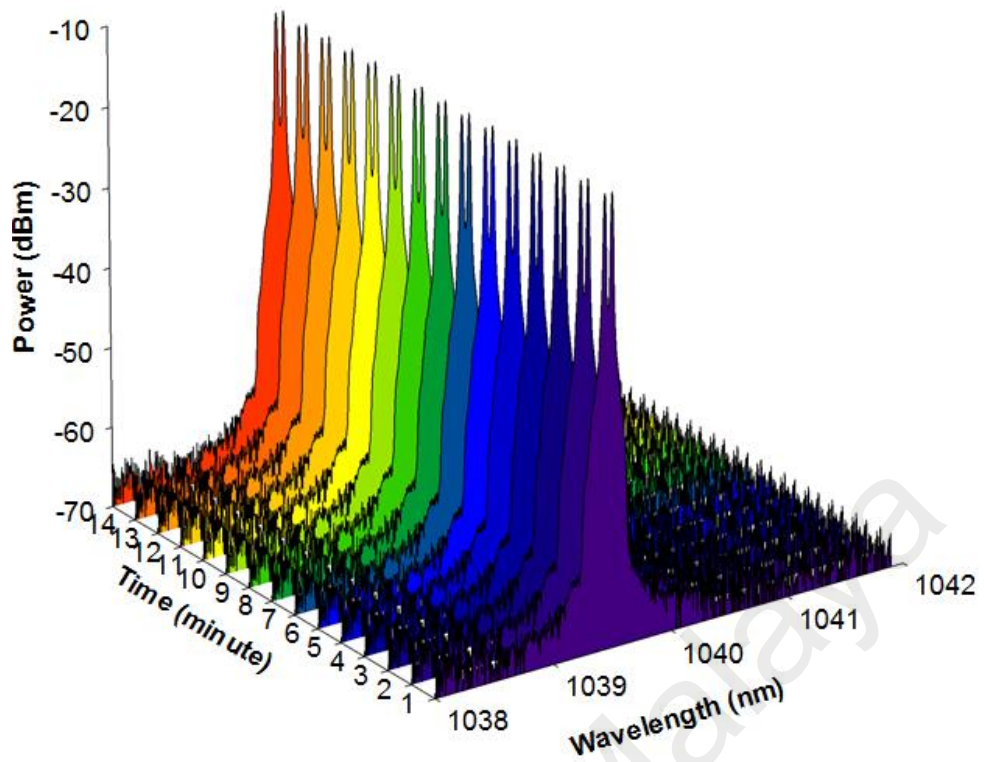


(b)

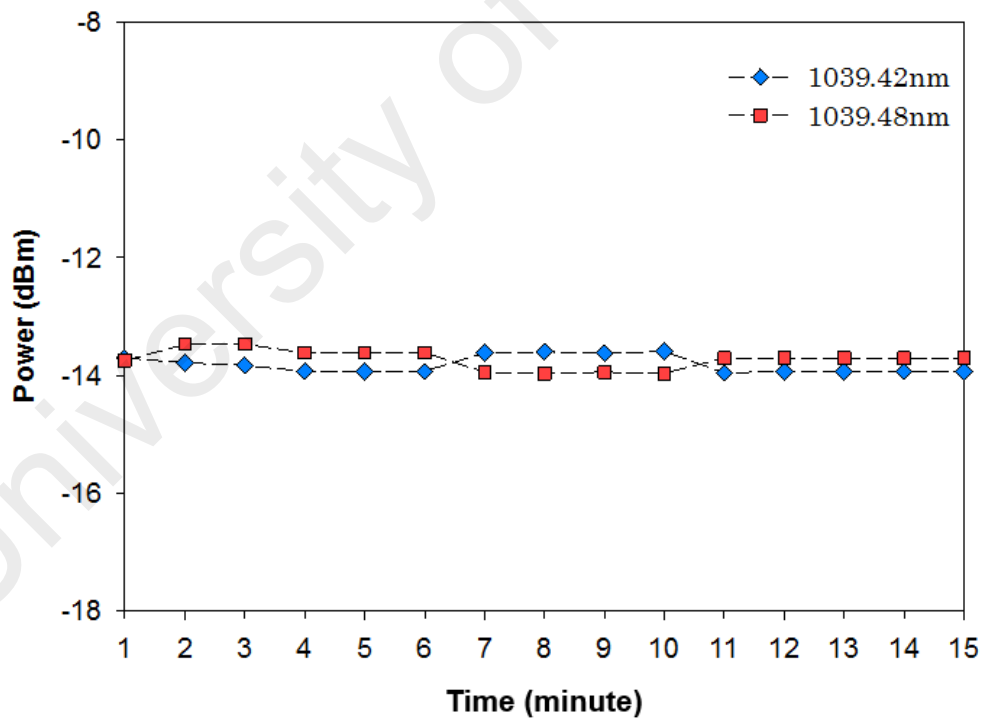
Figure 4.8: (a) The dual-wavelength spectrum with SMSR of 52 dB and (b) Set of dual-wavelengths with tunable spacing from 0.06 nm to 0.22 nm

Moreover, every dual-wavelength set is tested for stability over time in room temperature. In this work, the narrowest wavelength spacing is 0.06 nm and the broadest wavelength spacing is 0.22 nm. Figures 4.9 (a), 4.10 (a) and 4.11 (a) show 15 minutes stability scan of dual-wavelengths at wavelength spacing of 0.06 nm, 0.09 nm and 0.22 nm respectively. The maximum power fluctuation is less than 0.8 dBm, and is shown in Figures 4.9 (b), 4.10 (b) and 4.11 (b) where the wavelength shifting is less than 0.01 nm. The results of stability test indicated that the dual-wavelength generated in this setup is found to be very stable at room temperature.

University of Malaya

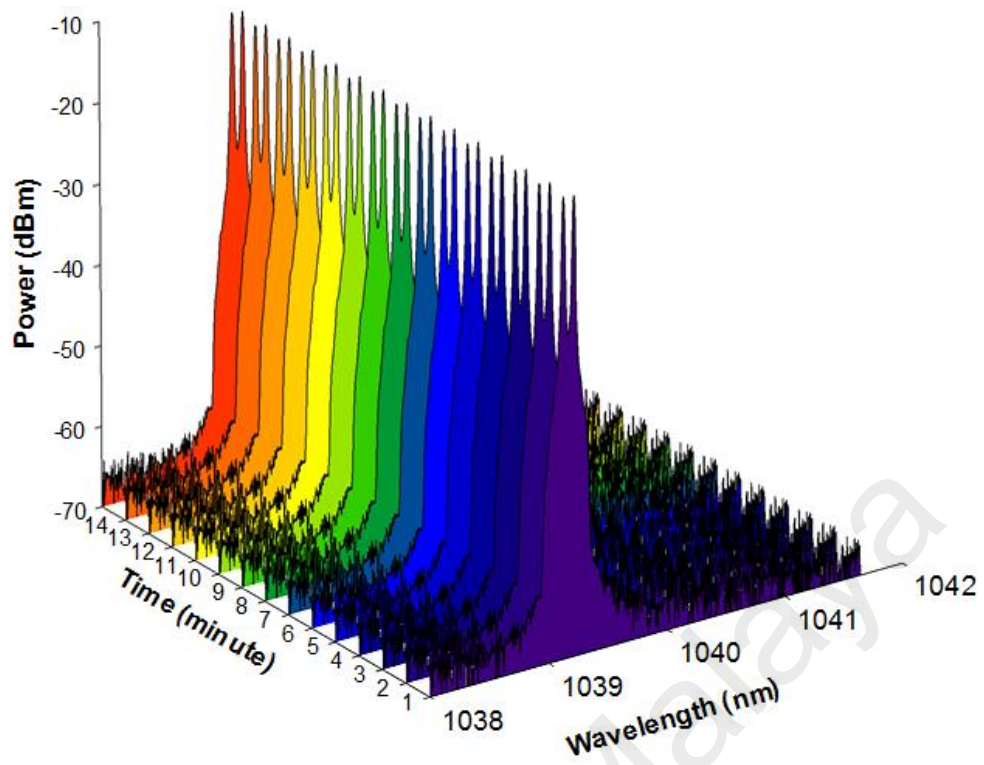


(a)

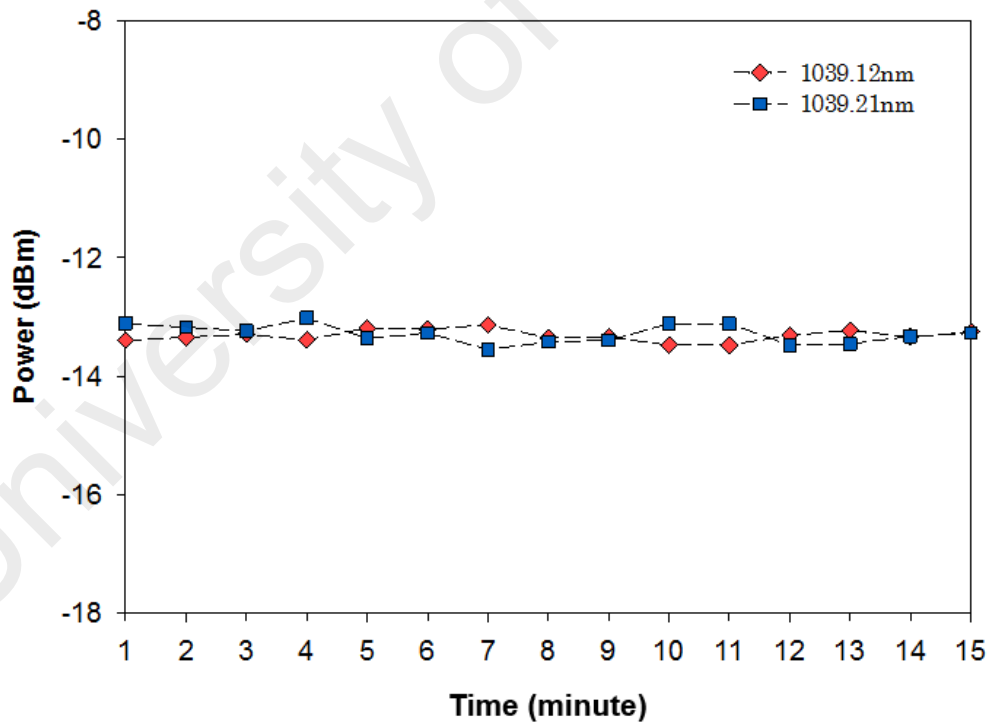


(b)

Figure 4.9: (a) Wavelength and (b) peak power stability test for wavelength spacing of 0.06 nm at $\lambda_1=1039.42$ nm and $\lambda_2=1039.48$ nm respectively

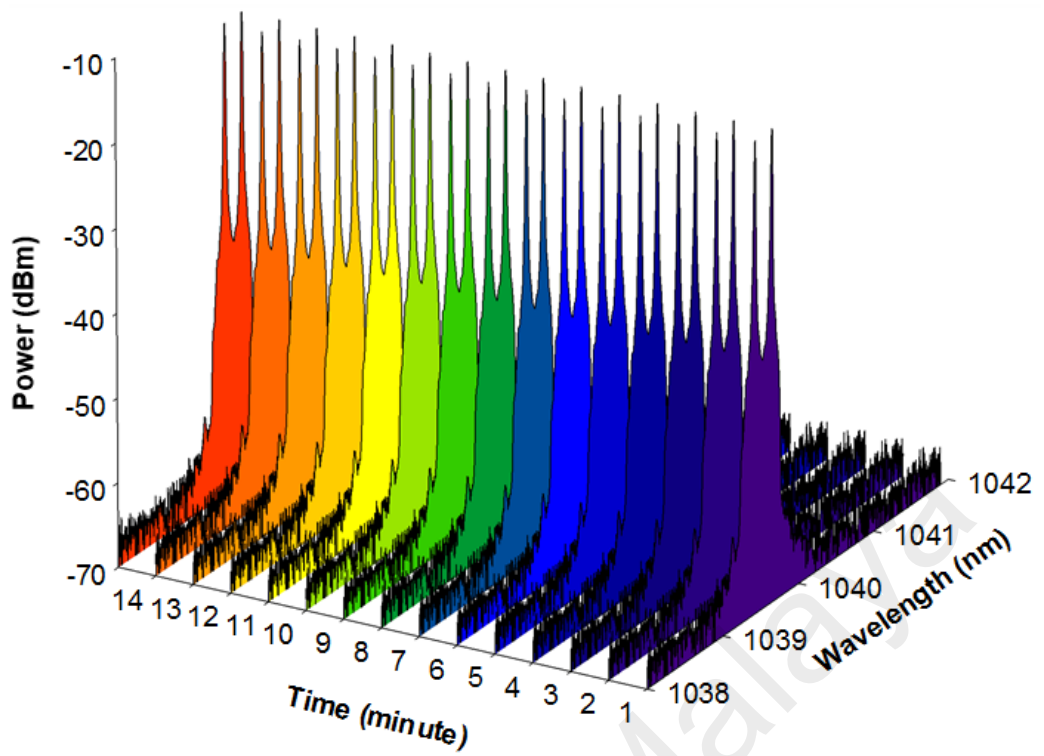


(a)

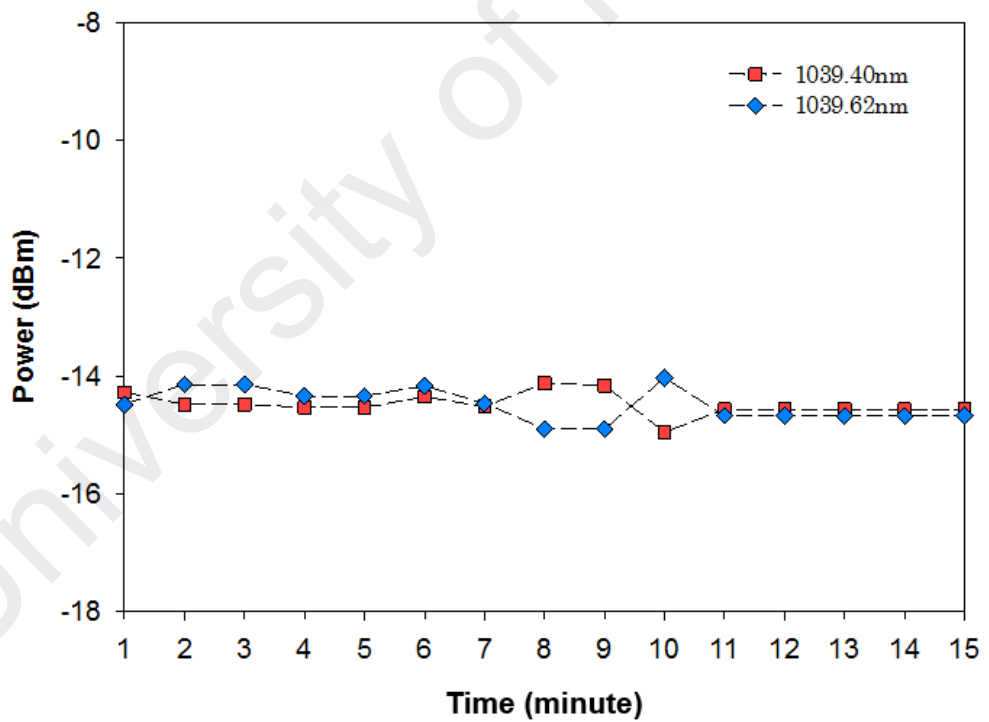


(b)

Figure 4.10: (a) Wavelength and (b) peak power stability test for wavelength spacing of 0.09 nm at $\lambda_1=1039.12$ nm and $\lambda_2=1039.21$ nm respectively



(a)



(b)

Figure 4.11 (a) Wavelength and (b) peak power stability test for wavelength spacing of 0.22 nm at $\lambda_1=1039.40$ nm and $\lambda_2=1039.62$ nm respectively

The wide tuning range of TBPF indicating the flexibility for tuning in various one-micron wavelength regions and narrow wavelength spacing by fine adjustment combination of PC and TBPF are the advantages of this proposed setup.

4.4 Tunable DWFL Using A Strain Technique

In this work, a simple YDF laser setup using microfiber based on Mach Zehnder Interferometer (MZI) is successfully employed for dual-wavelength operation. The strain technique is applied on the microfiber to generate tunable DWFL. The proposed setup also exhibits high SMSR of 48 dB, low power fluctuation that is lower than 0.6 dB and low wavelengths shifting of 0.01 nm resulting in stable operating condition in simple setup. The advantages of this setup are that the dual-wavelength generated using this technique has accurate distance at 2, 12, 87 and 190 μm by adjusting the micrometer drivers and these results are obtained consistently even when frequently repeated.

The design of tunable dual-wavelength generation setup is shown in Figure 4.12. A laser diode with centred wavelength of 974 nm (model LC96A74P-20R, Oclaro) is pumped to a 70 cm length of YDF (model DF1100, Fibercore) through the wavelength division multiplexing (WDM). A 980 nm port of WDM is spliced to LD while a common output port of WDM is attached to the ytterbium gain medium. The YDFA output is then linked to a polarization insensitive isolator to prevent undesirable feedback into the system. The isolator output is then linked to dual-tapered microfiber based MZI which is located between two xyz-translation stages (model MBT613/M,

Thorlabs) and then coupled to the input of 90:10 optical coupler (OC). The YDFL ring cavity setup is completed by channelling 90% output port of OC to a 1060 nm port of WDM while the 10% output port from optical coupler is then attached to the optical spectrum analyzer (OSA) (model AQ6373, YOKOGAWA) to measure the laser spectrum obtained in this experiment.

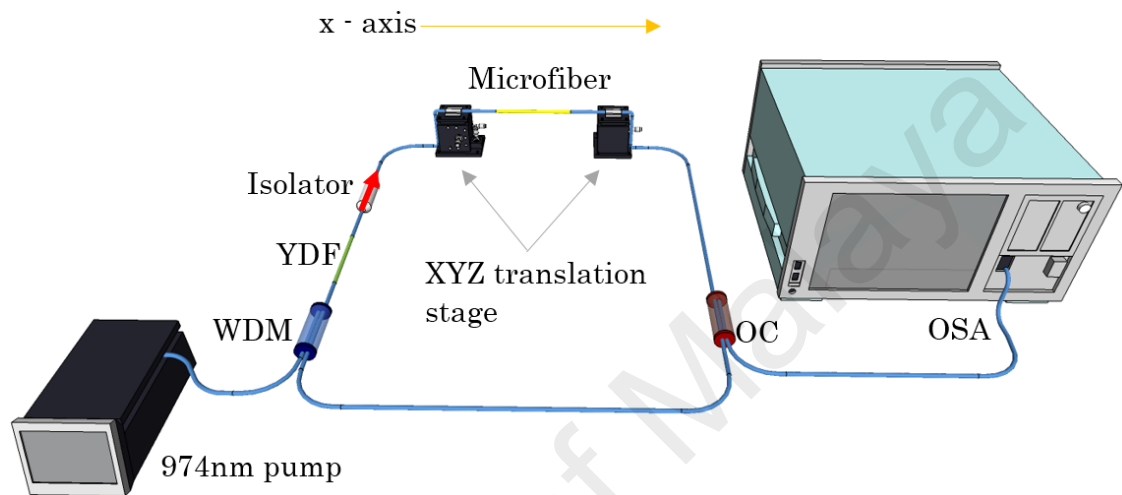


Figure 4.12: DWFL based strain technique proposed fiber ring setup

A Vaytran GPX-3000 series optical fiber processing workstation is used to fabricate dual-tapered microfiber based MZI where the specification of desirable design can be set accordingly. The cross section of fabricated dual-tapered microfiber with total length of 40 mm is shown in Figure 4.13 with taper waist diameter, taper transition length and taper waist lengths are 10 μm , 2 mm and 10 mm respectively. The transmission spectrum of unpolarized amplified spontaneous emission (ASE) with and without dual-tapered microfiber are depicted in Figure 4.14 at 175.4 mW. The interference comb (blue line) with free spectral range (FSR) of 8 nm is accountable for the lasing when the ring resonator is connected completely. Furthermore, when polarization state of laser in the ring cavity is controlled, lasing occurs at the peak of interference comb, and it is possible to switch the lasing wavelength. This will generate single or dual-wavelength laser.

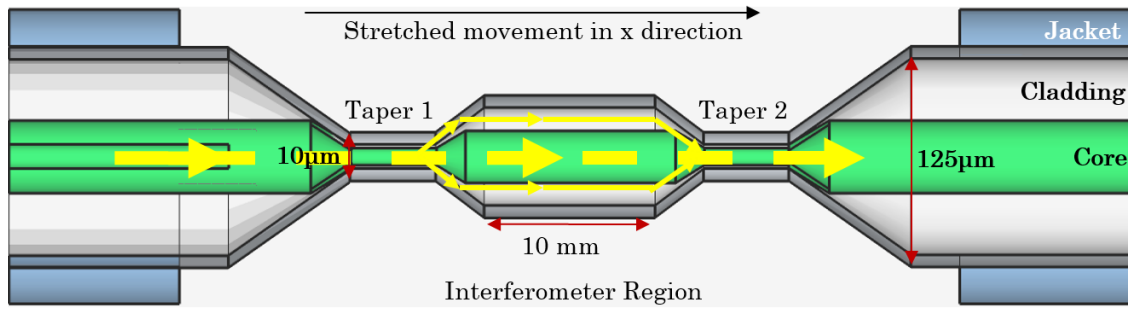


Figure 4.13: The cross-section of the microfiber MZI.

In this work, the lasing threshold is achieved at the pump power of 128.8 mW, as illustrated in the inset of Figure 4.14. The pump power can be increased up to 208.8 mW in order to obtain a very stable laser performance. Based on the strain technique setup, the tapered fiber is located between two xyz-translation stages that acts as a workstation where one stage holds the microber while another one moves the microfiber. A spectral filtering effect will possibly exist in the laser cavity. This spectral filtering effect shifted by tuning micrometer driver of the xyz-translation stage will move the platform stage horizontally, and eventually applying strain on the microfiber. This leads to the adjustment of birefringence to balance the gains and losses inside the ring cavity.

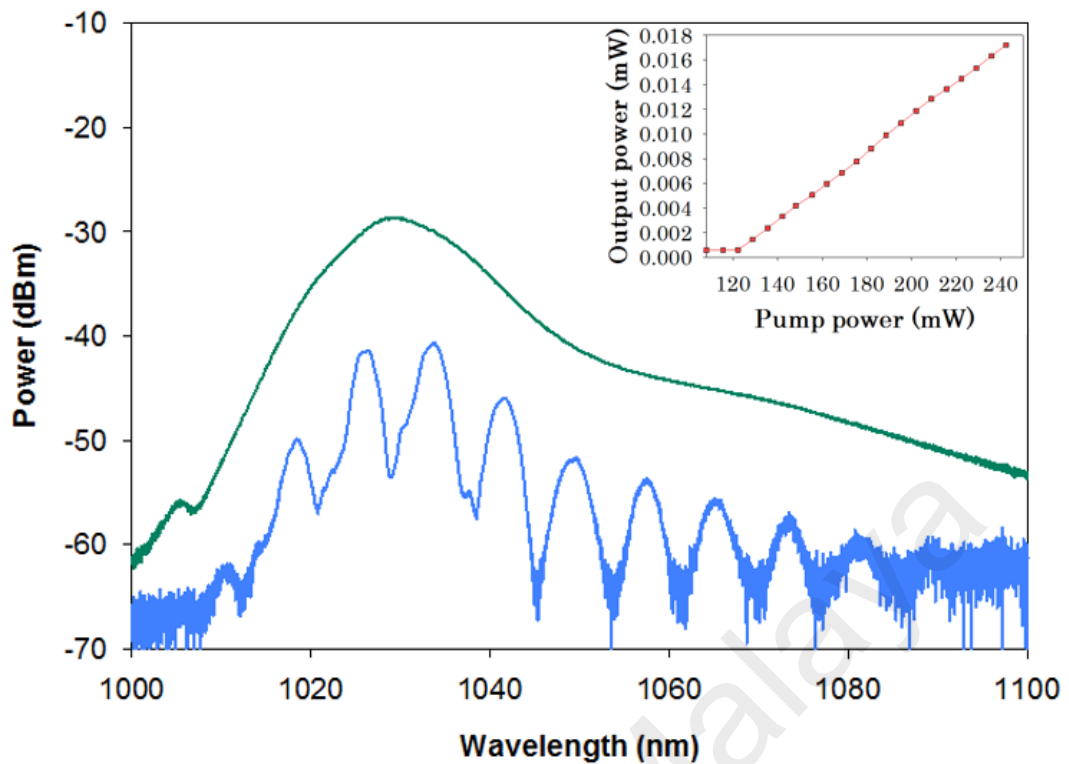


Figure 4.14: Amplified spontaneous emission spectrum of microfiber (blue) and excluded microfiber (green) at 175.4 mW. The lasing threshold at 128.8mW (inset)

Initially, at the starting point of zero, a single lasing wavelength with centered wavelength of 1030.40 nm and power of -15.54 dBm is obtained. Then, the micrometer is tuned accordingly to reach the maximum displacement of 350 μm . By doing this, the dual-wavelength spectrum is first achieved at the displacement of 2 μm as shown in Figure 4.15 with wavelength and power at 1029.07nm and -17.59 dBm, and 1036.95nm and -17.66 dBm respectively. The dual-wavelength's wavelength spacing is about 7.88nm due to the intra cavity birefringence, the 3dB linewidth is 0.03 nm and the side mode suppression ratio (SMSR) is about 48dB.

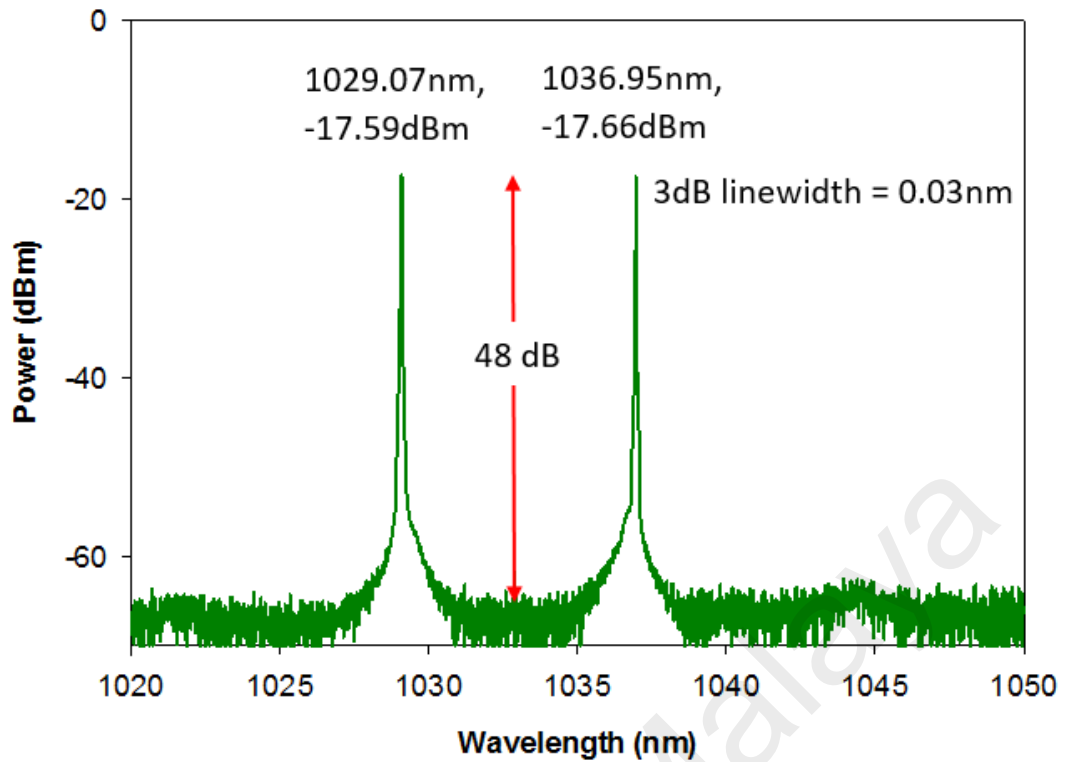


Figure 4.15: The dual-wavelength spectrum with SMSR of 48dB

By applying strain in this simple design of DWFL through fine-adjusting the micrometer driver, we obtained 4 sets of wavelength spacing for dual-wavelength profile in ring cavity length of 5 m at 2, 12, 87 and 190 μm displacements which corresponding strain applied onto fiber of 0.05×10^{-3} , 0.3×10^{-3} , 2.1×10^{-3} and 4.7×10^{-3} respectively. The results in Figure 4.16 revealed that SMSR exceeded 48 dB. Higher SMSR indicates higher stability of dual-wavelength laser achieved in this set up. Referring to Figure 4.16, the 4 sets of DWFL with various wavelength spacing are 7.88 nm from central wavelength of 1029.07 nm to 1036.95 nm, 7.62 nm at central wavelength from 1027.90 nm to 1035.52 nm, 11.59 nm from central wavelength of 1030.18 nm to 1041.77 nm, and 7.12 nm from central wavelength of 1034.76 nm to 1041.88 nm respectively.

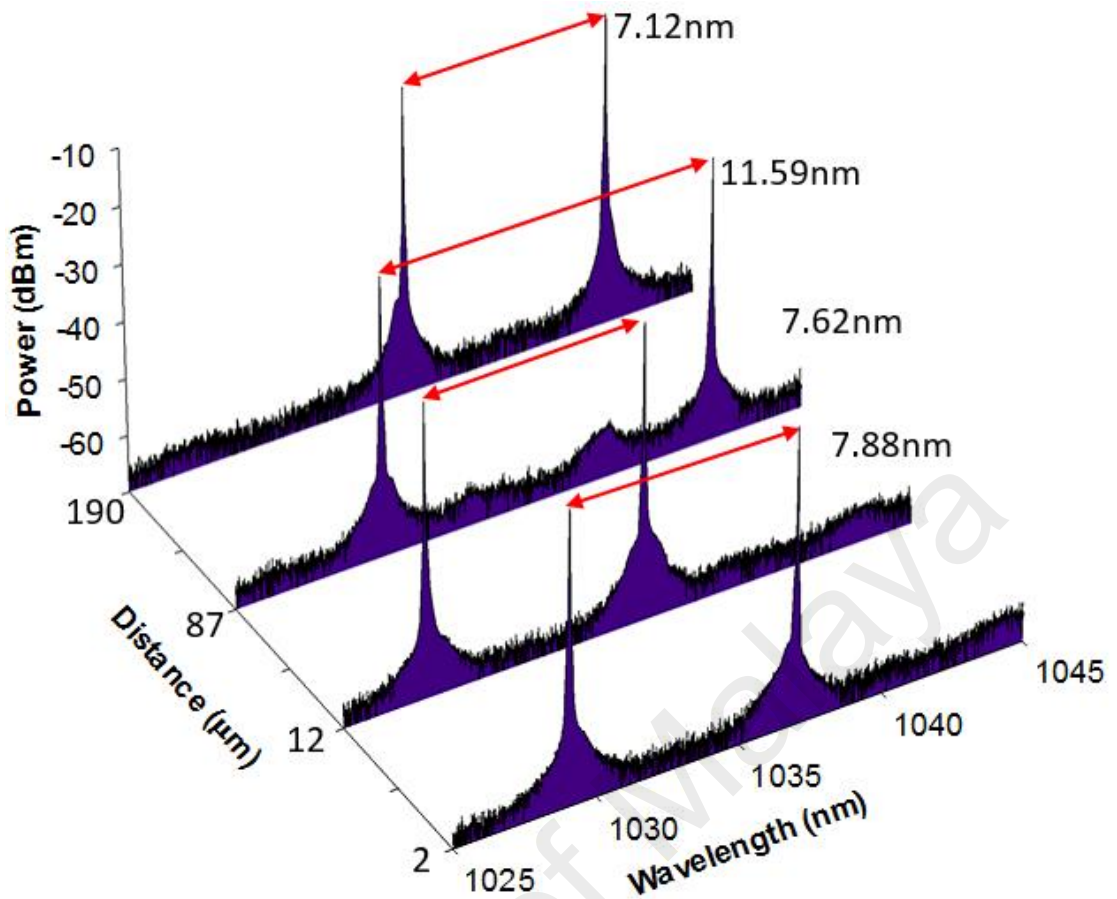


Figure 4.16: Set of dual-wavelengths with different wavelength spacing at certain distance from 2 μm to 190 μm

Moreover, every dual-wavelength set was tested for stability over time in room temperature. However, in this work, the stability result is shown for the narrowest wavelength spacing, which is 7.12 nm and the broadest wavelength spacing, which is 11.59 nm. Figure 4.17 (a) and Figure 4.18 (a) show the 20-minute stability scan of dual-wavelengths at the narrowest and broadest wavelength spacing, respectively. The maximum power fluctuation is less than ~ 0.6 dBm, and is illustrated in Figure 4.17 (b) and Figure 4.18 (b) where the wavelength shifting is less than 0.01 nm as shown in Figure 4.17 (c) and Figure 4.18 (c). The results of stability test showed that the dual-wavelength generated in this setup was very stable at room temperature.

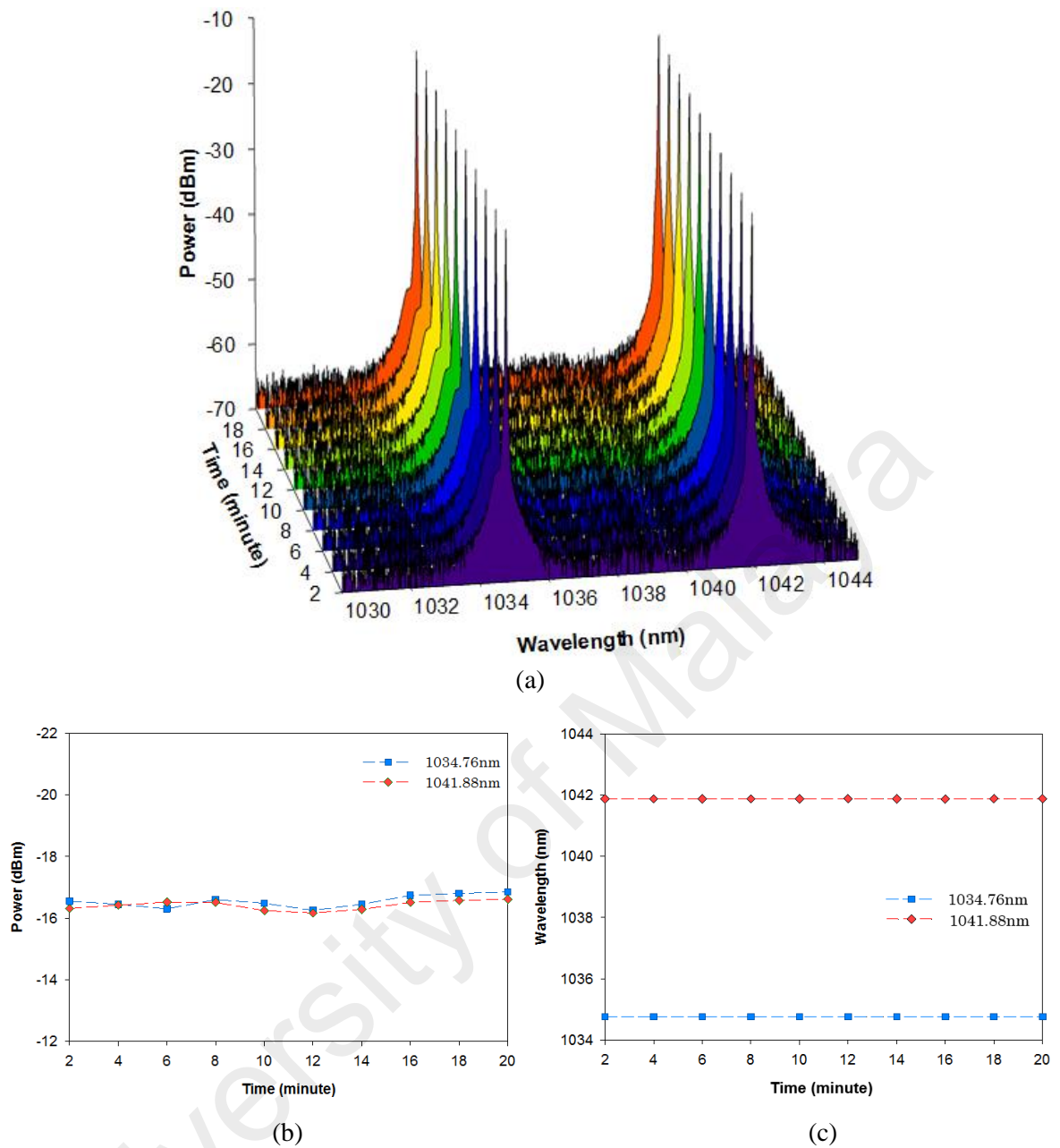


Figure 4.17: (a) Dual-wavelength (b) peak power and (c) wavelength shift stability test for wavelength spacing of 7.12 nm at $\lambda_1=1034.76$ nm and $\lambda_2=1041.88$ nm respectively

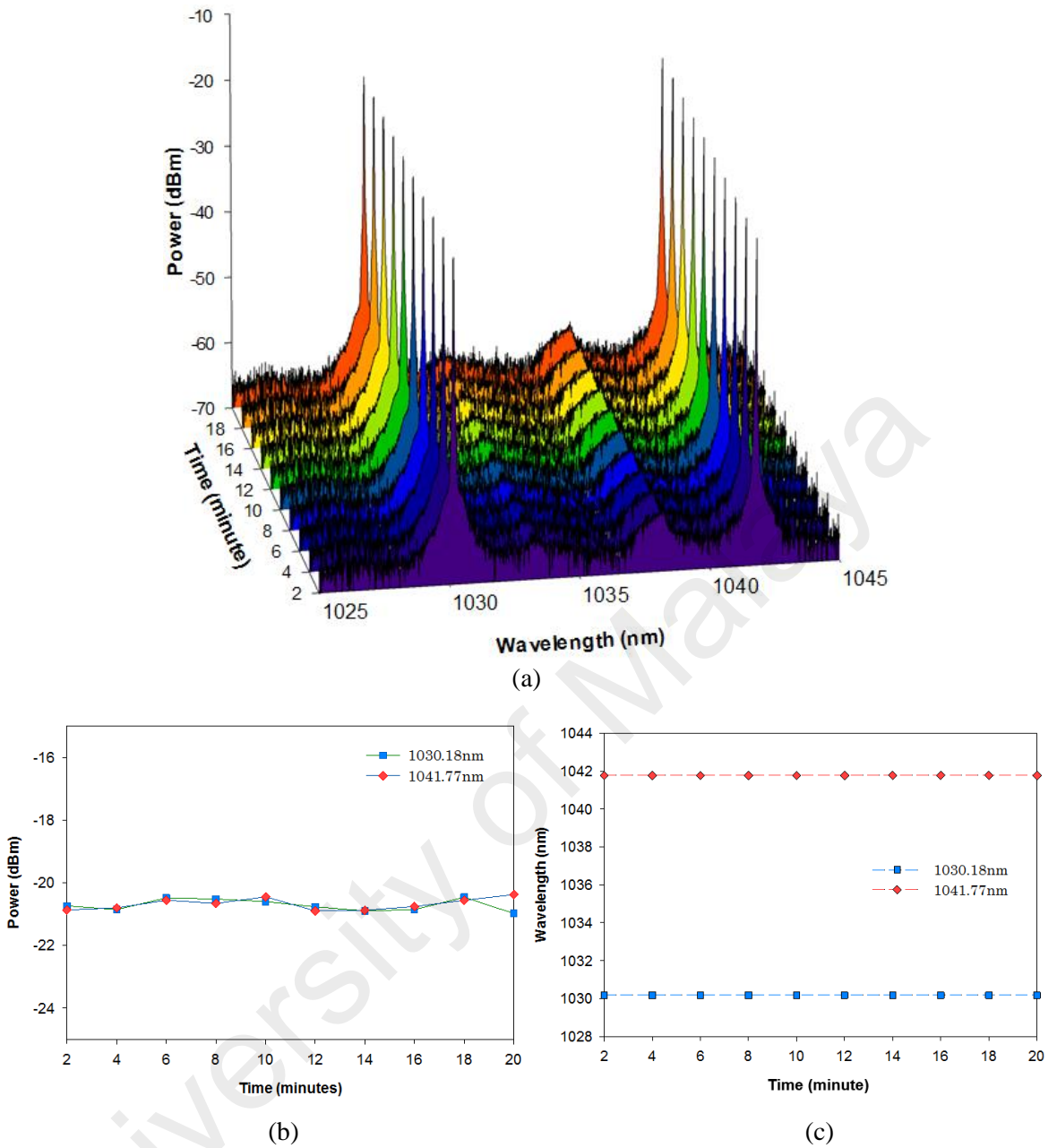


Figure 4.18: (a) Dual-wavelength (b) peak power and (c) wavelength shift stability test for wavelength spacing of 11.59 nm at $\lambda_1=1030.18$ nm and $\lambda_2=1041.77$ nm respectively

Additionally, the successful generation of DWFL is achieved by using the strain technique at certain distance and the results remain consistent after frequent repetition. This is the advantage of this study as compared to other designs of dual-wavelength generation by incorporating microfiber (Ahmad, H., Salim, M. A. M., Azzuhri, S. R., Zulkifli, M. Z., & Harun, S. W. 2015), photonic crystal fiber (Ahmad, H., *et al.*, 2013a; Chen, D., & Shen, L. 2007), and multimode fiber (MMF) (Cheng, J. Q., Zhang, L. L., Sharafudeen, K., Ma, Z. J., & Qiu, J. R. 2014) that adjusts the PC to get tunability of DWFL.

4.5 Tunable DWFL based on Side-Polished Fiber

In this work, a dual-wavelength operation using side polished fiber (SPF) is successfully demonstrated in simple YDF laser ring setup. By tuning the PC, the generation of tunable dual-wavelength lasing are achieved and the proposed setup also exhibits high SMSR of 50 dB, low power fluctuation that is lower than 0.9 dBm and less wavelengths shifting of 0.01 nm resulting in stable operation behavior in simple setup. There are 3 sets of DWFL at various wavelength spacings of 6.89 nm, 16.28 nm, and 22.16 nm.

Laser configuration of tunable dual-wavelength generation setup using side polished fiber as wavelength selective filter is shown in Figure 4.19. YDFA is formed together with a wavelength division multiplexer (WDM) coupler, with one input spliced to a laser diode with centred wavelength of 974 nm pump and the output linked to a 70 cm

YDF. The absorption rate of YDF (DF1100 Fibercore) at 977 nm is 1300 dB/m, with 5.7 dB/km of attenuation at 1200 nm. The cladding diameter is 124.8 μm , with a mode field diameter of 5.1 μm at operating wavelength of 1085 nm and a numerical aperture of 0.17. The output of YDFA is fusion-spliced to an optical insensitive isolator so that the ring laser operates unidirectionally. The output of isolator is then linked to side-polished fiber (SPF) with polished region of 17 mm and in turn, channeled to the polarization controller (PC) to manage the polarization state in the setup by adjusting three adjustable wave plates from the PC. The PC output is linked to the input port of 90:10 optical coupler and the 10% output port is attached to the optical spectrum analyzer model AQ 6373 Yokogawa, with 0.02 nm resolution whereas the 90 % output port is coupled back into the YDFA input through the 1060 nm port of WDM to form ring cavity.

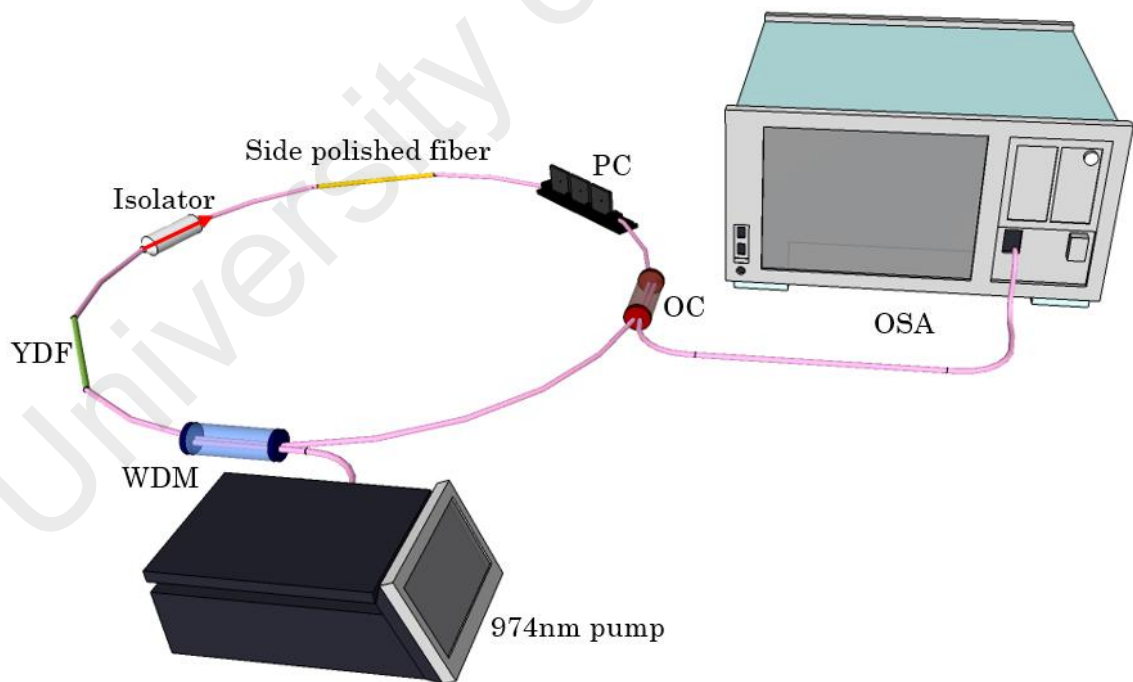


Figure 4.19: YDFL ring cavity experimental setup with a side-polished fiber

In this experiment, the lasing threshold is achieved at pump power of 62 mW, as depicted in Figure 4.20. The pump power reached up to 142.1 mW in order to obtain a very stable laser performance. A side-polished fiber was used as a wavelength selective filter (Zhang, S. X., *et al.*, 2014) to create a spectral filtering effect in laser cavity. This spectral filtering effect is responsible to generate dual- or multi-wavelength laser. Therefore, by adjusting the PC appropriately, the spectrum output of dual-wavelength laser obtained is as depicted in Figure 4.21, with wavelength and power at 1039.39 nm and -12.12 dBm, and 1046.28 nm and -12.50 dBm, respectively. The dual-wavelength's wavelength spacing is about 6.89 nm, which is due to the intra cavity birefringence. Whereas, the side mode suppression ratio (SMSR) is about 50 dB. A side-polished fiber is used to generate dual lasing beams. Therefore, SPF is suitable as wavelength selective filter.

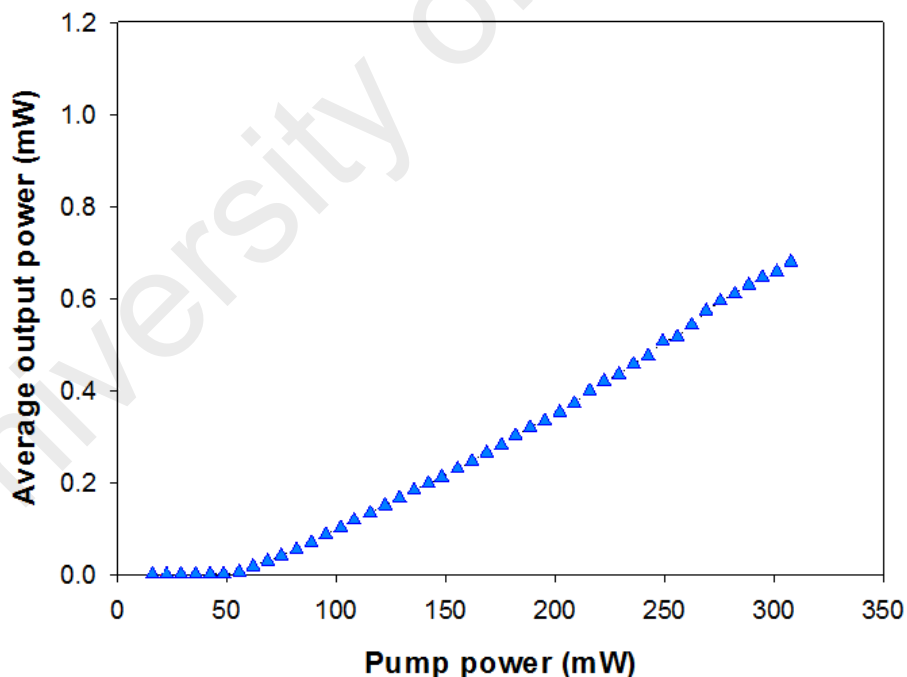


Figure 4.20: The lasing threshold for the side polished fiber setup in cavity ring

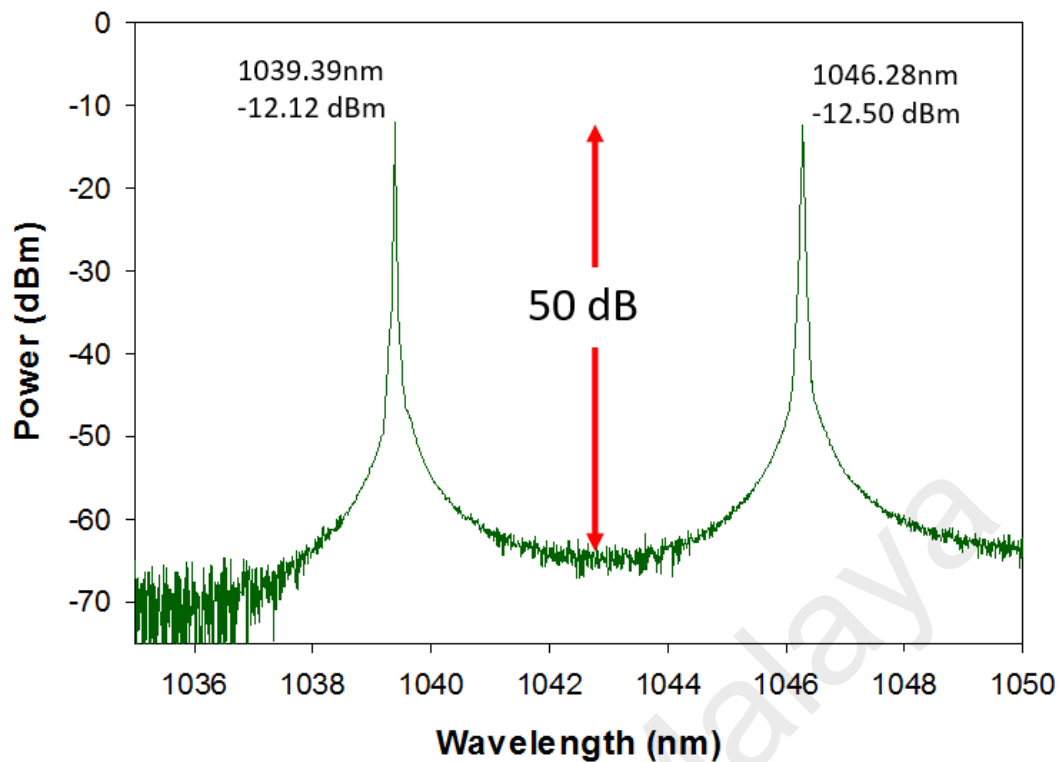


Figure 4.21: DWFL at 1039.39 nm and 1046.28 nm wavelength

In this experiment, the PC was adjusted to obtain dual-wavelength laser at the equal power level. Therefore, we obtained 3 sets of wavelength spacing for dual-wavelength profile, incorporating SPF in a simple cavity setup. Figure 4.22 shows all sets of dual-wavelength with different wavelength separation where the SMSR is observed to be ~50dB. Higher SMSR indicates higher stability of dual-wavelength laser achieved in this set up. Referring to Figure 4.22, there are 3 sets of DWFL with wavelengths spacing of 6.89 nm from central wavelength of 1039.39 nm to 1046.28 nm, 16.28 nm at central wavelength from 1042.07 nm to 1058.35 nm, and 22.16 nm from central wavelength of 1043.32 nm to 1065.48 nm respectively.

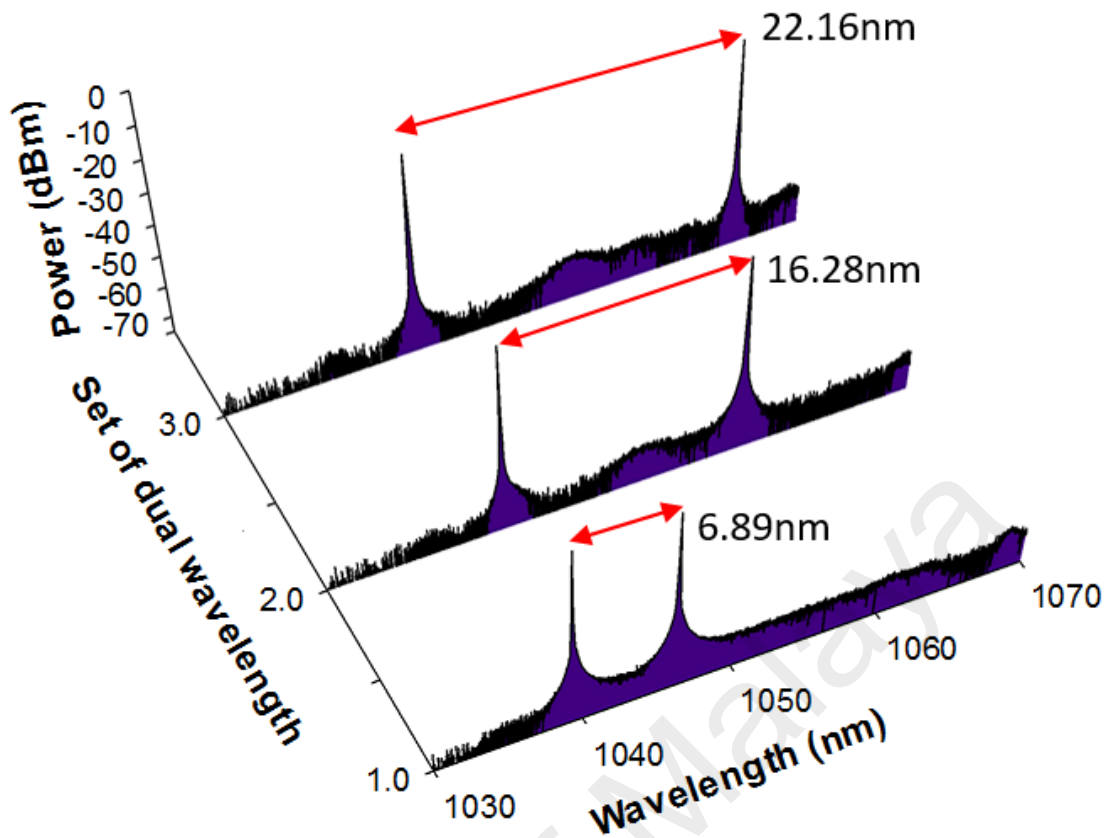
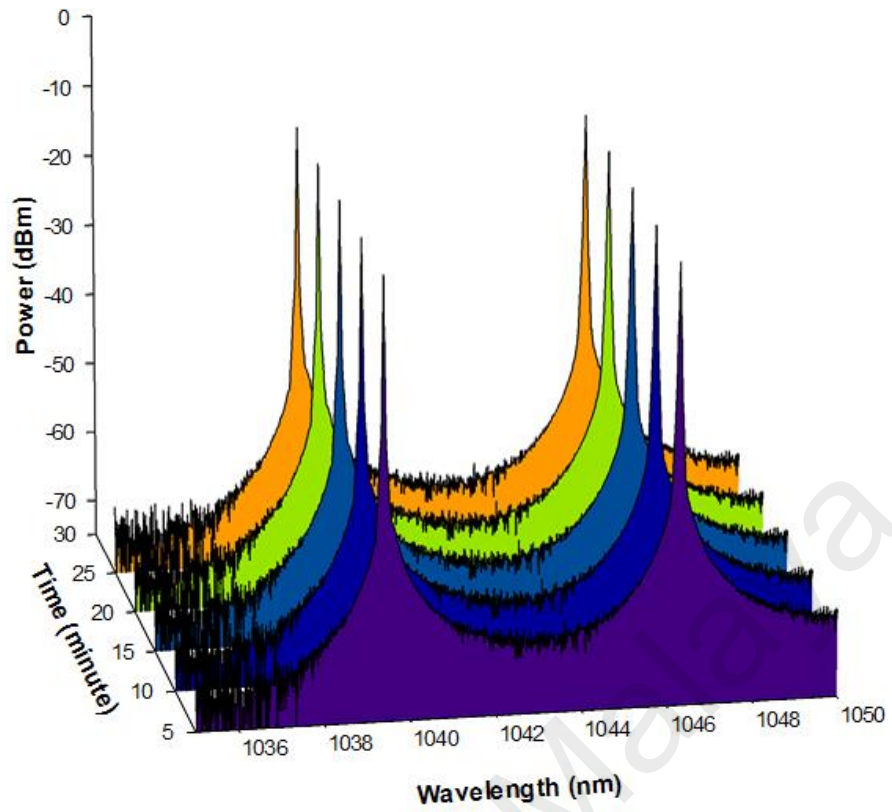
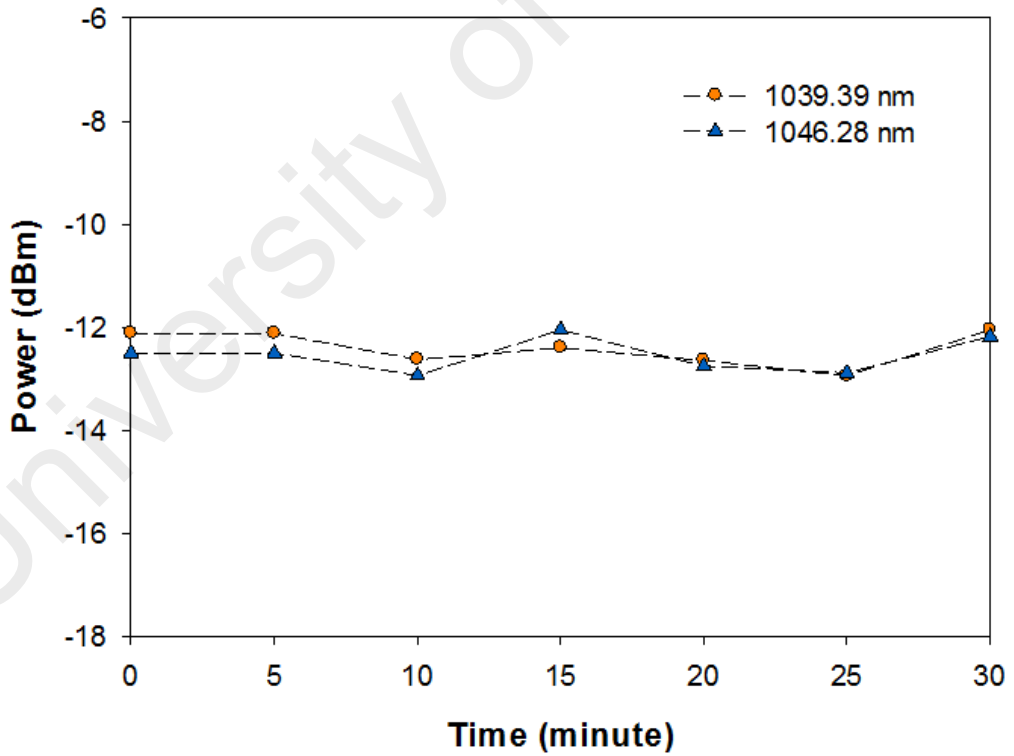


Figure 4.22: Dual-wavelengths spectrums with different wavelength spacing from 6.89 nm to 22.16 nm

Furthermore, all of the DWFL sets were tested for stability over time in room temperature. The stability result obtained for the narrowest wavelength spacing is 6.89 nm and the broadest wavelength spacing is 22.16 nm. Figure 4.23 (a), Figure 4.24 (a) and Figure 4.25 (a) illustrate the 30-minute stability scan of dual-wavelengths at 6.89 nm, 16.28nm and 22.16nm wavelength spacings respectively. The maximum power fluctuation of ~ 0.9 dBm is illustrated in Figure 4.23 (b), Figure 4.24 (b) and Figure 4.25 (b) respectively whereas the wavelength shift is less than 0.01 nm. The results of stability test showed that the dual-wavelength generated in this setup was very stable at room temperature.

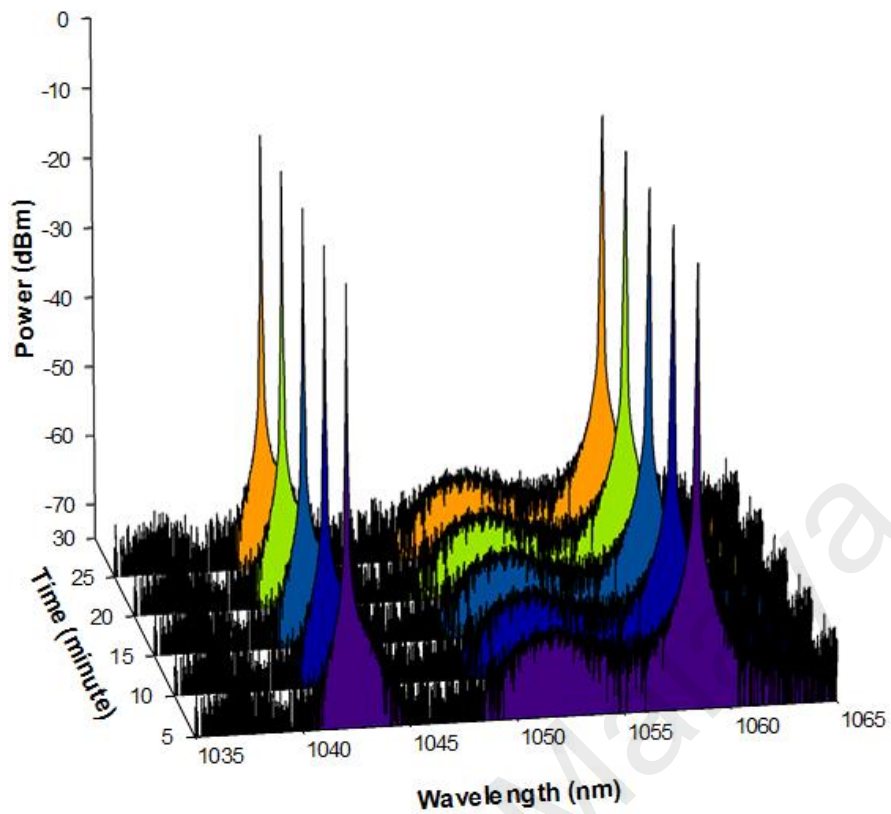


(a)

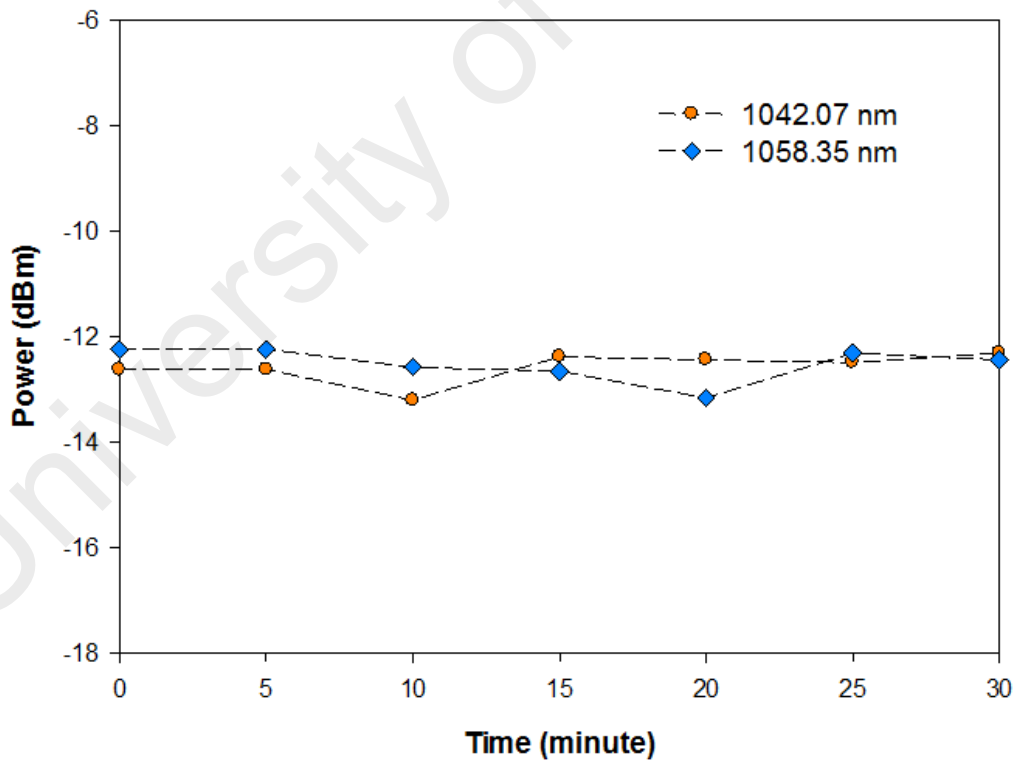


(b)

Figure 4.23: (a) Wavelength and (b) peak power stability test for wavelength spacing of 6.89 nm at $\lambda_1=1039.39$ nm and $\lambda_2=1046.28$ nm respectively

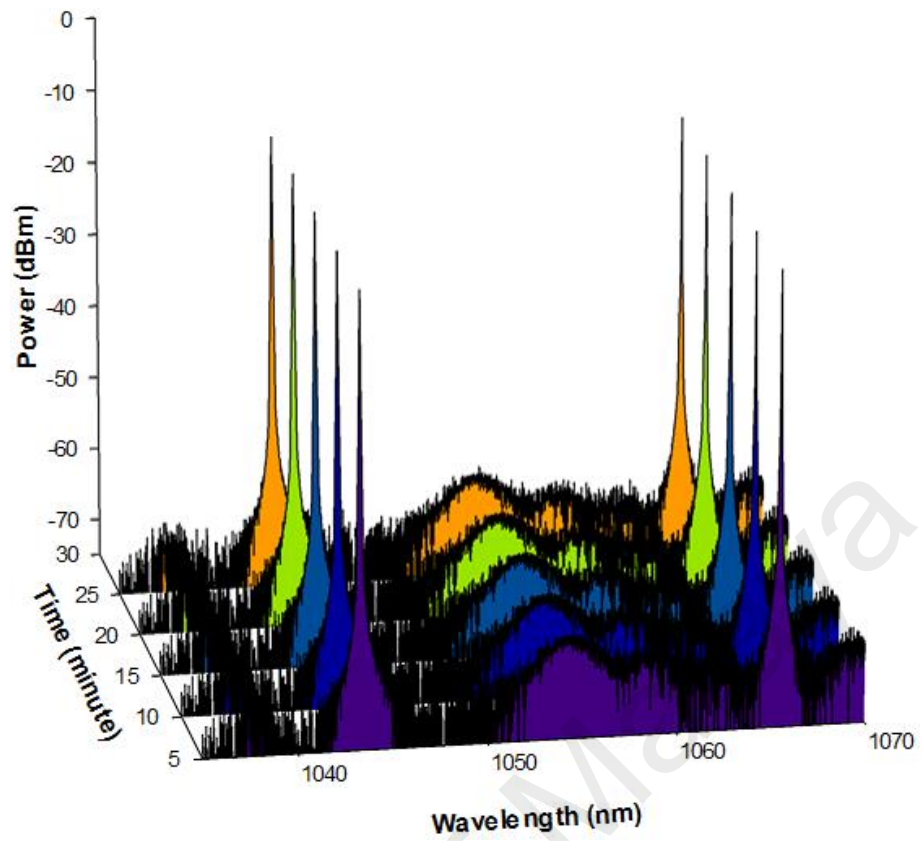


(a)

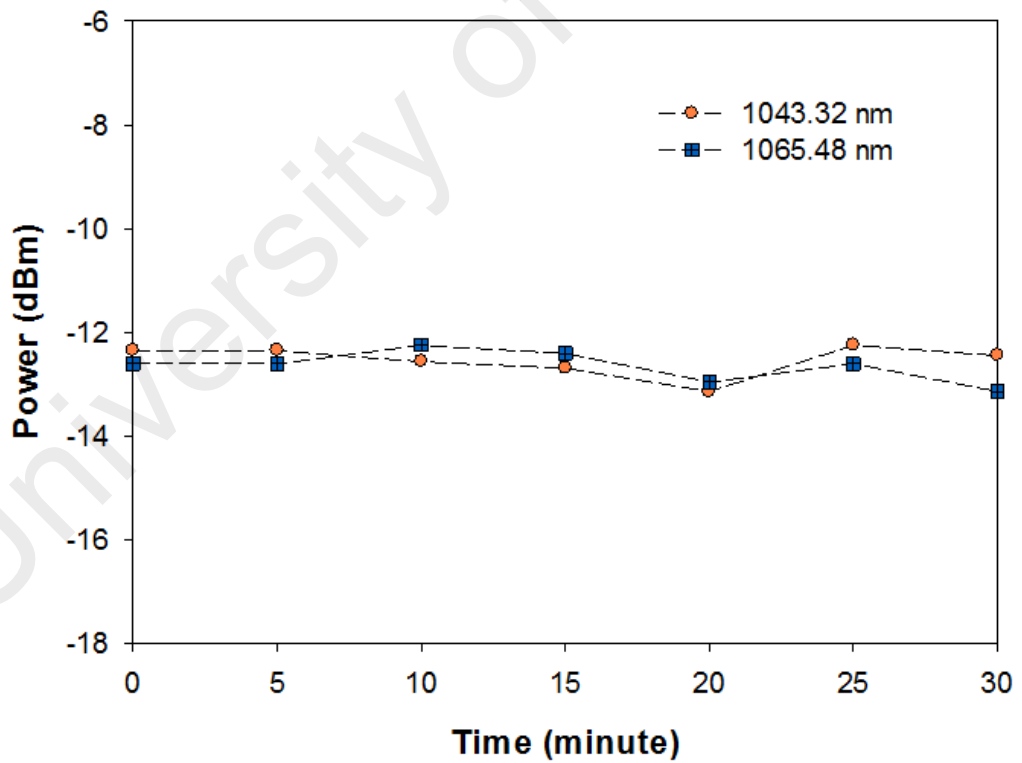


(b)

Figure 4.24: (a) Wavelength and (b) peak power stability test for wavelength spacing of 16.28 nm at $\lambda_1=1042.07$ nm and $\lambda_2=1058.35$ nm respectively



(a)



(b)

Figure 4.25: (a) Wavelength and (b) peak power stability test for wavelength spacing of 22.16 nm at $\lambda_1=1043.32$ nm and $\lambda_2=1065.48$ nm respectively

In this work, the dual-wavelength YDFL generation is demonstrated successfully. The tunability of dual-wavelength is achieved with three sets of wavelength spacing range centered at 6.89nm, 16.28nm, and 22.16nm. The SMSR was measured to be ~50dB and stable tunable dual-wavelength output less than ~0.9 dBm power fluctuation and less than 0.01 nm wavelengths shifting for a 30 minutes experiment period in room temperature.

4.6 Summary

In this chapter, the DWFL which employed YDF as a gain medium are demonstrated using two different wavelength selective filters, namely microfiber and side polished fiber. In the beginning, the dual-tapered microfiber MZI is demonstrated to generate stable dual-wavelength and single longitudinal mode operation. With regards to simple setup, lower cost of installation, and highly stable operation in room temperature are the key advantages in the one micron wavelength region. Then, the wide tuning range of TBPF and dual-tapered microfiber are both placed in the ring cavity to achieve narrow wavelength spacing by fine adjustment combination of PC and TBPF and the flexibility for tuning in various one-micron wavelength regions are the advantages of this proposed setup. Furthermore, by applying strain onto dual-tapered microfiber, the successful generation of DWFL is achieved and the results remain consistent after frequent repetition indicating a

precisely dual-wavelength spectrum. The side polished fiber is then used as a wavelength selective filter to generate DWFL in a low cost, simple setup and highly stable in room temperature.

The next chapter will describe the generation of dual-wavelength pulse laser by incorporating microfiber or side polished fiber as wavelength selective filters that have been explained in this chapter.

University of Malaya

CHAPTER 5: DUAL-WAVELENGTH PULSE LASER

5.1 Introduction

The dual-wavelength pulse laser has captured the interest of researchers in photonics due to its wide range of applications such as pump-probe processes, spectroscopy nonlinear frequency conversion (Zhao, Y., *et al.*, 2013), microwave or terahertz generation (Feng, S., *et al.*, 2013; Vodopyanov, K., *et al.*, 2006). Dual-wavelength pulse laser is efficiently generated by Q-switching operation where in this work, we prefer passively Q-switched because of its advantages like better flexibility and compactness, and low cost of deployment (Luo, Z., *et al.*, 2010; Wang, Z. T., Chen, Y., Zhao, C. J., Zhang, H., & Wen, H. C. 2012).

Passively Q-switching YDFL with its uniqueness and compactness has introduced an extensive variation of laser applications and various techniques to generate passive Q-switching in one micron region have been reported. One of the effective methods is to use an optical material. In this case, saturable absorber (SA) is the optical material used. For the past few decades, several SAs have been discovered and demonstrated as optical modulators to generate pulse laser operation. SESAM, for example, has become the most favoured SA due to its stability and flexibility. The expensive fabrication, complex packaging and fabrication (Ahmad, H., Salim, M. A. M., Azzuhri, S. R., Soltanian, M. R. K., & Harun, S. W. 2015; Ahmad, H., Salim, M. A. M., Soltanian, M. R. K., Azzuhri, S. R., & Harun, S. W. 2015), and narrow bandwidth (Schmidt, A., *et al.*, 2008) are the disadvantages of SESAM and prompted to explore other potential SAs such as carbon nanotubes (CNTs) ((Ahmad, H., Semangun, J. M., *et al.*, 2015; Gao, Y., *et al.*, 2013; Schmidt, A., *et al.*, 2008) and graphene (Liu, J., Wu, S. D., Yang, Q. H., &

Wang, P. 2011; Zhang, L., *et al.*, 2012) in Q-switching technology. Their interesting features such as simple fabrication process and ultrafast recovery time renders them as more suitable SAs for pulse laser application. However, CNTs suffers from a complex bandgap control (Bao *et al.*, 2009) that prevents saturable absorption at certain wavelength while graphene suffers from a small optical absorption and modulation depth (Bao *et al.*, 2009). Therefore, an extensive research has been deployed to discover new SA with features such as low-cost fabrication process, wavelength-independent, large modulation depth and high threshold damage would be ideal characteristics for an efficient SA.

In this work, we demonstrated pulse laser using a transition metal chalcogenides (TMD) which is MoSe₂, BP, TiO₂ and ZnO as new SAs. Wavelength selective filter is used in the ring cavity to generate DWFL. Therefore, the dual -wavelength Q-switched laser is designed and demonstrated in this work.

5.2 Q-switched DWFL based microfiber using MoSe₂ as SA

Recently, TMD based optical materials such as molybdenum diselenide (MoSe₂) are widely used in researches. In this work, we have achieved a dual-wavelength Q-switched YDFL using MoSe₂ film SA, which is a selenide-based TMDs. The Q-switched dual-wavelength laser was obtained by employing a microfiber as wavelength selective filter. The dual-wavelengths were centered from 1035.8 to 1040.2nm with wavelength spacing of 4.4 nm. The pulse repetition rates obtained from the setup ranged from 15.3 to 35.2 kHz thus demonstrating the MoSe₂ characteristic of saturable absorption for YDFL Q-switching operation.

In this experiment, the preparation and fabrication of few layers MoSe₂ were explained in chapter 3. The dual-detector measurement setup had been used to measure the saturable absorption of MoSe₂ SA thin film in chapter 3 as well. As a result, 13.5% modulation depth and ~0.03MW/cm² saturable intensity of MoSe₂ obtained in this work are as illustrated in Figure 5.1.

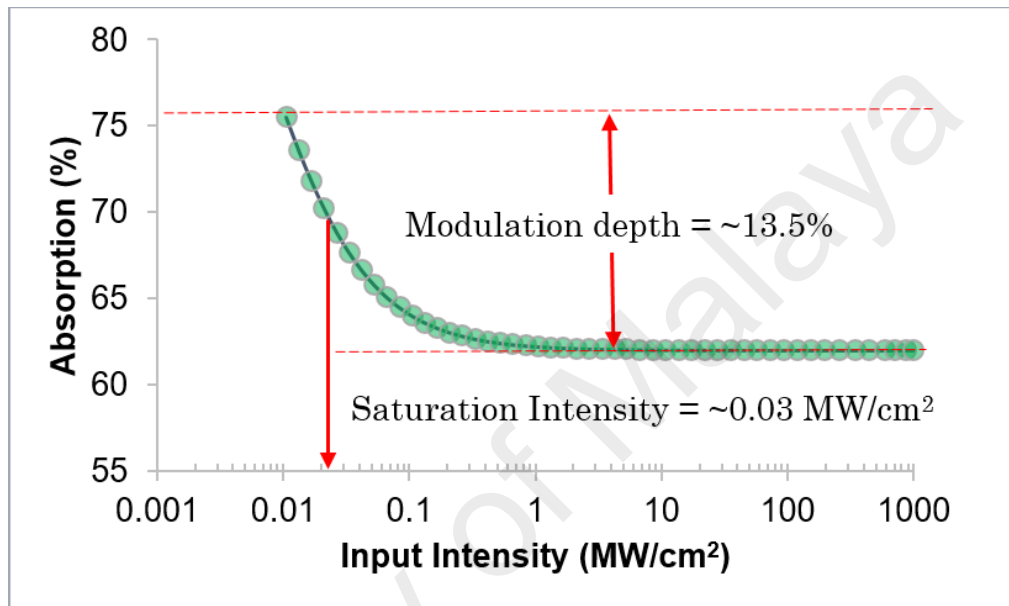


Figure 5.1: The characteristic of MoSe₂ saturable absorber

The configuration of DWFLs Q-Switched based MoSe₂ using a dual-tapered microfiber as wavelength selective filter is given schematically in Figure 5.2. The YDF comprising a length of 70 cm YDF model DF1100 Fibercore, with peak absorption of 1300 dB/m at 977 nm was utilized as a gain medium. Then, a 974 nm centered wavelength laser diode (LD) with maximum output power of 600mW model LC96A74P-20R, Oclaro was employed as pumping source for YDFL and was linked to a 980 nm port of wavelength division multiplexing (WDM). The WDM's common port was attached to the 70 cm-YDF, and then attached to an isolator to assure single direction of laser propagation. The isolator output was next channeled to the dual-taped microfiber, which works to generate dual-wavelength laser (H Ahmad, Salim, Azzuhri,

Jaddoa, & Harun, 2016). The output of the microfiber was then connected to MoSe₂ film saturable absorber which was located between the fiber ferrules, and then linked to input port of 90:10 optical coupler 1 (OC1). The 90% portion of the optical coupler was channeled to 1060 nm port of WDM to complete the cavity ring configuration. The 10% portion extracted from the cavity was used to analyze the signal behavior and was later linked to input port of 50:50 optical coupler 2 (OC2) which divides the generated pulse into two section. Therefore, the Q-switched signal can be observed simultaneously with one portion through an optical spectrum analyzer (OSA) model AQ6373 YOKOGAWA and another portion with a fiber optic photo detector connected to a digital oscilloscope (YOKOGAWA DLM2054). In addition to that, a 9kHz-7.8GHz frequency spectrum analyzer model MS2683A Anritsu and an optical power meter (THORLABS) was used to characterize the extracted signal generated from the cavity.

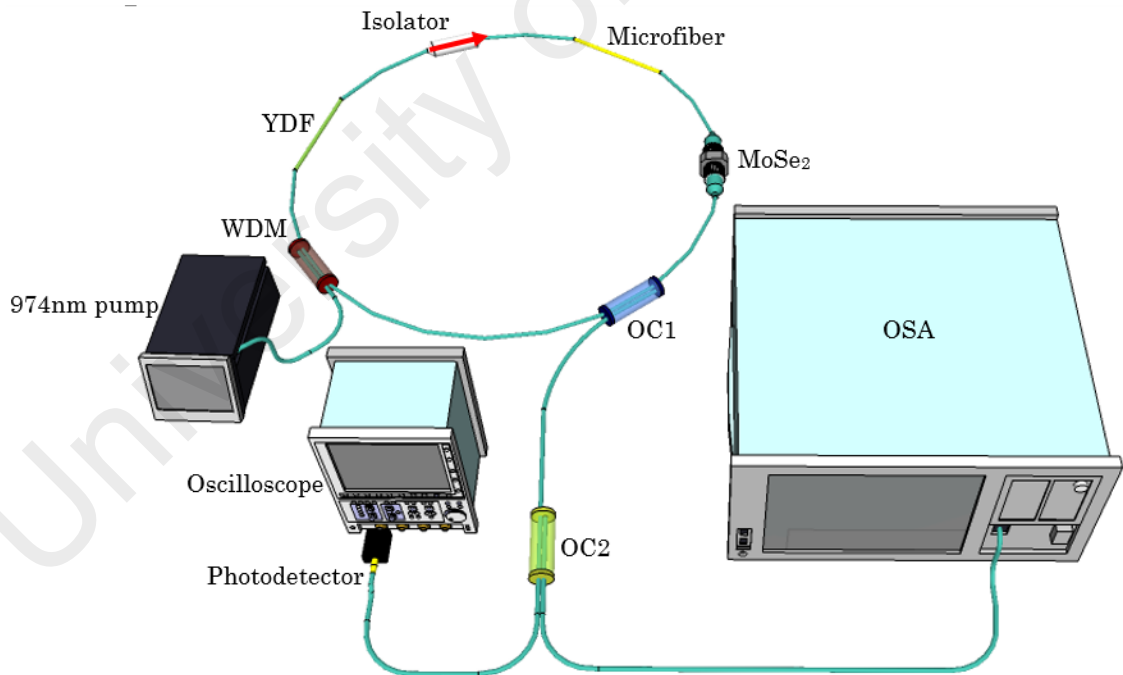
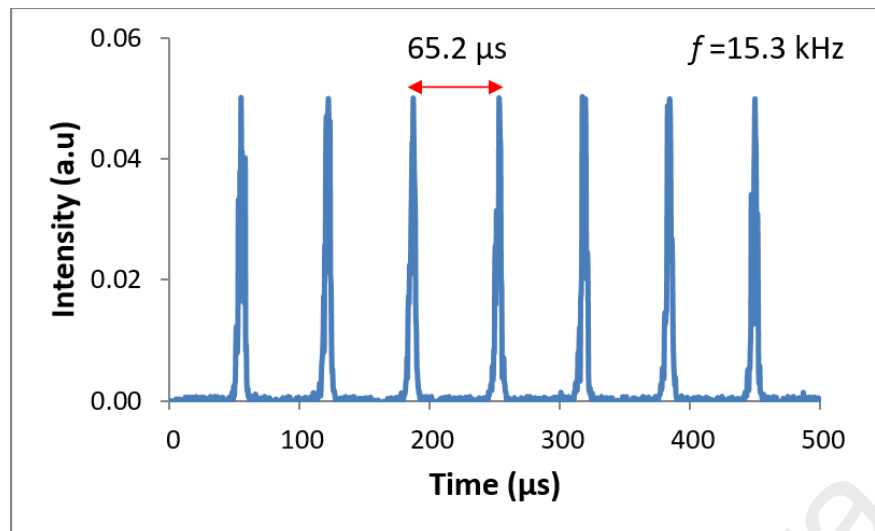
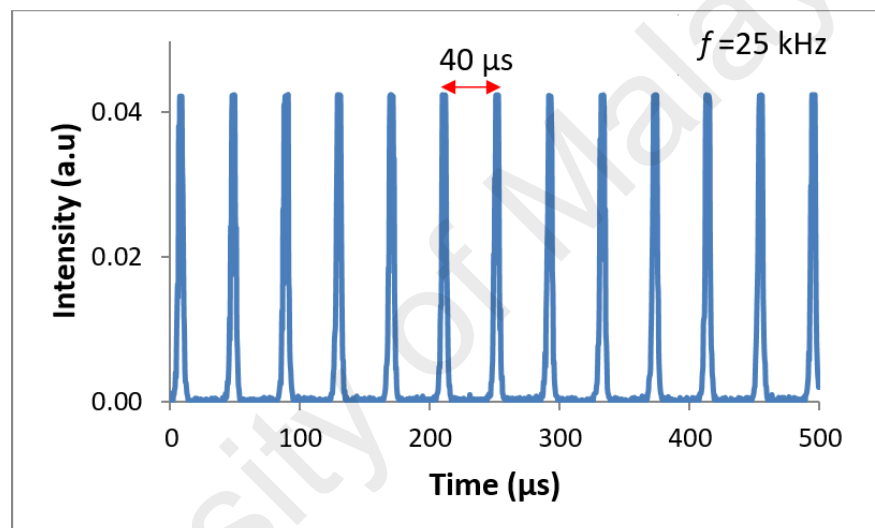


Figure 5.2: Configuration of MoSe₂ based Q-switched dual-wavelength in YDFL

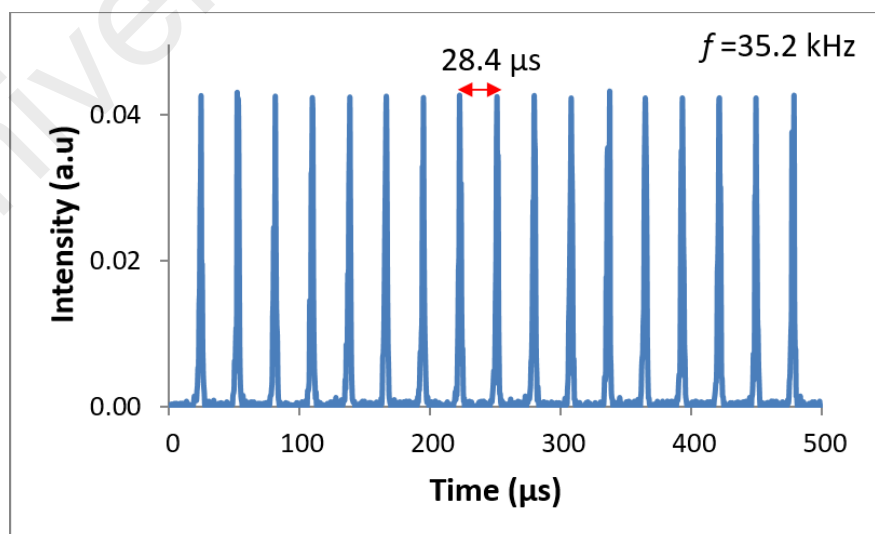
At 166.6 mW of pump power, initial observation of Q-switching mode was achieved with minimal repetition rate of 15.3 kHz, as illustrated in Figure 5.3 (a). Then, the pump power was steadily increased to 209.7mW and 261.2mW, the stable pulse trains with increasing repetition rate from 15.3 kHz to 25 and 35.2 kHz were monitored from the oscilloscope trace as illustrated in Figure 5.3 (b) and Figure 5.3 (c) respectively. The higher repetition rate is a common response for Q-switched once the pumped power was increased. In addition to that, the period was decreasing as the pump power increased, with a period of 65.2 μ s at 166.6 mW, and further decreasing to 28.4 μ s at 261.2 mW pump power. Furthermore, the pulse duration was also decreasing as a result of the gain compression (Herda, R., Kivistö, S., & Okhotnikov, O. G. 2008).



(a)



(b)



(c)

Figure 5.3: Output pulse trains with different frequency and period by increasing pump power at (a) 166.6 mW, (b) 209.7 mW and (c) 261.2 mW.

The stable output spectrum at 231.6mW as shown in Figure 5.4 (a), has a central dual-wavelength lasing at 1035.8nm and 1040.2nm with respective output power of -27.9 and -28.5 dBm. The corresponding pulse train, taken from the oscilloscope trace at 231.6 mW pump power with 29.4 kHz repetition rate is represented in Figure 5.4 (b). Figure 5.4 (c) illustrated the measured pulse width of 2.2 μ s, taken from the full width at half maximum (FWHM). Radio frequency spectrum analyzer (RFSA) was employed to observe the frequency domain traces as depicted in Figure 5.4 (d) with 29.4 kHz fundamental harmonic frequency (inset) and 48 dB peak-to-pedestal ratios. Furthermore, in Figure 5.4(d), no spectral modulation was recorded via RF output spectra, demonstrating the steady pulse repetition rate in the proposed setup.

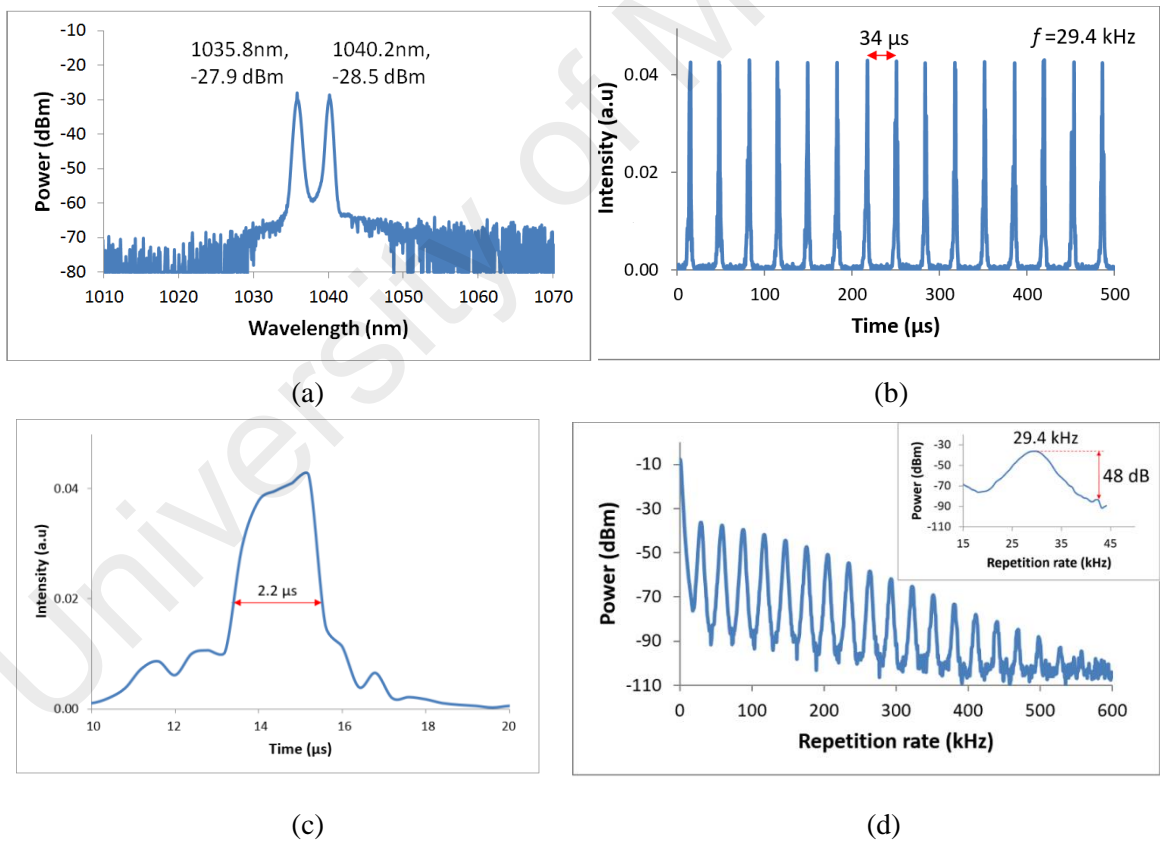
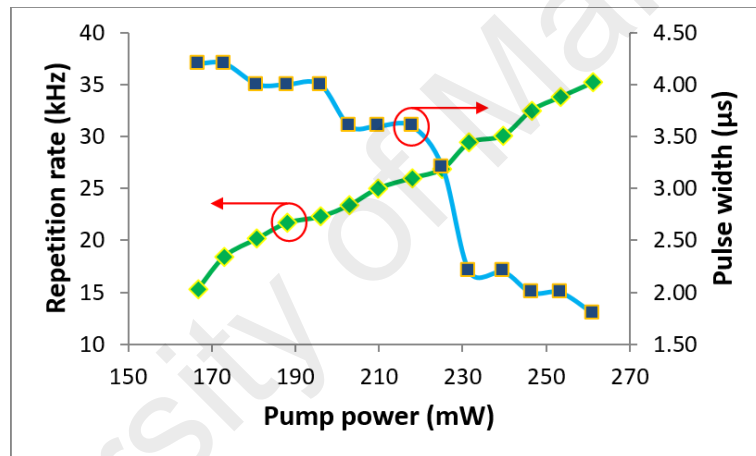
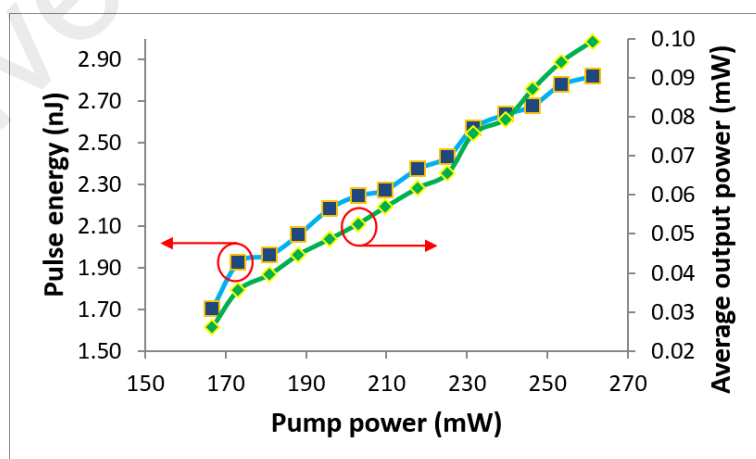


Figure 5.4: The centered dual-wavelength spectrum at 1035.8 nm and 1040.2 nm, b) Q-switched output pulse train with 34 μ s period, c) 2.2 μ s pulse width and (d) 29.4 kHz fundamental of RF spectra at pump power of 231.6 mW

Figure 5.5 (a) recorded the pulse duration and pulse repetition rate against the pump power of 166.6 mW until 261.2 mW. The Q-switched repetition rate increased from 15.3 kHz until 35.2 kHz while pulse width decreased from 4.2 μ s to 1.8 μ s. Nevertheless, as shown in Figure 5.5 (b), average output power and pulse energy were also computed and were increased as we raised the pump power. Moreover, the highest average output power was recorded at 0.1 mW. Whereas, the highest pulse energy obtained was 2.8 nJ at 261.2 mW maximum pump power. These results can be improved by utilizing a double-clad gain fiber in the ring setup (Zhou, D. P., Wei, L., Dong, B., & Liu, W. K. 2010).



(a)



(b)

Figure 5.5: (a) The repetition rate and pulse width and (b) the average output power and pulse energy against pump power.

We have successfully achieved the dual-wavelength Q-switched YDFL using MoSe₂ film as SA. The stable dual-wavelength Q-switching operation was centered at 1035.8 nm and 1040.2 nm. The frequency range from 15.3 kHz to 35.2 kHz with shortest pulse width and highest pulse energy were reported to be 1.8 μs and 2.8 nJ respectively. We anticipate that the findings obtained from this work will encourage advance development in passively Q-switching using TMD materials.

5.3 Q-switched DWFL based microfiber using BP as SA

Black Phosphorus (BP) is another 2D material that has the most stable allotrope of phosphorus with its unique properties present in highly anisotropic electric conductance and strain-controlled anisotropic electric mobility (Churchill, H. O., & Jarillo-Herrero, P. 2014; Koenig, S. P., *et al.*, 2014; Xia, F., *et al.*, 2014). BP has a layer-dependent direct band-gap that increases with the decreasing quantity of layers from 0.3 eV in bulk state to 2 eV in monolayer BP (Churchill, H. O., & Jarillo-Herrero, P. 2014; Xia, F., *et al.*, 2014). The characteristic of narrow gap of multilayer BP makes it a suitable SA as compared to that of graphene's and TMD materials's with zero band-gap and large band-gap, respectively (Koenig, S. P., *et al.*, 2014). Laser pulse generation using BP materials were first reported at the wavelength of 1.5 micron and two-micron region by depositing BP particles onto side-polished fiber while adhering to the scotch tape (Jiang, T., *et al.*, 2015). Besides that, there are various techniques that uses BP as SA such as deposited around the microfiber (Luo, Z. C., *et al.*, 2015), mechanical exfoliation method (Chen, Y., *et al.*, 2015) and BP gold-film mirror in Yb:LuYAG bulk laser (Kong, L., *et al.*, 2015), which is the only available Q-switched reported in the one-micron region.

Therefore, in this section we use the BP as a SA for dual-wavelength passively Q-switching in the one-micron region by mechanical exfoliation method. The dual-wavelength Q-switched operation was carried out using dual-taped microfiber as a wavelength selective filter centered at 1036.5 nm and 1039.2 nm. The pulse repetition rates obtained from the setup ranged from 6.5 to 62.5 kHz with shortest pulse width of 1.2 μ s and maximum pulse energy of 4 nJ.

Mechanical exfoliation method which is also known as ‘scotch-tape method’ was used to prepare the BP based SA (Chang, Y. M., *et al.*, 2010) and had been fabricated previously as explained in chapter 3. Mechanical exfoliation is advantageous with its simplicity, as the whole fabrication process does not involve any complex chemical treatment and expensive devices. On the other hand, this method lack of ability to control the desired thickness (number of layers) of BP based SA. Thus, the performances of BP was insufficient for passive mode locking.

The dual-detector measurement setup was used to characterize the saturable absorption of BP SA. The saturable intensity and modulation depth of BP were reported to be $\sim 0.03 \text{ MW/cm}^2$ and 30% respectively as shown in Figure 5.6. The modulation depth of this work is larger as compared to other similar reports such as 19.5% and 16.1% (Jiang, T., *et al.*, 2015), 18.55 and 8.1% (Chen, Y., *et al.*, 2015), 7.8% (Kong, L., *et al.*, 2015) and 3.31% (Park, K., *et al.*, 2015). The higher modulation depth of BP is due to the number of thick BP layer with multi-layers thickness larger than 10 layers (Chen, Y., *et al.*, 2015) and its ability for efficient optical absorption (Jiang, T., *et al.*, 2015).

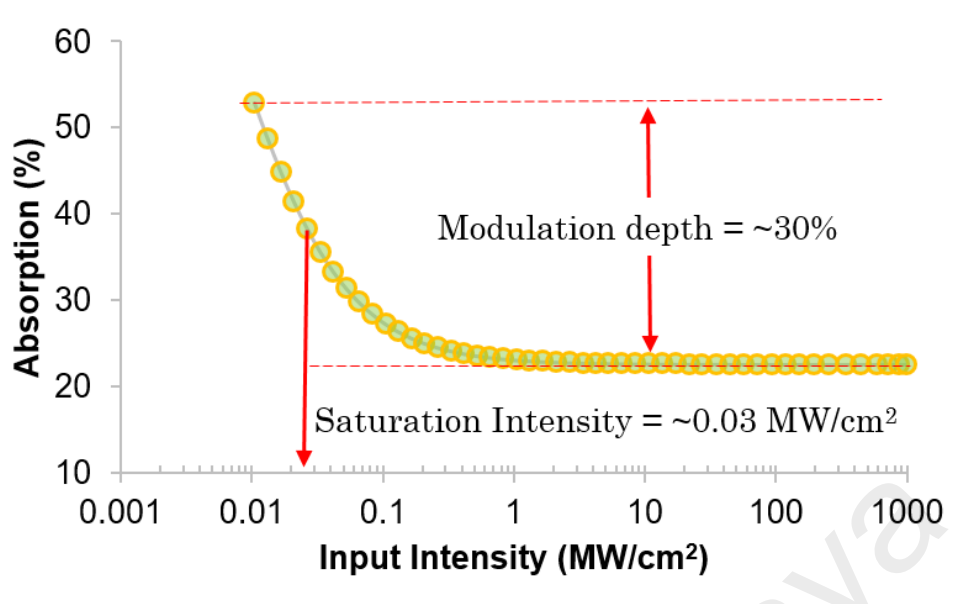


Figure 5.6: The saturable absorption characteristic of the Black Phosphorus SA

The configuration of Q-Switched DWFLs based BP using a microfiber as wavelength selective filter is schematically illustrated in Figure 5.7. The YDF comprising a length of 70cm YDF model DF1100 Fibercore, with peak absorption of 1300 dB/m at 977nm was utilized as a gain medium. Then, a 974 nm centered wavelength laser diode (LD) with maximum output power of 600 mW model LC96A74P-20R, Oclaro was employed as pumping source for YDFL and was linked to a 980 nm port of wavelength division multiplexing (WDM). The WDM common port was attached to 70 cm YDF, and then attached to a isolator to assure single direction of laser propagation. The isolator output was next linked to the dual-taped microfiber, which generates dual-wavelength laser (Ahmad, H., Salim, M. A. M., *et al.*, 2016). The output of the microfiber was then connected to BPSA which was located between the fiber ferrules, and then linked to input port of 90:10 optical coupler 1, (OC1). The 90% portion of optical coupler was channeled to reflection port of WDM to complete the cavity ring configuration. The 10% portion extracted from the cavity was used to analyze the signal behavior and was later linked to input port of 50:50 optical coupler 2, (OC2) which divides the generated pulse into two section. Therefore, the Q-switched signal can be observed simultaneously through one portion through an optical spectrum

analyzer (OSA) model AQ6373 YOKOGAWA and through another portion with a photo detector connected to digital oscilloscope (YOKOGAWA DLM2054). In addition to that, a 9kHz-7.8GHz frequency spectrum analyzer model MS2683A Anritsu and an optical power meter (THORLABS) were used to characterize the extracted signal generated from the cavity.

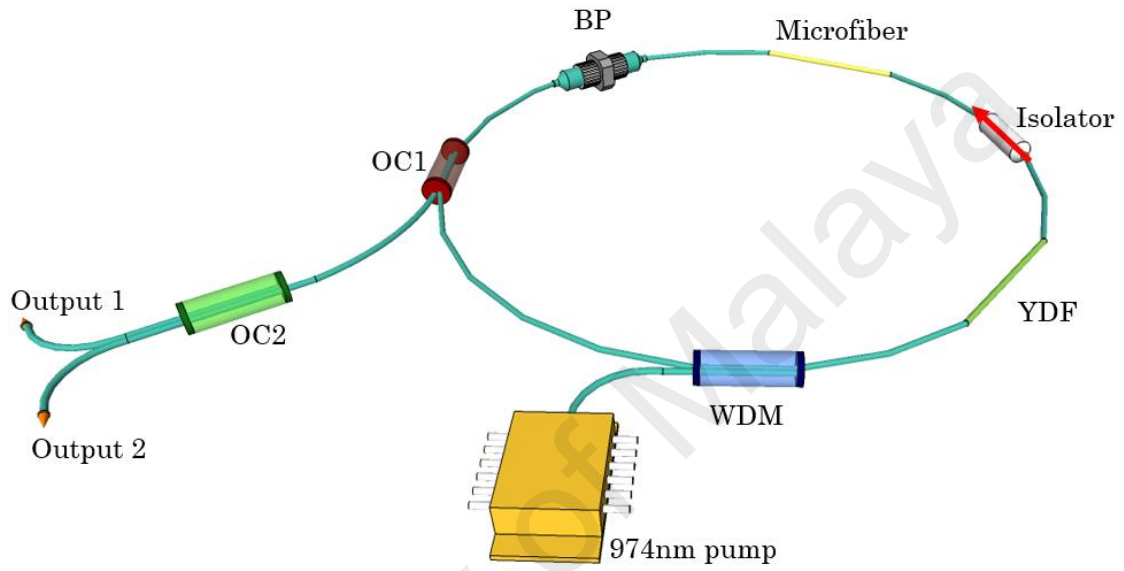


Figure 5.7: Experimental setup of Q-switched DWFLs in YDFL using BP as saturable absorber

Self starts Q-switched at the pump power of 143.9 mW in the dual-wavelength YDFL circuit with repetition rate of 6.5 kHz. When the pump power steadily increase from 143.9 mW to 202.9 mW, 239.7 mW and 297.1 mW as shown in Figure 5.8 (a) to Figure 5.8 (d) respectively, the stable pulse trains with increasing repetition rate from 6.5 kHz to 22.4, 32.4 and 62.5 kHz were monitored from the oscilloscope trace. On the other hand, the period decrease corresponding to increasing pump power due to typical properties of Q-switching operation.

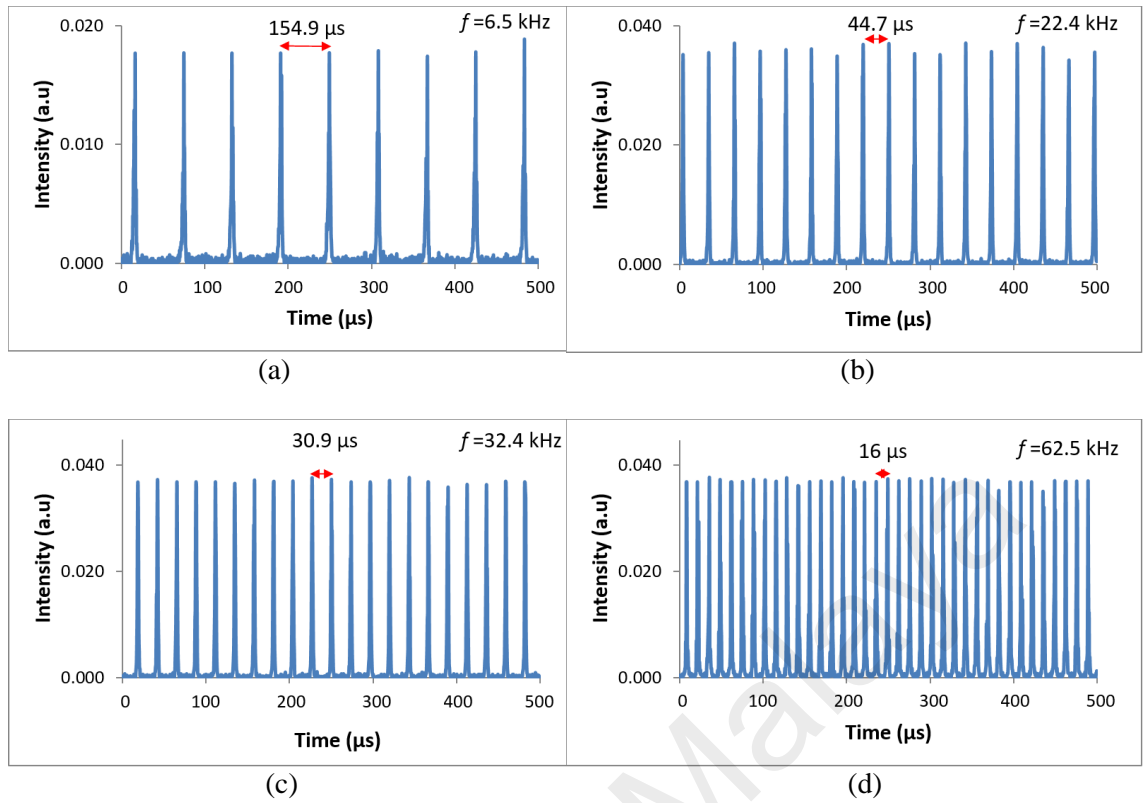


Figure 5.8: The repetition rate and period changes at (a) pump power of 143.9mW, (b) 202.9mW, (c) 239.7mW and (d) 297.1mW.

The stable output spectrum at 225.2mW, as shown in Figure 5.9 (a), has centered dual-wavelength of 1036.5 and 1039.2nm with respective output power of -22.5 and -21.3dBm. The corresponding pulse train, taken from the oscilloscope, as well as the pulse width as illustrated in Figure 5.9 (b) and Figure 5.9 (c) respectively have a repetition rate of 28.1 kHz. With regards to this, the period is 35.6 μs and the FWHM of pulse width is 1.6 μs . Then, the RFSA is used to measure in-frequency domain. As illustrated in Figure 5.9 (d), the broad harmonic spectrum traces with its fundamental frequency of 28.1 kHz and a peak-to-pedestal ratio of 46 dB (from the inset). This matches with the results obtained by oscilloscope thus demonstrating stable DWFLs Q-switched in our proposed setup.

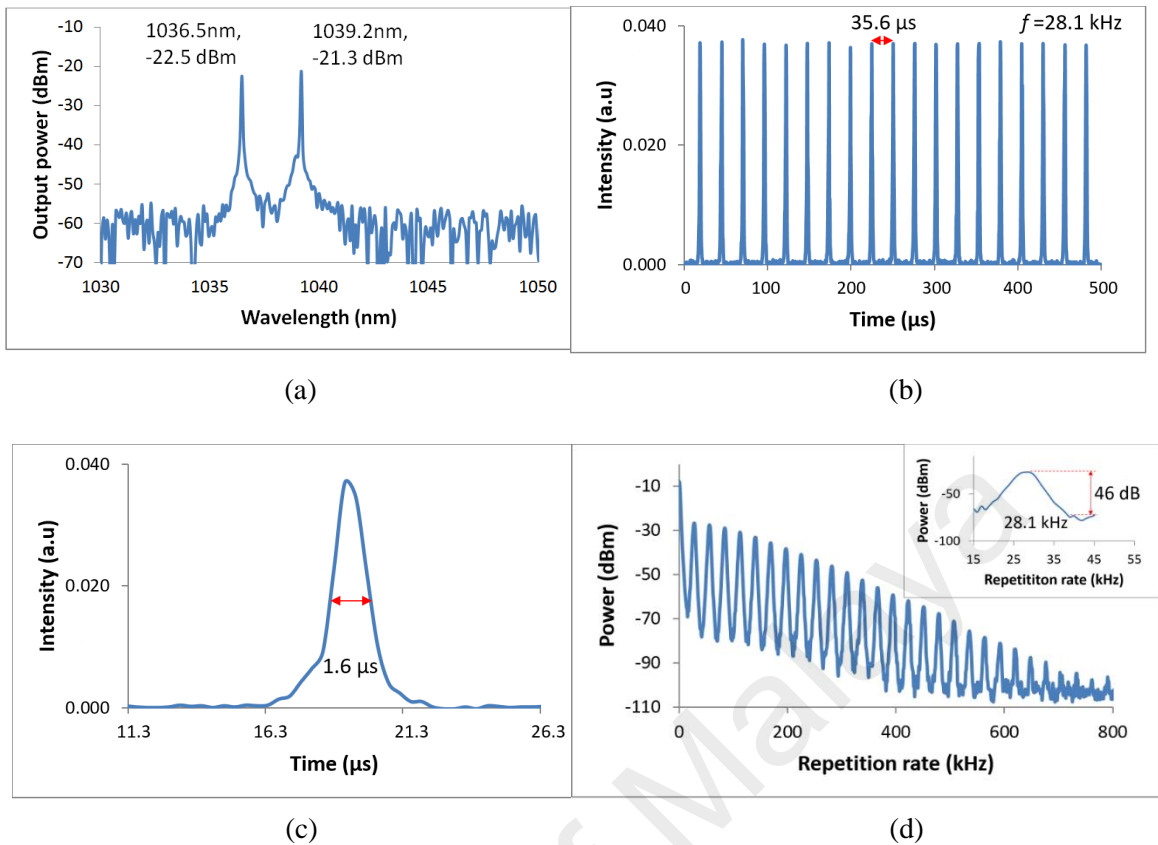
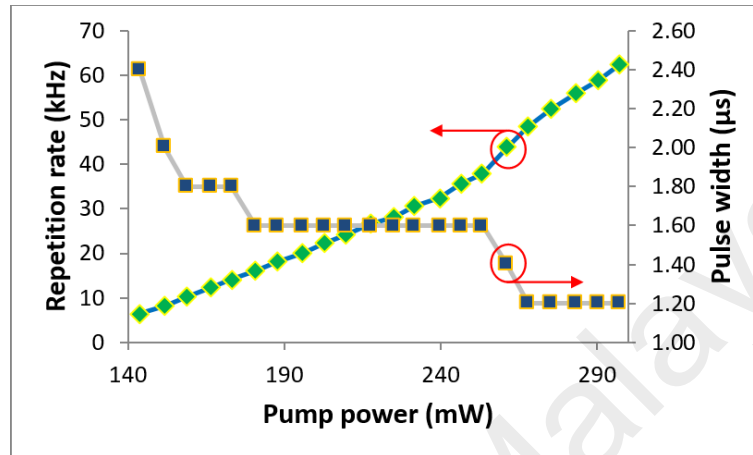


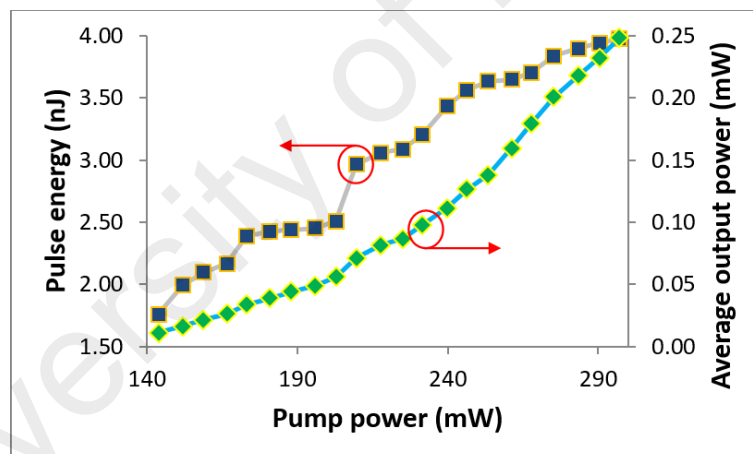
Figure 5.9: Characteristic of Q-switching at repetition rate of 28.1 kHz:
(a) dual-wavelength laser, (b) pulse duration, (c) pulse width and (d) frequency
domain at pump power of 225.2mW

The repetition rate as well as pulse width in relation to pump power is illustrated in Figure 5.10 (a). As the LD pump power increased from 143.9 to 297.1mW, the repetition rate of Q-switched hiked up from 6.5 to 62.5 kHz and corresponding pulse width decreased from 2.4 to 1.2 μs. Both results show the typical properties of Q-switched pulses. In addition, by optimizing the cavity setup especially by using short cavity design and optimizing the modulation depth of the BP based SA, the pulse width can be narrowed down further. As illustrated in Figure 5.10 (b), the single-pulse energy and calculated average output power were also measured in relation to pump power. The pulse energy and the average output power increased with the LD pump power

comprising maximum average output power of 0.25 mW, highest pulse energy of 4 nJ as well at maximum pump power of 297.1 mW. Furthermore, by utilizing a high-gain fiber, especially double-clad fibers the pulse energy can be increased further.



(a)



(b)

Figure 5.10: The repetition rate and pulse width and (b) the average output power and pulse energy in relation to pump power.

The Q-switched dual-wavelength using Black Phosphorusbased SA was successfully demonstrated. Stable Q-switched DWFLs centered at 1036.5 nm to 1039.2 nm. The pulse repetition rate tuning from 6.5 kHz to 62.5 kHz, highest pulse energy of 4 nJ and shortest pulse width of 1.2 μs. We anticipate that such findings from this work will encourage more development in the photonics field.

5.4 Q-switched DWFL based SPF using TiO₂ as SA

Titanium dioxide (TiO₂) is one of the nanomaterials that have attractive optical properties. A pump-probe measurement from (Elim, H., *et al.*, 2003) identified nonlinear absorption properties of TiO₂ with ultrafast recovery time of ~1.5 ps at room temperature. Additionally, Z-scan performed on TiO₂ thin film (Iliopoulos et al., 2009) showed transmittance peak nearby the focal plane and therefore, giving an indication that TiO₂ has a saturable-absorption-like behavior. Despite having a band gap at ~3.2 eV (~387 nm) (Karunagaran, B., Kim, K., Mangalaraj, D., Yi, J., & Velumani, S. 2005; Nambara, T., Yoshida, K., Miao, L., Tanemura, S., & Tanaka, N. 2007), when performing Z-scan using visible (Elim, H., *et al.*, 2003) and near infrared light (Iliopoulos, K., *et al.*, 2009), TiO₂ does reveal nonlinear optical response. Therefore, it exhibits the potential of TiO₂ as new optical material for SA.

In this study, we used a Q-switched YDFL utilizing a thin film TiO₂ passive SA. The spectrums are centered at 1034.7 nm and 1039 nm with pulse repetition rates obtained from the setup ranging from 31.2 to 64.5 kHz. These results show the potential of TiO₂ SA Q-switching operation in the one-micron region.

The dual-detector measurement system was used to measure the saturable absorption property of TiO₂ SA. Referring to the graph shown in Figure 5.11, the saturable intensity and modulation depth were 40% and 0.7 MW/cm², respectively. Furthermore, by enhancing the quality of TiO₂ SA, the modulation depth could be further optimized (Luo, Z., *et al.*, 2014).

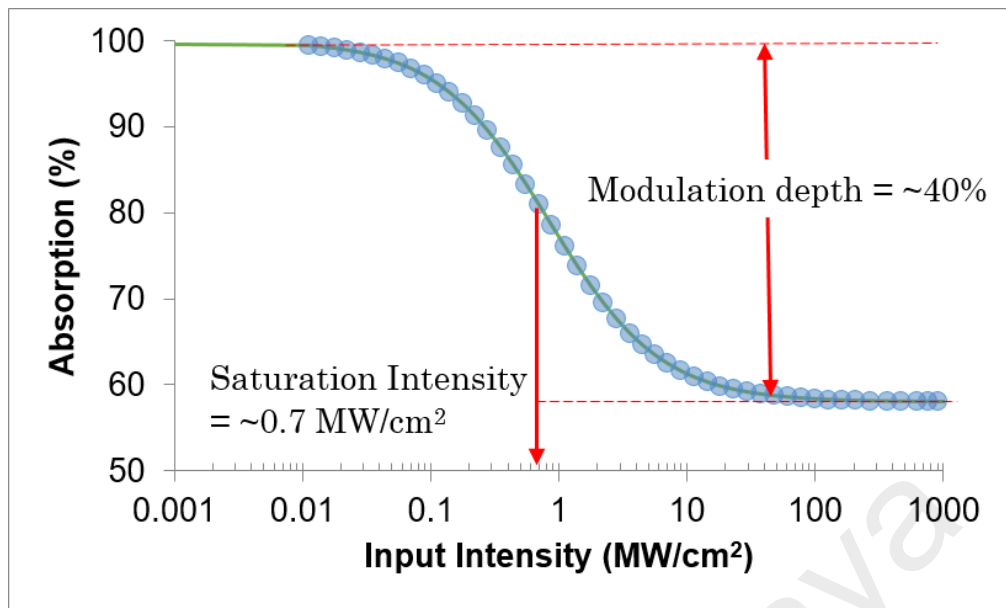


Figure 5.11: The saturable absorption distinctive of the TiO₂ SA.

The YDFL Q-switched incorporating TiO₂ as SA is illustrated in Figure 5.12. The laser setup consists of YDF as gain medium and the SA out of Titanium dioxide (TiO₂). The laser diode with centered wavelength of 974 nm (Oclaro Model LC96A74P-20R) is attached to a 980/1060 nm wavelength division multiplexer. A common port of WDM is connected to YDF (DF1100 Fibercore) with length of 70 cm having peak absorption of 1300 dB/m at 977nm. A YDFA is attached to a polarization insensitive isolator to avoid back reflection of laser in the cavity. The isolator output is linked to the thin film Titanium dioxide (TiO₂), which is in turn, connected to the 10dB optical coupler, and designated OC1. Then, 10% output port of OC1 is then channeled to 3dB optical coupler designated OC2. Therefore, the signal generated can be observed concurrently using optical spectrum analyzer (OSA) YOKOGAWA AQ6373 with a resolution of 0.02 nm through one signal portion and the other through signal portion with high-speed photodetector (Thorlabs D400FC) connected to digital oscilloscope (YOKOGAWA DLM2054). Moreover, a radio frequency spectrum analyzer, (Anritsu MS2683A, 9 kHz – 7.8 GHz) and optical power meter (Thorlabs, PM100USB) are also used to

measure the pulse signal. When TiO₂ SA is not present in the laser cavity, no pulsing is detected in the digital oscilloscope.

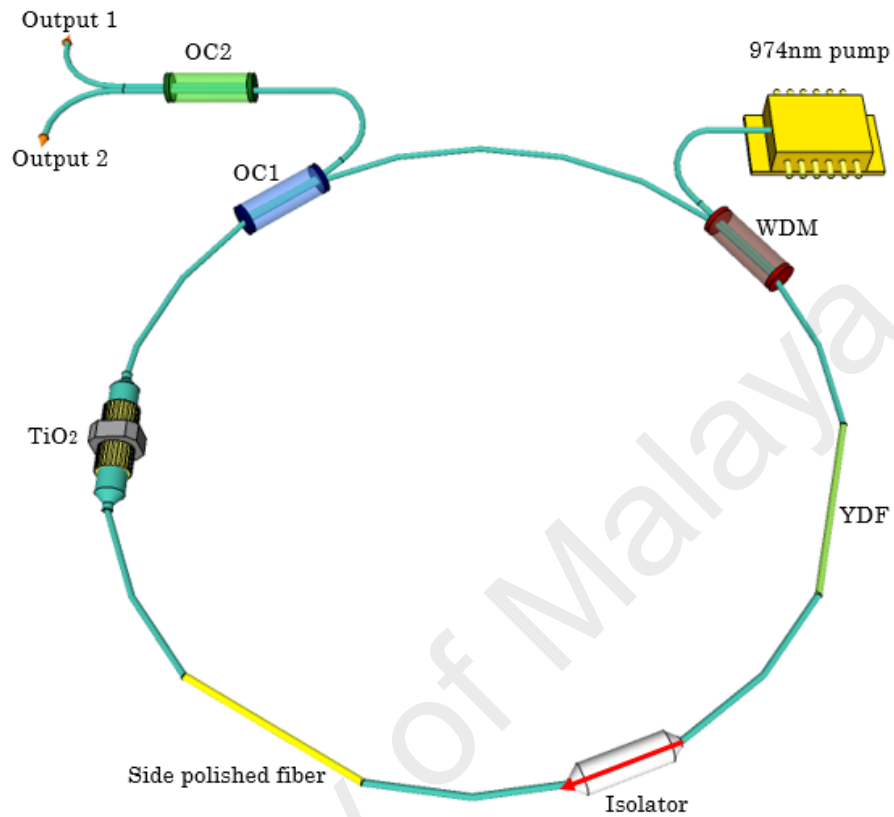


Figure 5.12: Configuration of titanium dioxide based saturable absorber in one micron region.

Laser setup starts its Q-switching pulse at the input power of 143.90 mW with repetition rates of 31.2 kHz, as illustrated in Figure 5.13(a). Figure 5.13(b) to figure 5.13 (d) show a stable pulse trains with increasing repetition rates as pump power is gradually increased from 143.90 mW to 180.90, 209.70 and 231.60 mW, respectively. Contradictorily, the period decreases with increasing pump power from 32 μ s to 16 μ s. These results show the reliant on the pump power as a common behavior of Q-switching operation.

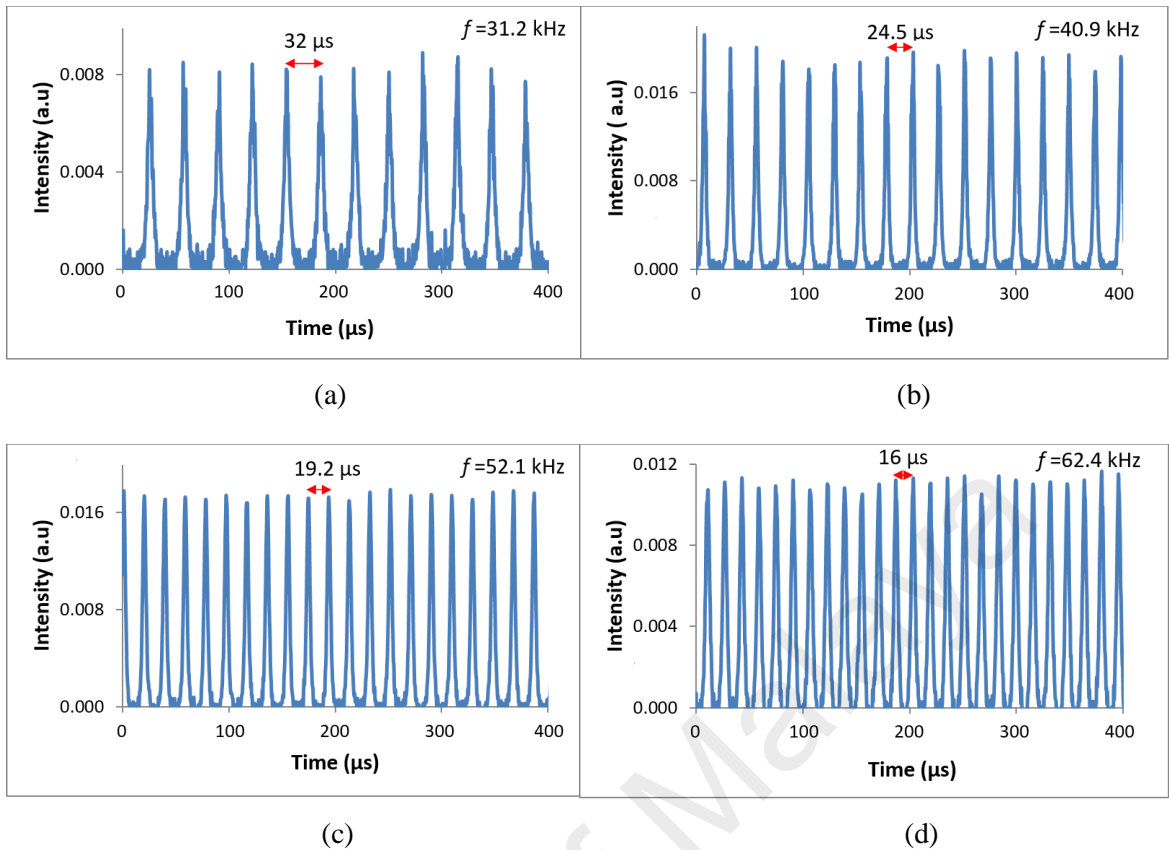


Figure 5.13: The pulse train of Q-switched at various pump power at (a) 143.90 mW and frequency of 31.2 kHz, (b) 180.90 mW and frequency of 40.9 kHz and (c) 209.70 mW and frequency of 52.13 kHz, (d) 231.60 mW and frequency of 62.4 kHz

Figure 5.14(a) shows the optical spectrum of dual-wavelength centered at 1034.7 nm and 1039 nm at pump power of 188 mW, taken from the OSA with output power of -18.8 dBm and -18.6 dBm, respectively. The corresponding Q-switching pulse train with frequency 43.5 kHz is illustrated in Figure 5.14 (b) and its single pulse profile is illustrated in Figure 5.14 (c). In addition to that, the pulse width was $3.7 \mu\text{s}$, measured from the full width at half maximum (FWHM). Figure 5.14 (d) illustrates the signal in repetition rate domain traces achieved by using the radio frequency spectrum analyzer (RFSA). The traces explain the first harmonic with repetition rate of 43.5 kHz as shown in inset of Figure 5.14 (d) with a peak-to-pedestal ratio of 53 dB. Furthermore, the passively Q-switching stable repetition rate indicated by the broadband of RF spectrum with no spectral modulation.

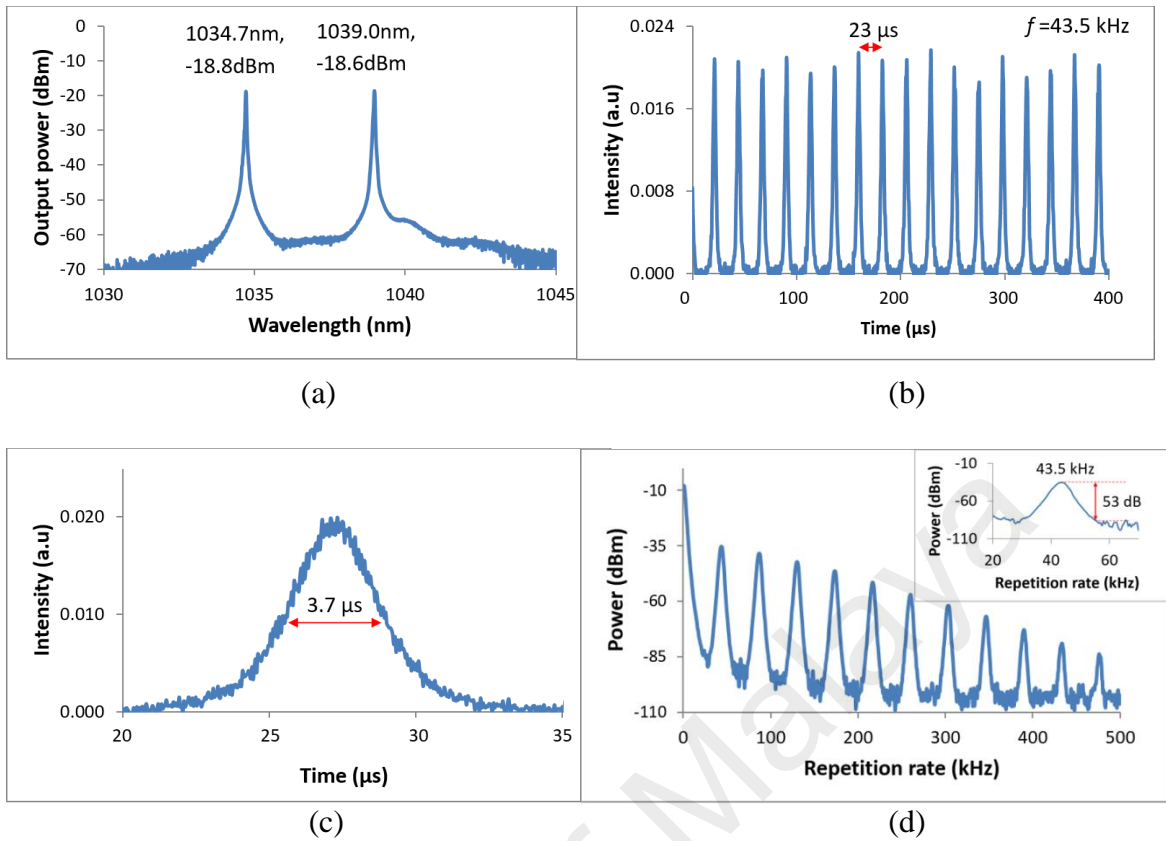
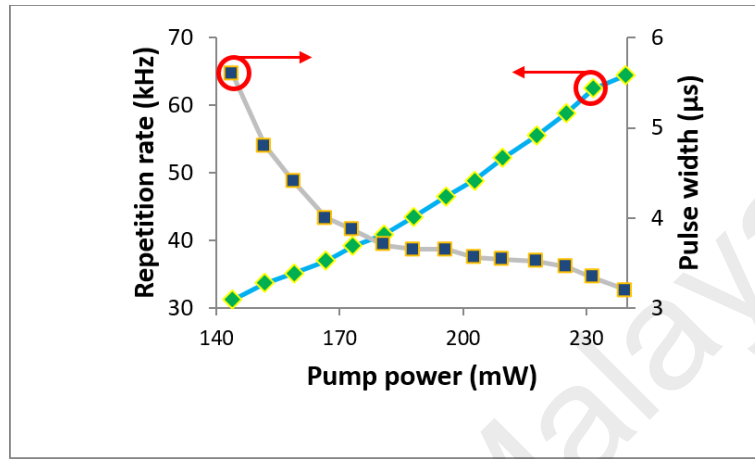


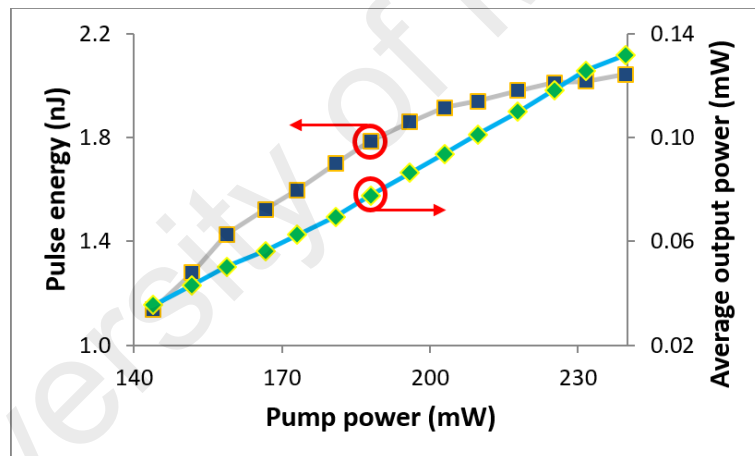
Figure 5.14: The characteristic of Q-switching at pump power of 188 mW and repetition rate of 43.5 kHz with (a) wavelength spectrum, (b) period, (c) single pulse profile and (d) RF output spectrum

Figure 5.15 (a) depicts the measured pulse width and pulse repetition rate as a function of pump power. As the pump power is increased from 143.90 mW to 239.70 mW, the repetition rates of Q-switched pulses are found to be increasing from 31.2 kHz to 64.5 kHz while the pulse width notably decreasing from 5.6 μs to 3.2 μs. The pulse width can be reduced further when parameters are optimized; for instance, shortening the cavity length and improving the modulation depth of the TiO₂ Q-switcher (Zhao, C., *et al.*, 2012). Furthermore, as illustrated in Figure 5.15 (b), the single-pulse energy and corresponding average output power were also measured. The pulse energy and the average output power were increasing with the increasing pump power. When the pump power is maximum, at 239.70 mW, the highest average output power is 0.13 mW. Whereas, the maximum pulse energy is 2 nJ, . Higher pulse energy can be

achieved using a high-gain fiber, like double-clad fiber, with high-performance TiO₂ SA, and further performance can be improvement when cavity designs are optimized (Zhou, D. P., *et al.*, 2010).



(a)



(b)

Figure 5.15: (a) The repetition rate and pulse width and (b) the pulse energy and average output power corresponding to pump power.

5.5 Q-switched DWFL based SPF using ZnO as SA

Zinc oxide (ZnO) is a metal oxide semiconductor of the II-VI group and has been studied over the few years by scientists, based on their optical and electrical properties. The main interest of this SA was due to its 3.4 eV direct band gap (Jagadish, C., & Pearton, S. J. 2011; Mang, A., & Reimann, K. 1995), a huge energy of 60 meV (Bagnall, D., *et al.*, 1997; Jagadish, C., & Pearton, S. J. 2011; Reynolds *et al.*, 1996) at room temperature.

In this research, we have demonstrated Q-switched dual-wavelengths ytterbium fiber laser centered at 1038 nm and 1039.2 nm wavelengths using ZnO as a SA and SPF as wavelength selective filter. The pulse repetition rates obtained ranged from 67.6 kHz to 104.2 kHz with pulse energy of 2 nJ.

The saturable intensity and modulation depth of ZnO were $\sim 0.01 \text{ MW/cm}^2$ and 22% respectively using dual-power detection measurement as described in chapter 3.

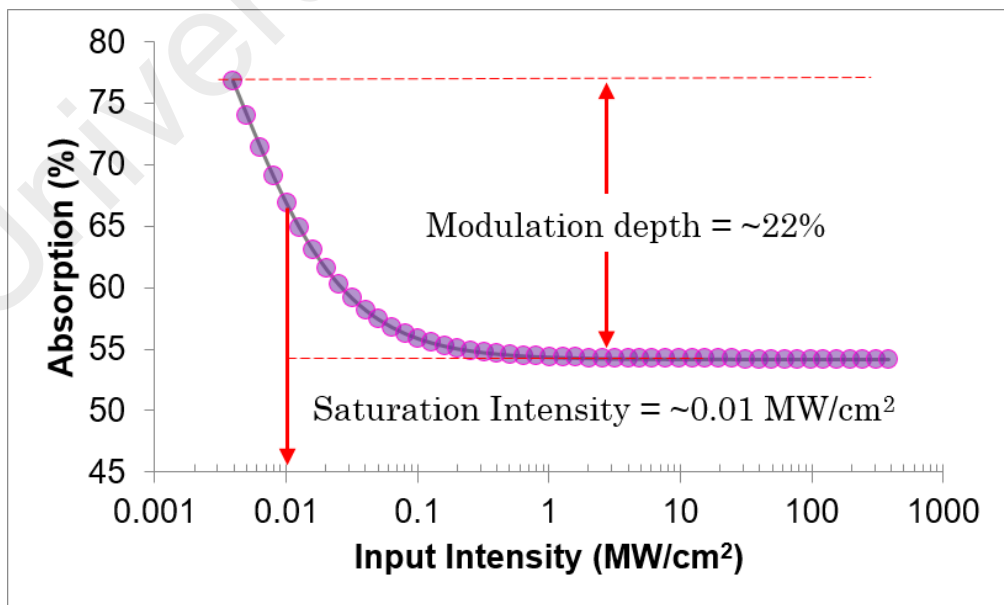


Figure 5.16: Saturation absorption characteristic of ZnO

In this experiment, Q-switched dual-wavelength setup is depicted in Figure 5.17, which comprises of 70 cm of Fibercore DF1100 ytterbium-doped fiber with 1300 dB/m peak absorption at 977nm, a side polished fiber or also known as “D-shaped fiber” due to its cross-section and zinc oxide thin film (ZnO) as a SA. The YDF was forward-pumped by a Oclaro LC96A74P-20R laser diode (LD) with 974 nm wavelength and a maximum pump power of 600 mW. The LD was coupled to the laser cavity via a 980/1060 nm wavelength division multiplexer (WDM). Then, a polarization insensitive isolator was fused into the laser cavity to avoid undesired backward reflection propagation and was attached to a side polished fiber that was employed to generate a dual-wavelength fiber laser (Zhang, S. X., *et al.*, 2014). ZnO thin film, which functions as a SA, was sandwiched between the two fiber ferrules. A 10-dB combined bi-conical optical coupler was used to tap 10% of total power in-order to monitor the optical spectrum, power and Q-switched pulses. 10% output port was later attached to a 3-dB optical coupler to enable simultaneous monitoring of pulse traces and wavelength spectrum. During the experiment, one of the output coupler was swapped to an OPM to measure the output power. A YOKOGAWA AQ6373 optical spectrum analyzer (OSA) with 0.02 nm resolution and a fast Thorlabs D400FC photodetector were connected to YOKOGAWA DLM2054 digital oscilloscope to monitor the wavelength spectrum and pulse train respectively. A 9 kHz – 7.8 GHz radio frequency spectrum analyzer (RFSA) model MS2683A by Anritsu is utilized to measure the pulse signal in frequency domain.

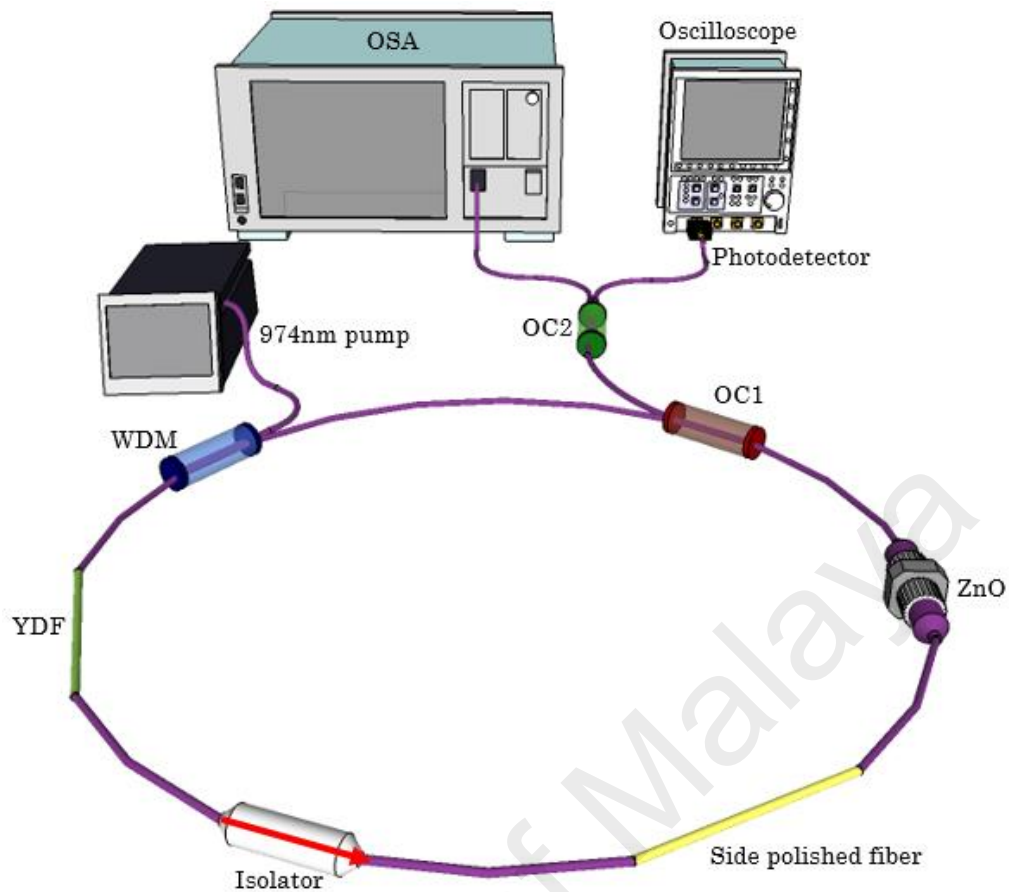


Figure 5.17: Configuration of Q-switched dual-wavelength based zinc oxide as saturable absorber in 1 μ m waveband

Initially, the dual-wavelengths YDFL runs in continuous wave (CW) operation without ZnO thin film SA. By inserting the ZnO thin film SA into the laser cavity and increasing the pump power to 188 mW, the Q-switching and dual-wavelength operations were simultaneously achieved. This can be observed via a digital oscilloscope as represented in Figure 5.18(a). The repetition rate of pulse train, f , rises from 67.6 kHz to 92.6 kHz while the period, reducing from 15.3 μ s to 10.7 μ s at four different pump power, specifically at 188mW, 217.8mW, 246.4mW and 253.4mW as shown in Figure 5.18 (a) to Figure 5.18 (d) respectively. This achievement is similar to our previous work (Ahmad, H., Salim, M. A. M., Azzuhri, S. R., Soltanian, M. R. K., & Harun, S. W. 2015; Ahmad, H., Salim, M. A. M., Soltanian, M. R. K., Azzuhri, S. R. & Harun, S. W. 2015) where the frequency correlates to the input pump power; the higher

the input power applied, the higher the frequency and the lower the pulse duration obtained.

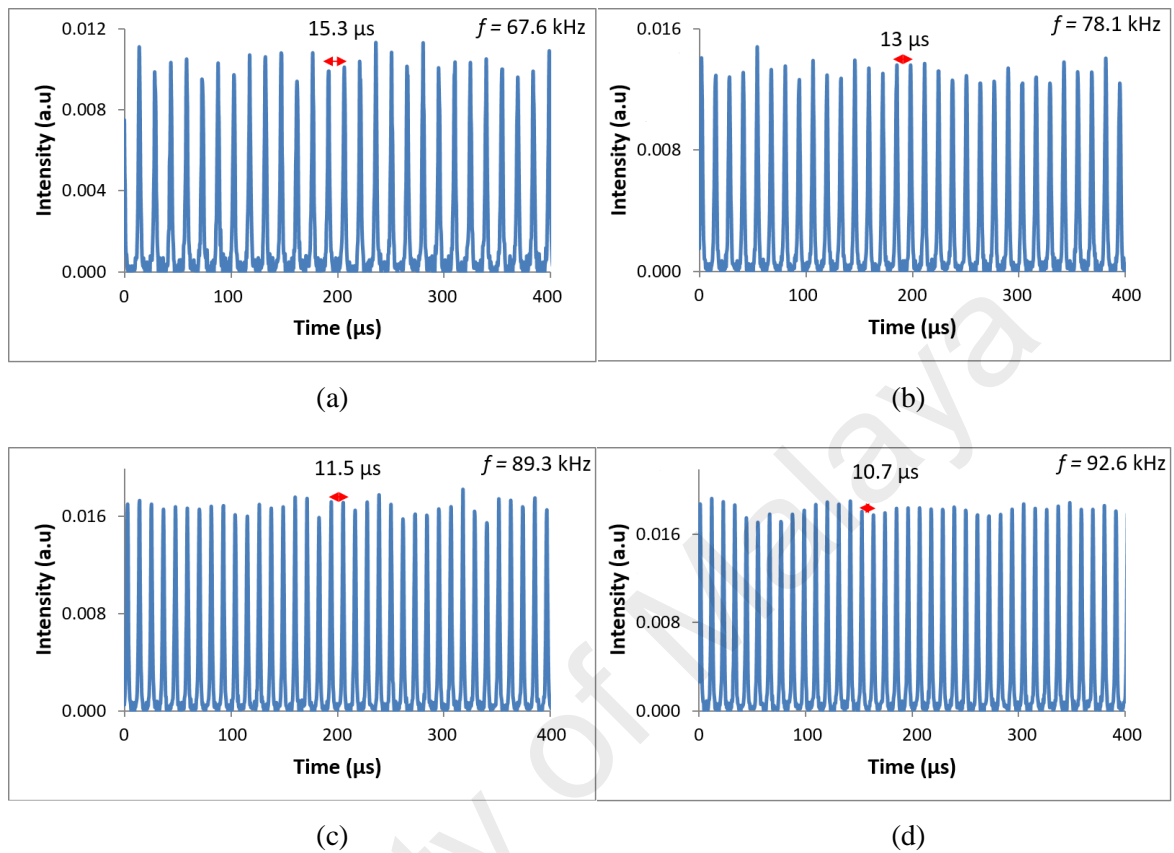
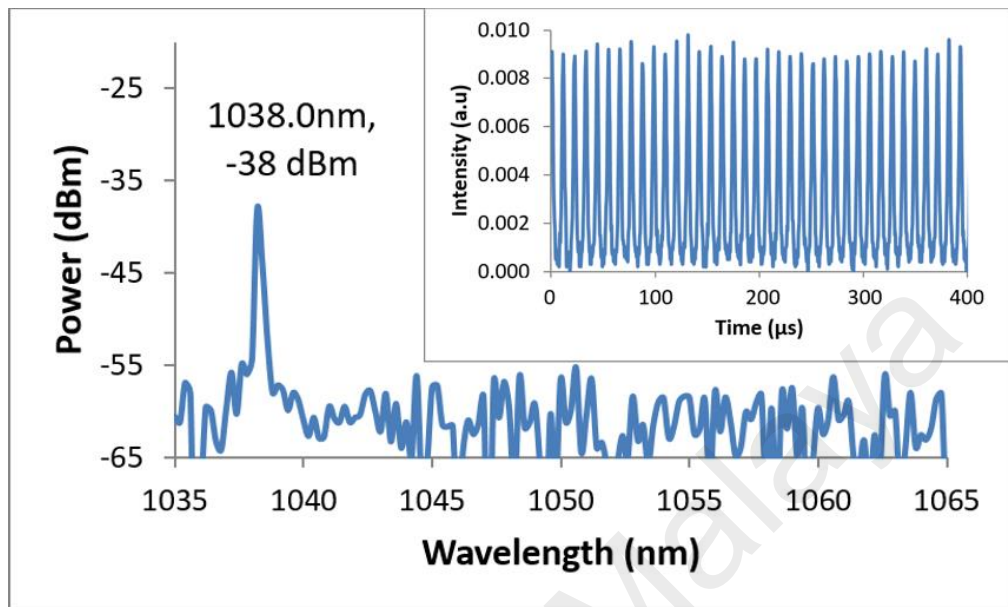


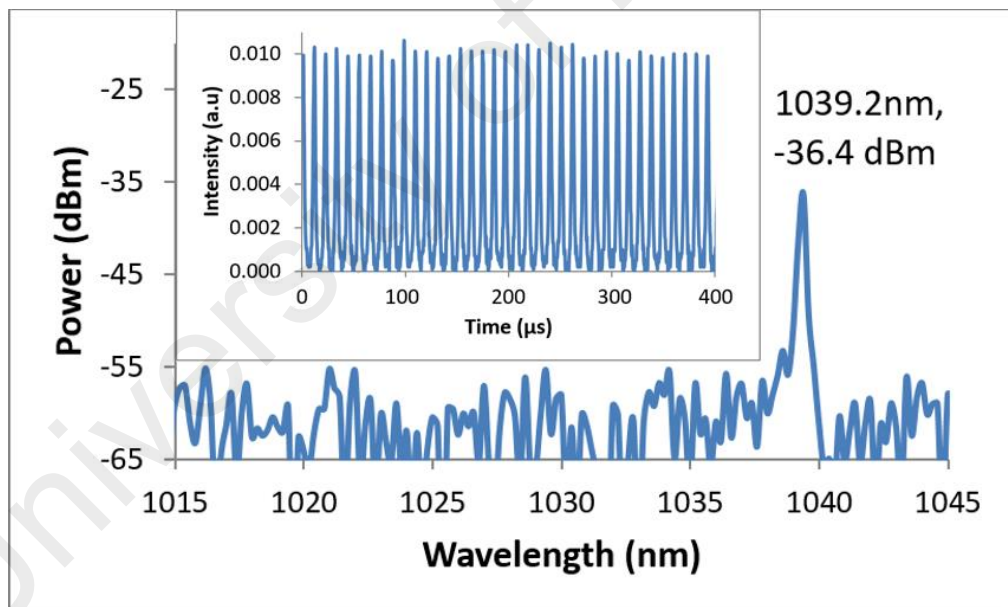
Figure 5.18: The pulse traces corresponding to four different stages of input power at (a) 188mW, (b) 217.8mW, (c) 246.4mW and (d) 253.4mW

The dual-wavelength spectrum had two lasings at 1038 nm and 1039.2 nm. At 253.4 mW pump power, the Q-switched dual-wavelengths pulse traces with frequency of 92.6 kHz is illustrated in Figure 5.18(d). In order to verify the synchronization pulses at dual-wavelengths, each wavelength at 1038 nm and 1039.2 nm were investigated separately using a tunable band pass filter (TBPf) (AGILTRON, FOTF-026122332). The TBPf was attached to one of the 50/50 optical coupler (OC2) output and fine adjustment at 1038 nm wavelength as shown in Figure 5.19 (a) and then continued at 1039.2nm as depicted in Figure 5.19 (b). Obviously, the pulse trains at 1038 nm (inset

of Figure 5.19 (a) and 1039.2nm (inset of Figure 5.19 (b)) show the same repetition rates of 92.6 kHz.



(a)



(b)

Figure 5.19: The dual-wavelength spectrum selected individually at (a) 1038 nm and (b) 1039.2 nm wavelength has same repetition rate of 92.6 kHz at pump power of 253.4 mW. (both insets: Q-switched with repetition rate of 92.6 kHz)

Then, the experiment is continued with Q-switched dual-wavelengths characterization at a maximum pump power of 275.3 mW as illustrated in Figure 5.20. A dual-wavelength spectrum with lasings at 1038 nm and 1039.2 nm wavelength is depicted in Figure 5.20 (a). The maximum repetition rate achieved is 104.2 kHz as observed in Figure 5.20 (b). A single pulse profile with 1.6 μ s pulse width is given in Figure 5.20 (c). Figure 5.20 (d) shows the frequency domain with repetition rate of 104.2 kHz (from the inset) obtained by radio frequency spectrum analyzer (RFSA) with \sim 50 dB SMSR indicating a stable Q-switched operation.

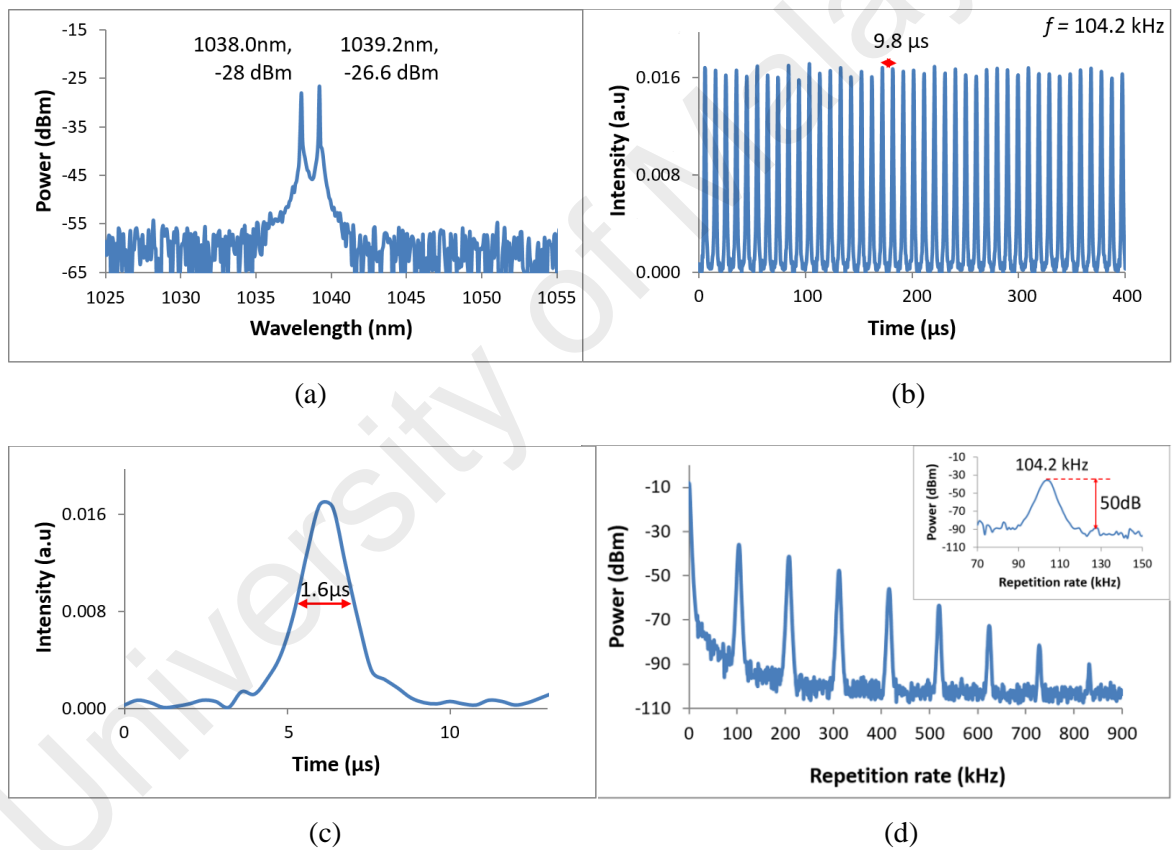
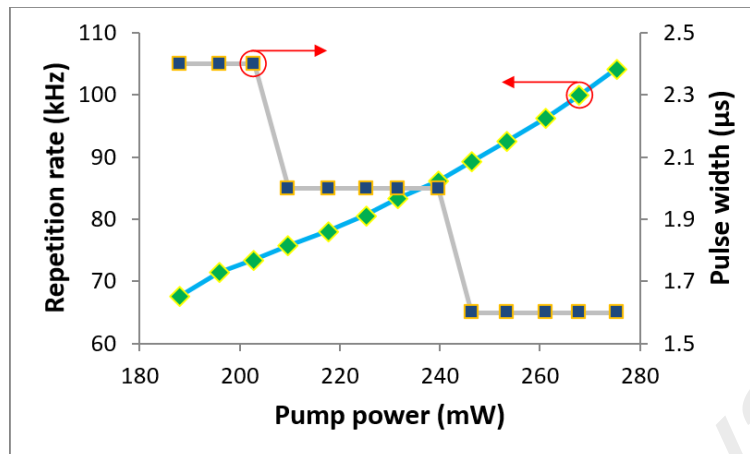
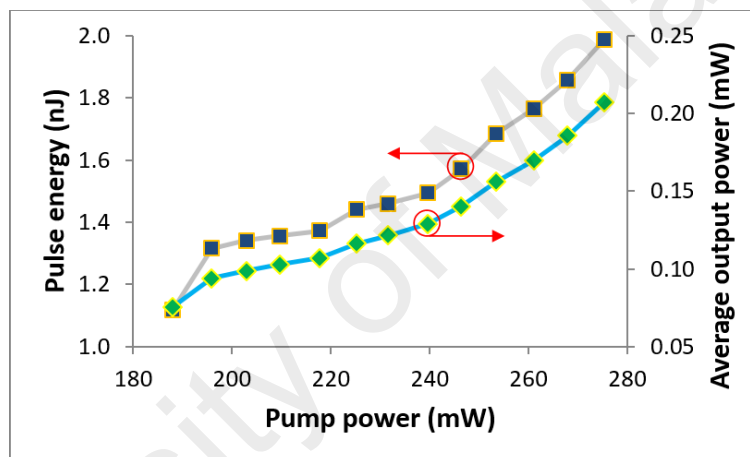


Figure 5.20: The Q-switched dual-wavelength characterization with repetition rate of 104.2 kHz at maximum pump power of 275.3 mW; (a) dual-wavelength spectrum, (b) Q-switched pulse train with period of 9.8 μ s, (c) FWHM of 1.6 μ s and (d) frequency domain spectrum

The trends of repetition rates and pulse durations corresponding to pump power are illustrated in Figure 5.21 (a). As we increased the input pump from 188 mW to 275.3 mW, the pulse repetition rate hiked up from 67.6 kHz to 104.2 kHz. However, the pulse duration decreases from 2.4 μ s to 1.6 μ s. We can improve these results by minimizing the cavity length and the cavity loss, and optimizing the modulation depth of SA (Zhao, C. J., *et al.*, 2012). Additionally, the single-pulse energy and average output power corresponding to pump power are also measured as depicted in Figure 5.21 (b). The pulse energy and average output power increase with increasing pump power. By increasing LD to 275.3 mW of maximum pump power, the highest pulse energy and maximum average output power obtained are 2 nJ and 0.2 mW, respectively.



(a)



(b)

Figure 5.21: (a) The pulse duration and repetition rate, and (b) the pulse energy and average output power corresponding to input pump power.

In a nutshell, a passively Q-switched dual-wavelength YDFL, lasings at 1038 nm and 1039.2 nm, respectively was successfully demonstrated. Dual-wavelength YDFL was produced using a side polished fiber and passive Q-switched was modulated by using ZnO thin film SA. Our stable dual-wavelength pulse was successfully attained with frequency from 67.6 kHz to 104.2 kHz, highest pulse energy of 2 nJ and the shortest pulse width of 1.6 μs, indicating ZnO as a potential SA for passive Q-switched dual-wavelengths pulse generation in the one-micron region.

5.6 Summary

In this chapter, the generation of dual-wavelength pulse laser are being presented. Firstly, in the first part, the generation of dual-wavelength fiber laser in continuous wave operation is presented by employing wavelength selective filter namely microfiber or side polished fiber. Then, the continuous wave turn to pulse laser by incorporating passively saturable absorber. Both wavelength selective filter and saturable absorber are important in order to provide a simultaneous dual-wavelength pulse laser in a simple ring cavity setup. Four type of saturable absorbers are employed to produce Q-switched laser namely molybdenum diselenide, black phosphorus, titanium dioxide and zinc oxide as shown in Table 5.1. The proposed setup successfully demonstrated a passively Q-switched that requires a compact yet robust and cost-effective pulse laser.

Table 5.1: Characteristics of Q-switched YDFL by different SAs

Characteristics	MoSe ₂	BP	TiO ₂	ZnO
Pump Threshold, (mW)	166.6	143.9	143.9	188
Dual-wavelength, (nm)	1035.8 and 1040.2	1036.5 and 1039.2	1034.7 and 1039	1038 and 1039.2
Repetition rate, (kHz)	15.3 - 35.2	6.5 - 62.5	31.2 - 64.5	67.6 - 104.2
Minimum pulse width, (μs)	1.8	1.2	3.2	1.6
Maximum pulse energy, (nJ)	2.8	4	2	2
Modulation depth, (%)	13.5	30	40	22
Saturable Intensity, (MW/cm ²)	~0.03	~0.03	~0.7	~0.01

CHAPTER 6: CONCLUSION

6.1 Conclusion

In conclusion, this research has successfully demonstrated and achieved all the objectives in this research work. The first objective is to design and characterize dual-tapered microfiber based Mach Zehnder Interferometer in generating dual-wavelength fiber laser. It is then followed by generating narrow wavelength spacing of DWFL as the second objective. The third objective is to explore techniques used in generating tunable dual-wavelength and in this case we successfully applied strain technique to tune the dual-wavelength generation. Then, we employed SPF as a wavelength selective filter to generate DWFL, which is the fourth objective in this work. Finally, we have also achieved the fifth objective, whereby we have successfully generated passively Q-switched dual-wavelength by incorporating new saturable absorber.

We start the research work by designing the ring cavity of ytterbium-doped fiber laser that is used for dual-wavelength generation and passively Q-switched operation in the one-micron region. Then, we fabricated dual-tapered microfiber based Mach Zehnder Interferometer as a wavelength selective filter. The first microfiber was designed using in-house tapered machine with waist diameter of 2 μm and insertion loss of 7 dB. The consequent dual-wavelength lasing with single longitudinal mode was successfully demonstrated in ytterbium-doped fiber ring laser. The generation of dual-wavelength fiber laser can be tuned up to 7 sets by adjusting the polarization controller with narrowest wavelength spacing of 0.94 nm and high SMSR of 50 dB. A stable DWFL operation with maximum power fluctuation of 0.8 dBm for 30 minutes in room temperature is achieved as well.

Then, with the same microfiber of 2 μm waist diameter used in YDFL, the tunable band pass filter (TBPF) was incorporated together with microfiber to generate narrow wavelength spacing of DWFL. Fine tuning the tunable band pass filter and adjusting the polarization controller (PC), 3 sets of stable dual-wavelength with narrow wavelength spacing of 0.06 nm, 0.09 nm and 0.22 nm were achieved with SMSR of 50 dB. The system offers stable dual-wavelength operation with maximum wavelength shift and power fluctuation were less than 0.01nm and 0.8 dB, respectively.

Second microfiber was fabricated with commercial tapered machine, namely Vytran GPX-3000 series. The dual-tapered microfiber fabricated using this machine has a waist diameter of 10 μm and insertion loss of 10 dB. In this work, the microfiber is employed in the ring cavity where it is placed between two xyz-translation stages. However, the polarization controller is not used in this proposed setup. The strain is applied on the microfiber by adjusting the micrometer driver of xyz translation stage. As a result, 4 sets of dual-wavelength generation at a precise displacement of 2, 12, 87 and 190 μm were achieved and these results remain consistent even after repeated trials. Instead of using polarization controller at previous work, we can also apply strain techniques for tuning the dual-wavelength laser. The SMSR, maximum wavelength shift and power fluctuation were 48 dB, less than 0.01 nm and 0.6 dB indicates stable operation in the one-micron region.

Another wavelength selective filter used in this work is side polished fiber. The commercial side polished fiber is attained from the Phoenix manufacturer with a polished length of 17 mm. The side polished fiber is used in the ring cavity to generate DWFL. By tuning the polarization controller, 3 sets of dual-wavelength was obtained with wavelength spacing of 6.70 nm, 16.87 nm, and 22.05 nm respectively. The SMSR was measured to be 50 dB with stable tunable dual-wavelength output of less than 0.9

dB power fluctuations and 0.01 nm wavelength shifting for 30 minutes in room temperature.

Both dual-tapered microfiber with waist diameter of 2 μm and 10 μm , and side polished fiber with polished length of 17 mm were used as wavelength selective filter together with passive saturable absorber to generate dual-wavelength Q-switched generation.

Q-switched dual-wavelength using molybdenum diselenide, MoSe_2 from Transition Metal Dichalcogenides (TMD) group as a passive saturable absorber in generating Q-switched pulse, and a 10 μm waist diameter of dual-tapered microfiber were employed to generate dual-wavelength laser. The combination of MoSe_2 SA and microfiber resulted in the simultaneous generation of Q-switched dual-wavelength in the YDF ring cavity. In this work, the stable dual-wavelength Q-switching operation was centered at 1035.8 nm and 1040.2 nm wavelength and repetition rate ranges from 15.3 kHz to 35.2 kHz with highest pulse energy and shortest pulse width found to be 2.8 nJ and 1.8 μs , respectively.

Subsequently, with the same microfiber of 10 μm waist diameter as wavelength selective filter, the saturable absorber used next was the black phosphorus. Both the microfiber and BP SA generate dual-wavelength Q-switched with repetition rate from 6.5 kHz to 62.5 kHz, highest pulse energy of 4 nJ and shortest pulse width of 1.2 μs whereas the centered dual-wavelength was obtained at 1036.5 nm to 1039.2 nm.

Moreover, side polished fiber with polished length of 17 mm was used as wavelength selective filter and titanium dioxide (TiO_2) was used as the passive saturable absorber in this work. The generated Q-switched dual-wavelength generation has repetition rate ranging from 31.2 kHz to 64.5 kHz with maximum pulse energy of 2.0 nJ and shortest

pulse width of 3.2 μs . Whereas, dual-wavelength spectrum centered at 1034.7 nm and 1039 nm was obtained in room temperature.

Finally, we employed zinc oxide (ZnO) as saturable absorber and side polished fiber in the ring cavity to generate dual-wavelength Q-switched in YDF laser. The dual-wavelength spectrum are obtained at 1038 nm and 1039.2 nm respectively. The stable dual-wavelength pulse was attained with repetition rate from 67.6 kHz to 104.2 kHz, together with the highest pulse energy of 2 nJ and the shortest pulse width of 1.6 μs , indicating that ZnO is a potential SA for passive Q-switched dual-wavelength pulse generation in the one-micron region.

University of Malaysia

Future Works

The dual-wavelength generation in ytterbium-doped fiber laser demonstrated and successfully achieved in this work can be further studied in term of:

Dual-Wavelength Mode Locked

The development of dual-wavelength fiber laser for ultrafast mode locked is one of the future works that could be done using passive saturable absorber. A few techniques such as optical deposition can be employed to fabricate the saturable absorber. Whereas, the wavelength selective filters like microfiber or side polished fiber can be used to generate dual-wavelength spectrum in the cavity.

Microwave and Terahertz Generation

Dual-wavelength fiber laser have potential in generating microwave and terahertz radiations by interaction of narrow wavelength spacing propagating in the same laser cavity. Further research should extent the study on new techniques or approaches to design dual-wavelength fiber laser to generate single longitudinal mode (SLM) output in simple ring cavity.

Multi-wavelength Generation

For future research work, we would like to generate multi-wavelength laser in YDF. In this work, we have successfully generated dual-wavelength laser using microfiber and side polished fiber. Perhaps by using other type of wavelength selective filter and by finding alternative design, the multi-wavelength laser can be improved.

University of Malaya

REFERENCES

- Agrawal, G. (2001). *Applications of nonlinear fiber optics*: Academic Press.
- Ahmad, H., Dernaika, M., Kharraz, O. M., Alimadad, M., Ibrahim, M. F., Lim, K. S., & Harun, S. W. (2014). A tuneable, power efficient and narrow single longitudinal mode fibre ring laser using an inline dual-taper fibre Mach–Zehnder filter. *Laser Physics*, 24(8), 085111.
- Ahmad, H., Latif, A. A., Zulkifli, M.Z, Awang, N. A., & Harun, S. W. (2012). High power dual-wavelength tunable fiber laser in linear and ring cavity configurations. *Chinese Optics Letters*, 10(1), 010603.
- Ahmad, H., Salim, M. A. M., Soltanian, M. R. K., Azzuhri, S. R., Harun, S. W., & Yasin, M. (2015). Generation of stable and narrow spacing dual-wavelength ytterbium-doped fiber laser using a photonic crystal fiber. *Journal of Modern Optics*, 1-6.
- Ahmad, H., Rashid, F. A. A., Azzuhri, S. R., Salim, M. A. M., Shaharuddin, R., Ismail, M. A., & Razak, M. Z. (2016). The generation of passive dual wavelengths Q-switched YDFL by MoSe₂ film. *Laser Physics Letters*, 13(11), 115102.
- Ahmad, H., Salim, M. A. M., Azzuhri, S. R., Jaddoa, M., & Harun, S. W. (2016). Tunable dual-wavelength ytterbium-doped fiber laser using a strain technique on microfiber Mach–Zehnder interferometer. *Applied Optics*, 55(4), 778-782.
- Ahmad, H., Salim, M. A. M., Azzuhri, S. R., Soltanian, M. R. K., & Harun, S.W. (2015). A passively Q-switched ytterbium-doped fiber laser based on a few-layer Bi₂Se₃ saturable absorber. *Laser Physics*, 25(6), 065102.
- Ahmad, H., Salim, M. A. M., Soltanian, M. R. K., Azzuhri, S. R., & Harun, S. W. (2015). Passively dual-wavelength Q-switched ytterbium doped fiber laser using Selenium Bismuth as saturable absorber. *Journal of Modern Optics*, 62(19), 1550-1554.

- Ahmad, H., Salim, M. A. M., Azzuhri, S. R., & Harun, S. W. (2016). Highly stable and tunable narrow-spacing dual-wavelength ytterbium-doped fiber using a microfiber Mach–Zehnder interferometer. *Optical Engineering*, 55(2), 026114–026114.
- Ahmad, H., Salim, M. A. M., Azzuhri, S. R., Soltanian, M. R. K., & Harun, S. W. (2015). A passively Q-switched ytterbium-doped fiber laser based on a few-layer Bi₂Se₃ saturable absorber. *Laser Physics*, 25(6). doi:Artn 06510210.1088/1054-660x/25/6/065102
- Ahmad, H., Salim, M. A. M., Azzuhri, S. R., Zulkifli, M. Z., & Harun, S. W. (2015). Dual wavelength single longitudinal mode Ytterbium-doped fiber laser using a dual-tapered Mach-Zehnder interferometer. *Journal of the European Optical Society-Rapid Publications*, 10. doi:Artn 1501310.2971/Jeos.2015.15013
- Ahmad, H., Salim, M. A. M., Soltanian, M. R. K., Azzuhri, S. R., & Harun, S. W. (2015). Passively dual-wavelength Q-switched ytterbium doped fiber laser using Selenium Bismuth as saturable absorber. *Journal of Modern Optics*, 62(19), 1550-1554. doi:10.1080/09500340.2015.1050471
- Ahmad, H., Semangun, J. M., Azzuhri, S. R., Zulkifli, M. Z., Awang, N. A., & Harun, S. W. (2015). Passively mode-locked laser using an entirely centred erbium-doped fiber. *Laser Physics*, 25(4). doi:Artn 04510510.1088/1054-660x/25/4/045105
- Ahmad, H., Soltanian, M. R. K., Narimani, L., Amiri, I., Khodaei, A., & Harun, S. W. (2015). Tunable S-Band Q-Switched Fiber Laser Using Bi₂Se₃ as the Saturable Absorber. *IEEE Photonics Journal*, 7(3), 1-8.
- Ahmad, H., Soltanian, M. R. K., Pua, C. H., Zulkifli, M. Z., & Harun, S. W. (2013a). Narrow Spacing Dual-Wavelength Fiber Laser Based on Polarization Dependent Loss Control. *IEEE Photonics Journal*, 5(6). doi : Artn 150270610.1109/Jphot.2013.2293613
- Ahmad, H., Soltanian, M. R. K., Pua, C. H., Zulkifli, M. Z., & Harun, S. W. (2013b). Narrow Spacing Dual-Wavelength Fiber Laser Based on Polarization Dependent Loss Control. *IEEE Photonics Journal*, 5(6), 1502706-1502706. doi:10.1109/jphot.2013.2293613

- Ahmad, H., Suthaskumar, M., Tiu, Z., Zarei, A., & Harun, S. W. (2016). Q-switched Erbium-doped fiber laser using MoSe₂ as saturable absorber. *Optics & Laser Technology*, 79, 20-23.
- Ando, Y., Zhao, X., Shimoyama, H., Sakai, G., & Kaneto, K. (1999). Physical properties of multiwalled carbon nanotubes. *International Journal of Inorganic Materials*, 1(1), 77-82. doi:Doi 10.1016/S1463-0176(99)00012-5
- Avadhanulu, M. (2001). *An Introduction To Lasers Theory And Applications*: S. Chand Limited.
- Bagnall, D., Chen, Y., Zhu, Z., Yao, T., Koyama, S., Shen, M. Y., & Goto, T. (1997). Optically pumped lasing of ZnO at room temperature. *Applied Physics Letters*, 70(17), 2230-2232.
- Bao, Q. L., Zhang, H., Wang, Y., Ni, Z. H., Yan, Y. L., Shen, Z. X., Tang, D. Y. (2009). Atomic-Layer Graphene as a Saturable Absorber for Ultrafast Pulsed Lasers. *Advanced Functional Materials*, 19(19), 3077-3083. doi:Doi 10.1002/Adfm.200901007
- Brambilla, G. (2010, 24-27 Oct. 2010). *Optical microfiber passive components*. Paper presented at the 9th International Conference on Optical Communications and Networks (ICOON 2010).
- Brambilla, G., Jung, Y., & Renna, F. (2010). Optical fiber microwires and nanowires manufactured by modified flame brushing technique: properties and applications. *Frontiers of Optoelectronics in China*, 3(1), 61-66. doi:10.1007/s12200-009-0081-1
- Braun, J. H., Baidins, A., & Marganski, R. E. (1992). TiO₂ pigment technology: a review. *Progress in Organic Coatings*, 20(2), 105-138.
- Chang, Y. M., Kim, H., Lee, J. H., & Song, Y.-W. (2010). Multilayered graphene efficiently formed by mechanical exfoliation for nonlinear saturable absorbers in fiber mode-locked lasers. *Applied Physics Letters*, 97(21), 211102.

- Chen, D., & Shen, L. (2007). Switchable and tunable Erbium-doped fiber ring laser incorporating a birefringent and highly nonlinear photonic crystal fiber. *Laser Physics Letters*, 4(5), 368-370. doi:10.1002/lapl.200610118
- Chen, L. R., & Gu, X. (2007). Dual-wavelength Yb-doped fiber laser stabilized through four-wave mixing. *Optics Express*, 15(8), 5083-5088. doi:10.1364/OE.15.005083
- Chen, Y., Jiang, G., Chen, S., Guo, Z., Yu, X., Zhao, C., . . . Tang, D. (2015). Mechanically exfoliated black phosphorus as a new saturable absorber for both Q-switching and Mode-locking laser operation. *Optics Express*, 23(10), 12823-12833.
- Cheng, J. Q., Zhang, L. L., Sharafudeen, K., Ma, Z. J., & Qiu, J. R. (2014). Room-temperature switchable triple-wavelength operation of an erbium-doped fiber laser. *Laser Physics*, 24(1). doi:Artn 01510210.1088/1054-660x/24/1/015102
- Cho, W. B., Kim, J. W., Lee, H. W., Bae, S., Hong, B. H., Choi, S. Y., Rotermund, F. (2011). High-quality, large-area monolayer graphene for efficient bulk laser mode-locking near 1.25 μm . *Optics Letters*, 36(20), 4089-4091.
- Churchill, H. O., & Jarillo-Herrero, P. (2014). Two-dimensional crystals: Phosphorus joins the family. *Nature Nanotechnology*, 9(5) 330.
- Derickson, D. (1998). *Fiber optic test and measurement*. Paper presented at the Fiber optic test and measurement/edited by Dennis Derickson. Upper Saddle River, NJ: Prentice Hall, c1998.
- Durairaj, V. (2013). Amplification in Ytterbium-doped fibers (Master's Thesis). Retrieved from <https://aaltodoc.aalto.fi>
- Elim, H., Ji, W., Yuwono, A., Xue, J., & Wang, J. (2003). Ultrafast Optical Nonlinearity in PMMA-TiO₂ Nanocomposites. *arXiv preprint cond-mat/0301153*.

- Feifei, Y., Sigang, Y., Hongwei, C., Minghua, C., & Shizhong, X. (2011). 60-nm-Wide Tunable Single-Longitudinal-Mode Ytterbium Fiber Laser With Passive Multiple-Ring Cavity. *IEEE Photonics Technology Letters*, 23(22), 1658-1660. doi:10.1109/LPT.2011.2166112
- Feng, S., Lu, S., Peng, W., Li, Q., Qi, C., Feng, T., & Jian, S. (2013). Photonic generation of microwave signal using a dual-wavelength erbium-doped fiber ring laser with CMFBG filter and saturable absorber. *Optics & Laser Technology*, 45, 32-36.
- Feng, X., Liu, Y., Fu, S., Yuan, S., & Dong, X. (2004). Switchable dual-wavelength ytterbium-doped fiber laser based on a few-mode fiber grating. *IEEE Photonics Technology Letters*, 16(3), 762-764.
- Feng, X., Liu, Y., Yuan, S., Kai, G., Zhang, W., & Dong, X. (2004). L-band switchable dual-wavelength erbium-doped fiber laser based on a multimode fiber Bragg grating. *Optics Express*, 12(16), 3834-3839.
- Gao, L., Zhu, T., Zeng, J., & Chiang, K. S. (2013). Temporal response measurement of magnetic fluids based on D-shaped fiber intermodal interferometer. *Applied Physics Express*, 6(5), 052502.
- Gao, Y., Zhao, T. Z., Li, C. Y., Ge, W. Q., Wu, Q., Shi, Z. H., . . . Wang, Y. G. (2013). Diode-side-pumped passively Q-switched Nd:YAG laser at 1123 nm with reflective single walled carbon nanotube saturable absorber. *Optics Communications*, 286, 261-264. doi:Doi 10.1016/J.Optcom.2012.08.045
- Hanna, D., Percival, R., Perry, I., Smart, R., Suni, P., Townsend, J., & Tropper, A. (1988). *Continuous-wave oscillation of a monomode ytterbium-doped fibre laser*. Paper presented at the IEEE Colloquium on All-Fibre Devices.
- Harun, S. W., Lim, K. S., Jasim, A. A., & Ahmad, H. (2010). Dual wavelength erbium-doped fiber laser using a tapered fiber. *Journal of Modern Optics*, 57(21), 2111-2113. doi:10.1080/09500340.2010.522740

- Herda, R., Kivistö, S., & Okhotnikov, O. G. (2008). Dynamic gain induced pulse shortening in Q-switched lasers. *Optics Letters*, 33(9), 1011-1013.
- Iliopoulos, K., Kalogerakis, G., Vernardou, D., Katsarakis, N., Koudoumas, E., & Couris, S. (2009). Nonlinear optical response of titanium oxide nanostructured thin films. *Thin Solid Films*, 518(4), 1174-1176. doi:10.1016/j.tsf.2009.02.154
- Ismaeel, R., Lee, T., Ding, M., Belal, M., & Brambilla, G. (2013). Optical microfiber passive components. *Laser & Photonics Reviews*, 7(3), 350-384.
- Jagadish, C., & Pearton, S. J. (2011). *Zinc oxide bulk, thin films and nanostructures: processing, properties, and applications*: Elsevier.
- Janotti, A., & Van de Walle, C. G. (2009). Fundamentals of zinc oxide as a semiconductor. *Reports on Progress in Physics*, 72(12), 126501.
- Jasim, A. A., Muhammad, M. Z., Zulkifli, A. Z., Ahmada, F., Ahmad, H., & Harun, S. W. (2012). Fabrication and Characterization of a 2× 2 Microfiber coupler. *Optoelectronics and Advanced Materials-Rapid Communications*, 6, 7-11.
- Jian, F., Ying-Ying, X., Shao-Fang, T., Yang, L., & Shuo, S. (2010). Transverse Multimode Evolution in Non-Adiabatic Optical Micro/Nanofiber Tapers. *Chinese Physics Letters*, 27(1), 014202.
- Jiang, L., Yang, J., Wang, S., Li, B., & Wang, M. (2011). Fiber Mach-Zehnder interferometer based on microcavities for high-temperature sensing with high sensitivity. *Optics Letters*, 36(19), 3753-3755.
- Jiang, T., Yin, K., Zheng, X., Yu, H., & Cheng, X.-A. (2015). Black phosphorus as a new broadband saturable absorber for infrared passively Q-switched fiber lasers. *arXiv preprint arXiv:1504.07341*.

- Karunagaran, B., Kim, K., Mangalaraj, D., Yi, J., & Velumani, S. (2005). Structural, optical and Raman scattering studies on DC magnetron sputtered titanium dioxide thin films. *Solar Energy Materials and Solar Cells*, 88(2), 199-208. doi:10.1016/j.solmat.2004.03.008
- Kashiwagi, K., & Yamashita, S. (2010). *Optical Deposition of Carbon Nanotubes for Fiber-based Device Fabrication*: INTECH Open Access Publisher.
- Kivisto, S., Hakulinen, T., Kaskela, A., Aitchison, B., Brown, D. P., Nasibulin, A. G., Okhotnikov, O. G. (2009). Carbon nanotube films for ultrafast broadband technology. *Optics Express*, 17(4), 2358-2363. doi:Doi 10.1364/Oe.17.002358
- Koenig, S. P., Doganov, R. A., Schmidt, H., Neto, A. C., & Oezylmaz, B. (2014). Electric field effect in ultrathin black phosphorus. *Applied Physics Letters*, 104(10), 103106.
- Kong, L., Qin, Z., Xie, G., Guo, Z., Zhang, H., Yuan, P., & Qian, L. (2015). Multilayer black phosphorus as broadband saturable absorber for pulsed lasers from 1 to 2.7 μm wavelength. *arXiv preprint arXiv:1508.04510*.
- Kumar, S., & Schwingenschlogl, U. (2015). Thermoelectric Response of Bulk and Mono layer MoSe_2 and WSe_2 . *Chemistry of Materials*, 27(4), 1278-1284. doi:10.1021/cm504244b
- Kuznetsov, V. N., & Serpone, N. (2006). Visible light absorption by various titanium dioxide specimens. *The Journal of Physical Chemistry B*, 110(50), 25203-25209.
- Larciprete, M., Haertle, D., Belardini, A., Bertolotti, M., Sarto, F., & Günter, P. (2006). Characterization of second and third order optical nonlinearities of ZnO sputtered films. *Applied Physics B*, 82(3), 431-437.
- Laroche, M., Chardon, A. M., Nilsson, J., Shepherd, D. P., Clarkson, W. A., Girard, S., & Moncorge, R. (2002). Compact diode-pumped passively Q-switched tunable Er-Yb double-clad fiber laser. *Optics Letters*, 27(22), 1980-1982. doi:Doi 10.1364/Ol.27.001980

- Li, J. L., Musha, M., Shirakawa, A., Ueda, K. I., & Zhong, L. X. (2006). Dual-wavelength-switching operation based on optical bistability in pump-bypassed ytterbium-doped fiber laser. *Applied Physics B*, 85(4), 545-548. doi:10.1007/s00340-006-2366-z
- Li, L., Xia, L., Xie, Z., & Liu, D. (2012). All-fiber Mach-Zehnder interferometers for sensing applications. *Optics Express*, 20(10), 11109-11120.
- Li, Y., & Bao, X. (2008). The observation of comblike transmission spectrum from a tapered single mode fiber tip. *Applied Physics Letters*, 93(26), -. doi:doi:http://dx.doi.org/10.1063/1.3059574
- Liu, D., Ngo, N. Q., Ning, G., Shum, P., & Tjin, S. C. (2006). Tunable microwave photonic notch filter using a dual-wavelength fiber laser with phase modulation. *Optics Communications*, 266(1), 240-248.
- Liu, J., Wu, S. D., Yang, Q. H., & Wang, P. (2011). Stable nanosecond pulse generation from a graphene-based passively Q-switched Yb-doped fiber laser. *Optics Letters*, 36(20), 4008-4010.
- Lu, P., Men, L., Sooley, K., & Chen, Q. (2009). Tapered fiber Mach-Zehnder interferometer for simultaneous measurement of refractive index and temperature. *Applied Physics Letters*, 94(13), -. doi:doi:http://dx.doi.org/10.1063/1.3115029
- Lu, S., Miao, L., Guo, Z., Qi, X., Zhao, C., Zhang, H., Fan, D. (2015). Broadband nonlinear optical response in multi-layer black phosphorus: an emerging infrared and mid-infrared optical material. *Optics Express*, 23(9), 11183-11194.
- Lu, X., Utama, M. I. B., Lin, J. H., Gong, X., Zhang, J., Zhao, Y. Y., Xiong, Q. H. (2014). Large-Area Synthesis of Monolayer and Few-Layer MoSe₂ Films on SiO₂ Substrates. *Nano Letters*, 14(5), 2419-2425. doi:10.1021/nl5000906
- Luo, Z.-C., Liu, M., Guo, Z.-N., Jiang, X.-F., Luo, A.-P., Zhao, C.-J., Zhang, H. (2015). Microfiber-based few-layer black phosphorus saturable absorber for ultra-fast fiber laser. *Optics Express*, 23(15), 20030-20039.

- Luo, Z., Huang, Y., Zhong, M., Li, Y., Wu, J., Xu, B., . . . Weng, J. (2014). 1-, 1.5-, and 2- μm fiber lasers Q-switched by a broadband few-layer MoS_2 saturable absorber. *Journal of Lightwave Technology*, 32(24), 4077-4084.
- Luo, Z., Li, Y., Zhong, M., Huang, Y., Wan, X., Peng, J., & Weng, J. (2015). Nonlinear optical absorption of few-layer molybdenum diselenide (MoSe_2) for passively mode-locked soliton fiber laser [Invited]. *Photonics Research*, 3(3), A79-A86.
- Luo, Z., Zhou, M., Weng, J., Huang, G., Xu, H., Ye, C., & Cai, Z. (2010). Graphene-based passively Q-switched dual-wavelength erbium-doped fiber laser. *Optics Letters*, 35(21), 3709-3711.
- Luxon, J. T., & Summitt, R. (1969). Interpretation of the infrared absorption spectra of stannic oxide and titanium dioxide (rutile) powders. *The Journal of Chemical Physics*, 50(3), 1366-1370.
- Mahad, F. D., Supa'at, M., & Sahmah, A. (2009). EDFA gain optimization for WDM system. *Elektrika*, 11(1), 34-37.
- Mang, A., & Reimann, K. (1995). Band gaps, crystal-field splitting, spin-orbit coupling, and exciton binding energies in ZnO under hydrostatic pressure. *Solid State Communications*, 94(4), 251-254.
- Nambara, T., Yoshida, K., Miao, L., Tanemura, S., & Tanaka, N. (2007). Preparation of strain-included rutile titanium oxide thin films and influence of the strain upon optical properties. *Thin Solid Films*, 515(5), 3096-3101. doi:10.1016/j.tsf.2006.09.004
- Nilsson, J., Clarkson, W., Selvas, R., Sahu, J., Turner, P., Alam, S.-U., & Grudinin, A. (2004). High-power wavelength-tunable cladding-pumped rare-earth-doped silica fiber lasers. *Optical Fiber Technology*, 10(1), 5-30.
- Park, K., Lee, J., Lee, Y. T., Choi, W. K., Lee, J. H., & Song, Y. W. (2015). Black phosphorus saturable absorber for ultrafast mode-locked pulse laser via evanescent field interaction. *Annalen der Physik*, 527(11-12), 770-776.

Paschotta, R. Encyclopedia of laser physics and technology.

Paschotta, R., Nilsson, J., Barber, P., Caplen, J., Tropper, A. C., & Hanna, D. C. (1997). Lifetime quenching in Yb doped fibres. *Optics Communications*, 136(5-6), 375-378.

Paschotta, R., Nilsson, J., Tropper, A. C., & Hanna, D. C. (1997). Ytterbium-doped fibre amplifiers. *IEEE Journal of quantum electronics*, 33(7), 1049-1056.

Pask, H., Carman, R. J., Hanna, D. C., Tropper, A. C., Mackechnie, C. J., Barber, P. R., & Dawes, J. M. (1995). Ytterbium-doped silica fiber lasers: versatile sources for the 1-1.2 μm region. *IEEE Journal of Selected Topics in Quantum Electronics*, 1(1), 2-13.

Peng, W., Yan, F., Li, Q., Tan, S., Liu, S., Feng, S., & Feng, T. (2013). A tunable self-seeded Brillouin/erbium fiber laser utilizing an asymmetrical twin core fiber based Mach-Zehnder interferometer. *Laser Physics*, 23(3), 035101. doi:10.1088/1054-660x/23/3/035101

Peng, W., Yan, F., Li, Q., Yin, G., Feng, S., Feng, T., & Tan, S. (2013). Tunable self-seeded multiwavelength Brillouin-erbium fiber laser using an in-line two-taper Mach-Zehnder interferometer. *Optics & Laser Technology*, 45, 348-351. doi:10.1016/j.optlastec.2012.06.025

Peter, Y., & Cardona, M. (2010). *Fundamentals of semiconductors: physics and materials properties*: Springer Science & Business Media.

Popa, D., Sun, Z., Hasan, T., Torrisi, F., Wang, F., & Ferrari, A. C. (2011). Graphene Q-switched, tunable fiber laser. *Applied Physics Letters*, 98(7). doi:Artn 073106Doi 10.1063/1.3552684

Popa, D., Sun, Z., Torrisi, F., Hasan, T., Wang, F., & Ferrari, A. C. (2010). Sub 200 fs pulse generation from a graphene mode-locked fiber laser. *Applied Physics Letters*, 97(20). doi:Artn 203106Doi 10.1063/1.3517251

- Poustie, A. J., Harper, P., & Finlayson, N. (1994). Multiwavelength fiber laser using a spatial mode beating filter. *Optics Letters*, 19(10), 716-718.
- Qian, J.-r., Su, J., & Hong, L. (2008). A widely tunable dual-wavelength erbium-doped fiber ring laser operating in single longitudinal mode. *Optics Communications*, 281(17), 4432-4434.
- Reynolds, D. C., Look, D. C., & Jogai, B. (1996). Optically pumped ultraviolet lasing from ZnO. *Solid State Communications*, 99(12), 873-875.
- Schmidt, A., Rivier, S., Steinmeyer, G., Yim, J. H., Cho, W. B., Lee, S., Aguiló, M. (2008). Passive mode locking of Yb: KLuW using a single-walled carbon nanotube saturable absorber. *Optics Letters*, 33(7), 729-731.
- Schmidt, A., Rivier, S., Steinmeyer, G., Yim, J. H., Cho, W. B., Lee, S., Griebner, U. (2008). Passive mode locking of Yb : KLuW using a single-walled carbon nanotube saturable absorber. *Optics Letters*, 33(7), 729-731. DOI: 10.1364/Ol.33.000729
- Siegman, A. E. (1986). Lasers University Science Books. *Mill Valley, CA*, 37.
- Skorczakowski, M., Swiderski, J., Pichola, W., Nyga, P., Zajac, A., Maciejewska, M., Bragagna, T. (2010). Mid-infrared Q-switched Er:YAG laser for medical applications. *Laser Physics Letters*, 7(7), 498-504. DOI 10.1002/lapl.201010019
- SM Ytterbium Doped Fiber*. (2013). Retrieved from: www.fibercore.com
- Song, Y., Zhan, L., Hu, S., Ye, Q., & Xia, Y. (2004). Tunable multiwavelength Brillouin-erbium fiber laser with a polarization-maintaining fiber Sagnac loop filter. *IEEE Photonics Technology Letters*, 16(9), 2015-2017.
- Sun, Z., Hasan, T., & Ferrari, A. C. (2012). Ultrafast lasers mode-locked by nanotubes and graphene. *Physica E-Low-Dimensional Systems & Nanostructures*, 44(6), 1082-1091. doi:DOI 10.1016/j.physe.2012.01.012

- Tadakuma, M., Aso, O., & Namiki, S. (2000, 7-10 March 2000). *A 104 GHz 328 fs soliton pulse train generation through a comb-like dispersion profiled fiber using short high nonlinearity dispersion fibers*. Paper presented at the Optical Fiber Communication Conference, 2000.
- Thompson, T. L., & Yates, J. T. (2006). Surface science studies of the photoactivation of TiO₂ new photochemical processes. *Chemical Reviews*, *106*(10), 4428-4453.
- Tongay, S., Zhou, J., Ataca, C., Lo, K., Matthews, T. S., Li, J., Wu, J. (2012). Thermally driven crossover from indirect toward direct bandgap in 2D semiconductors: MoSe₂ versus MoS₂. *Nano Letters*, *12*(11), 5576-5580.
- Villatoro, J., Minkovich, V. P., & Monzón-Hernández, D. (2006). Compact modal interferometer built with tapered microstructured optical fiber. *IEEE Photonics Technology Letters*, *18*(11), 1258-1260.
- Vodopyanov, K., Fejer, M., Yu, X., Harris, J., Lee, Y.-S., Hurlbut, W. C., Lynch, C. (2006). Terahertz-wave generation in quasi-phase-matched GaAs. *Applied Physics Letters*, *89*(14), 141119.
- Wang, H., Li, Y. G., Chen, X. D., Huang, B., Lu, F. Y., & Lu, K. C. (2009). Highly efficient dual-wavelength ytterbium-doped fiber linear cavity laser based on cascaded fiber Bragg gratings. *Laser Physics*, *19*(6), 1257-1262. doi:10.1134/s1054660x09060139
- Wang, Z. L. (2004). Zinc oxide nanostructures: growth, properties and applications. *Journal of Physics: Condensed Matter*, *16*(25), R829.
- Wang, Z. T., Chen, Y., Zhao, C. J., Zhang, H., & Wen, S. C. (2012). Switchable Dual-Wavelength Synchronously Q-Switched Erbium-Doped Fiber Laser Based on Graphene Saturable Absorber. *IEEE Photonics Journal*, *4*(3), 869-876. doi:10.1109/jphot.2012.2199102
- Williams, R. J., Jovanovic, N., Marshall, G. D., & Withford, M. J. (2010). All-optical, actively Q-switched fiber laser. *Optics Express*, *18*(8), 7714-7723. doi:Doi 10.1364/Oe.18.007714

- Wilson, J., & Yoffe, A. (1969). The transition metal dichalcogenides discussion and interpretation of the observed optical, electrical and structural properties. *Advances in Physics*, 18(73), 193-335.
- Woodward, R. I., Howe, R. C. T., Runcorn, T. H., Hu, G., Torrisi, F., Kelleher, E. J. R., & Hasan, T. (2015). Wideband saturable absorption in few-layer molybdenum diselenide (MoSe₂) for Q-switching Yb-, Er- and Tm-doped fiber lasers. *Optics Express*, 23(15), 20051-20061. doi:10.1364/OE.23.020051
- Woodward, R. I., & Kelleher, E. J. (2015). 2D saturable absorbers for fibre lasers. *Applied Sciences*, 5(4), 1440-1456.
- Wright, M. W., & Valley, G. C. (2005). Yb-doped fiber amplifier for deep-space optical communications. *Journal of Lightwave Technology*, 23(3), 1369-1374. doi:10.1109/JLT.2005.843532
- Wright, M. W., & Valley, G. C. (2005). Yb-doped fiber amplifier for deep-space optical communications. *Journal of Lightwave Technology*, 23(3), 1369.
- Xia, F., Wang, H., & Jia, Y. (2014). Rediscovering black phosphorus as an anisotropic layered material for optoelectronics and electronics. *Nature Communications*, 5.
- Xia, J., Huang, X., Liu, L. Z., Wang, M., Wang, L., Huang, B., Meng, X. M. (2014). CVD synthesis of large-area, highly crystalline MoSe₂ atomic layers on diverse substrates and application to photodetectors. *Nanoscale*, 6(15), 8949-8955. doi:10.1039/c4nr02311k
- Xia, L., Shum, P., & Cheng, T. H. (2007). Photonic generation of microwave signals using a dual-transmission-band FBG filter with controllable wavelength spacing. *Applied Physics B-Lasers and Optics*, 86(1), 61-64.
- Xing, G. C., Guo, H. C., Zhang, X. H., Sum, T. C., & Huan, C. H. A. (2010). The Physics of ultrafast saturable absorption in graphene. *Optics Express*, 18(5), 4564-4573. doi:Doi 10.1364/Oe.18.004564

Xinhuan, F., Yange, L., Shenggui, F., Shuzhong, Y., & Xiaoyi, D. (2004). Switchable dual-wavelength ytterbium-doped fiber laser based on a few-mode fiber grating. *IEEE Photonics Technology Letters*, 16(3), 762-764. doi:10.1109/LPT.2004.823722

Xinju, L. (2010). *Laser technology*: CRC Press.

Yasuno, Y., Hong, Y., Makita, S., Yamanari, M., Akiba, M., Miura, M., & Yatagai, T. (2007). In vivo high-contrast imaging of deep posterior eye by 1- μ m swept source optical coherence tomography and scattering optical coherence angiography. *Optics Express*, 15(10), 6121-6139. doi:10.1364/OE.15.006121

Yin, Z. F., Wu, L., Yang, H. G., & Su, Y. H. (2013). Recent progress in biomedical applications of titanium dioxide. *Physical Chemistry Chemical Physics*, 15(14), 4844-4858.

Yu, Y., Liaw, S., Hsu, W., Shih, M., & Chen, N. (2015). Single longitudinal mode Ytterbium doped fiber lasers with large proposed tuning range. *Optical and Quantum Electronics*, 47(2), 131-137.

Yue, Z., Chui, P. C., & Wong, K. K. Y. (2013). Multiwavelength Single-Longitudinal-Mode Ytterbium-Doped Fiber Laser. *IEEE Photonics Technology Letters*, 25(4), 385-388. doi:10.1109/LPT.2013.2238917

Zamarreño, C. R., Zubiate, P., Sagües, M., Matias, I., & Arregui, F. (2013). Experimental demonstration of lossy mode resonance generation for transverse-magnetic and transverse-electric polarizations. *Optics Letters*, 38(14), 2481-2483.

Zetie, K., Adams, S., & Tocknell, R. (2000). How does a Mach-Zehnder interferometer work? *Physics Education*, 35(1), 46.

Zhang, F., Chu, P. L., Lai, R., & Chen, G. R. (2005). Dual-wavelength chaos generation and synchronization in erbium-doped fiber lasers. *IEEE Photonics Technology Letters*, 17(3), 549-551.

- Zhang, L., Fan, J. T., Wang, J. H., Hu, J. M., Lotya, M., Wang, G. Z., Feng, Y. (2012). Graphene incorporated Q-switching of a polarization-maintaining Yb-doped fiber laser. *Laser Physics Letters*, 9(12), 888-892. doi:Doi 10.7452/Lapl.201210090
- Zhang, Q., Zeng, X., Pang, F., Wang, M., & Wang, T. (2012). Switchable multiwavelength fiber laser by using a compact in-fiber Mach–Zehnder interferometer. *Journal of Optics*, 14(4), 045403. doi:10.1088/2040-8978/14/4/045403
- Zhang, S. X., Liu, C. Y., & Ye, H. A. (2014). Development of Side-Polished Fiber Filters. *Applied Mechanics and Materials*, 602-605, 2740-2743. doi:10.4028/www.scientific.net/AMM.602-605.2740
- Zhao, C., Zou, Y., Chen, Y., Wang, Z., Lu, S., Zhang, H., Tang, D. (2012). Wavelength-tunable picosecond soliton fiber laser with topological insulator: Bi₂Se₃ as a mode locker. *Optics Express*, 20(25), 27888-27895.
- Zhao, C. J., Zhang, H., Qi, X., Chen, Y., Wang, Z. T., Wen, S. C., & Tang, D. Y. (2012). Ultra-short pulse generation by a topological insulator based saturable absorber. *Applied Physics Letters*, 101(21). doi:Artn 21110610.1063/1.4767919
- Zhao, H. M., Lou, Q. H., Zhou, J., Zhang, F. P., Doug, J. X., Wei, Y. R., & Wang, Z. J. (2007). Stable pulse-compressed acousto-optic Q-switched fiber laser. *Optics Letters*, 32(19), 2774-2776. doi:Doi 10.1364/Ol.32.002774
- Zhao, Y., Li, X., Xu, M., Yu, H., Wu, Y., Wang, Z., Xu, X. (2013). Dual-wavelength synchronously Q-switched solid-state laser with multi-layered graphene as saturable absorber. *Optics Express*, 21(3), 3516-3522.
- Zhou, D.-P., Wei, L., Dong, B., & Liu, W.-K. (2010). Tunable passively-switched erbium-doped fiber laser with carbon nanotubes as a saturable absorber. *IEEE Photonics Technology Letters*, 22(1), 9-11.
- Zhou, P., Wang, X., Xiao, H., Ma, Y., & Chen, J. (2012). Review on recent progress on Yb-doped fiber laser in a variety of oscillation spectral ranges. *Laser Physics*, 22(5), 823-831. doi:10.1134/S1054660X12050404

Zhou, Y., Chui, P. C., & Wong, K. K. Y. (2013). Multiwavelength Single-Longitudinal-Mode Ytterbium-Doped Fiber Laser. *IEEE Photonics Technology Letters*, 25(4), 385-388. doi:Doi 10.1109/Lpt.2013.2238917

University of Malaya

LIST OF PUBLICATIONS AND PAPERS PRESENTED

List of Publication

1. H. Ahmad, **M. A. M. Salim**, S. Azzuhri, M. Zulkifli, and S. Harun, "Dual wavelength single longitudinal mode Ytterbium-doped fiber laser using a dual-tapered Mach-Zehnder interferometer," *Journal of the European Optical Society-Rapid Publications*, vol. 10, 2015.
2. H. Ahmad, **M. A. M. Salim**, S. R. Azzuhri, M. Soltanian, S. Harun, and M. Yasin, "Generation of an ultra-stable dual-wavelength ytterbium-doped fiber laser using a photonic crystal fiber," *Laser Physics*, vol. 26, p. 025101, 2015.
3. H. Ahmad, **M. A. M. Salim**, M. R. K. Soltanian, S. R. Azzuhri, S. W. Harun, and M. Yasin, "Generation of stable and narrow spacing dual-wavelength ytterbium-doped fiber laser using a photonic crystal fiber," *Journal of Modern Optics*, pp. 1-6, 2015.
4. H. Ahmad, **M. A. M. Salim**, S. R. Azzuhri, M. Soltanian, and S. Harun, "A passively Q-switched ytterbium-doped fiber laser based on a few-layer Bi₂Se₃ saturable absorber," *Laser Physics*, vol. 25, p. 065102, 2015.
5. H. Ahmad, **M. A. M. Salim**, M. Soltanian, S. R. Azzuhri, and S. Harun, "Passively dual-wavelength Q-switched ytterbium doped fiber laser using Selenium Bismuth as saturable absorber," *Journal of Modern Optics*, vol. 62, pp. 1550-1554, 2015.
6. H. Ahmad, **M. A. M. Salim**, S. R. Azzuhri, and S. W. Harun, "Highly stable and tunable narrow-spacing dual-wavelength ytterbium-doped fiber using a microfiber Mach-Zehnder interferometer," *Optical Engineering*, vol. 55, pp. 026114-026114, 2016.

7. H. Ahmad, **M. A. M. Salim**, S. R. Azzuhri, M. Jaddoa, and S. Harun, "Tunable dual-wavelength ytterbium-doped fiber laser using a strain technique on microfiber Mach-Zehnder interferometer," *Applied Optics*, vol. 55, pp. 778-782, 2016.
8. H. Ahmad, Z. C. Tiu, A. Zarei, M. Suthaskumar, **M. A. M. Salim**, and S. W. Harun, "Domain-wall dark pulse generation in fiber laser incorporating MoS₂," *Applied Physics B*, vol. 122, pp. 1-5, 2016.
9. M. Jaddoa, M. Razak, **M. A. M. Salim**, A. Sharbirin, N. Nayan, M. Ismail, *et al.*, "Tunable single wavelength erbium-doped fiber ring laser based on in-line Mach-Zehnder strain," *Optik-International Journal for Light and Electron Optics*, 2016.
10. H. Ahmad, **M. A. M. Salim**, Z. Ali, M. Ismail, K. Thambiratnam, A. Latif, *et al.*, "Titanium dioxide-based Q-switched dual wavelength in the 1 micron region," *Chinese Optics Letters*, vol. 14, p. 091403, 2016.
11. F. Rashid, S. R. Azzuhri, **M. A. M. Salim**, R. Shaharuddin, M. Ismail, M. Ismail, *et al.*, "Using a black phosphorus saturable absorber to generate dual wavelengths in a Q-switched ytterbium-doped fiber laser," *Laser Physics Letters*, vol. 13, p. 085102, 2016.
12. H. Ahmad, **M. A. M. Salim**, K. Thambiratnam, S. Norizan, and S. Harun, "A black phosphorus-based tunable Q-switched ytterbium fiber laser," *Laser Physics Letters*, vol. 13, p. 095103, 2016.
13. H. Ahmad, F. A. A. Rashid, S. R. Azzuhri, **M. A. M. Salim**, R. A. Shaharuddin, M. A. Ismail, and M. Z. A. Razak. "The generation of passive dual wavelengths Q-switched YDFL by MoSe₂ film." *Laser Physics Letters* 13, no. 11, 115102, 2016
14. H. Ahmad, **M. A. M. Salim**, M. F. Ismail, and S. W. Harun. "Q-switched ytterbium-doped fiber laser with zinc oxide based saturable absorber." *Laser Physics* 26, no. 11, 115107, 2016

15. A. S. Zulkhairi, Saaidal R. Azzuhri, R. A. Shaharuddin, M. F. Jaddoa, **M. A. M. Salim**, A. A. Jasim, and H. Ahmad. "Switchable multiwavelength ytterbium-doped fiber laser using a non-adiabatic microfiber interferometer." *Laser Physics* 27, no. 5 (2017): 055104.
16. H. Ahmad, and **M. A. M. Salim**. "TiO₂-Based Q-Switched Ytterbium-Doped Fiber Laser." *IEEE Journal of Quantum Electronics* 53, no. 5 (2017): 1-6.
17. **M. A. M. Salim**, H Ahmad, Saaidal R Azzuhri, M Z A Razak and S W Harun. "Tunable wavelength generation in the 1 μ m region incorporating a 16-channel arrayed waveguide grating (AWG)." *Laser Physics* 27 (2017) 125101
18. **M. A. M. Salim**, R A Shaharuddin, M A Ismail, S W Harun, H Ahmad and Saaidal R Azzuhri. "Bi₂Te₃ based passively Q-switched at 1042.76 and 1047 nm wavelength." *Laser Physics* 27 (2017) 125102

List of oral and poster presentation

1. **M.A.M. Salim**, H. Ahmad, Saaidal R. Azzuhri and S.W. Harun (August 2016). Dual-Wavelength based Microfiber Q-Switched incorporating Molybdenum Diselenide. Photonics Conference and Meeting (PCM 2016). University of Malaya, Kuala Lumpur
2. **M.A.M. Salim**, H. Ahmad, Saaidal R. Azzuhri, M.Z.A. Razak and S.W. Harun (August 2016): Tunable Wavelength Generation in 1-Micron Region Incorporating 16-Channels Arrayed Waveguide Grating (AWG). International Graduate Conference on Engineering, Science and Humanities (IGCESH 2016). Universiti Teknologi Malaysia, Johor Bahru
3. **M.A.M. Salim**, H. Ahmad, S.W. Harun, N. Bidin and G. Krishnan (September 2017). Generation of an Ultrafast Femtosecond Soliton Fiber Laser by Carbon Nanotube as Saturable Absorber. International Laser Technology and Optics Symposium 2017 (ILATOS 2017). Pulai Springs Resort, Johor Bahru.